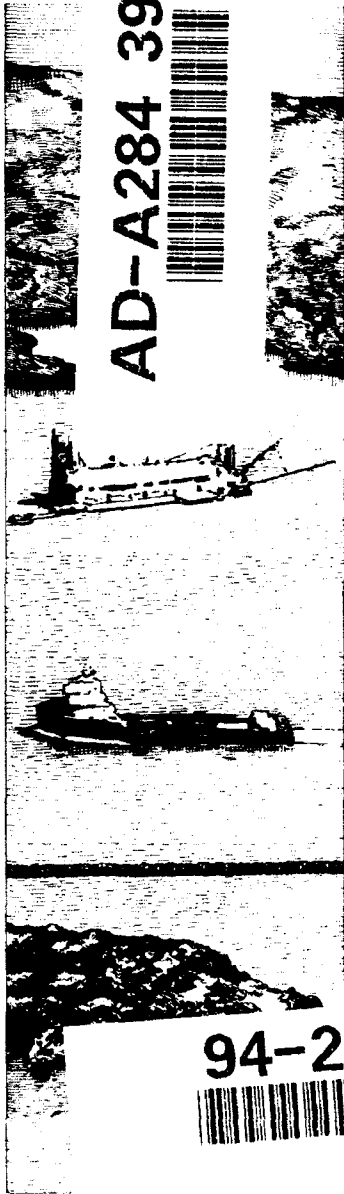




US Army Corps  
of Engineers

AD-A284 391



94-29814



*94P*

DREDGING RESEARCH PROGRAM

CONTRACT REPORT DRP-94-4

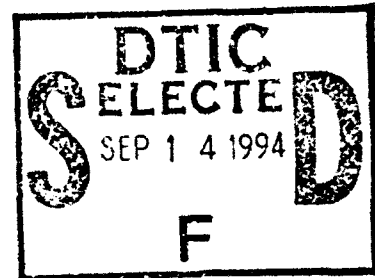
1

**FLUID MUD AND WATER WAVES:  
A BRIEF REVIEW OF INTERACTIVE PROCESSES  
AND SIMPLE MODELING APPROACHES**

by

Ashish J. Mehta, Say-Chong Lee, Yigong Li

Coastal and Oceanographic Engineering Department  
University of Florida  
Gainesville, Florida 32611



July 1994

Final Report

Approved for Public Release; Distribution Unlimited

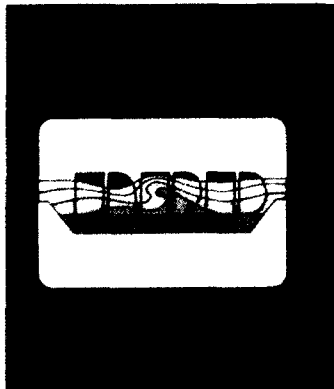
Prepared for DEPARTMENT OF THE ARMY  
U.S. Army Corps of Engineers  
Washington, DC 20314-1000

Under Work Unit No. 32590

Monitored by U.S. Army Engineer Waterways Experiment Station  
3909 Halls Ferry Road, Vicksburg, Mississippi 39180-6199

94

3



The Dredging Research Program (DRP) is a seven-year program of the U.S. Army Corps of Engineers. DRP research is managed in these five technical areas:

- Area 1 - Analysis of Dredged Material Placed in Open Water
- Area 2 - Material Properties Related to Navigation and Dredging
- Area 3 - Dredge Plant Equipment and Systems Processes
- Area 4 - Vessel Positioning, Survey Controls, and Dredge Monitoring Systems
- Area 5 - Management of Dredging Projects

The contents of this report are not to be used for advertising, publication, or promotional purposes. Citation of trade names does not constitute an official endorsement or approval of the use of such commercial products.



PRINTED ON RECYCLED PAPER



US Army Corps  
of Engineers  
Waterways Experiment  
Station

# Dredging Research Program Report Summary



## *Fluid Mud and Water Waves: A Brief Review of Interactive Processes and Simple Modeling Approaches (CR DRP-94-4)*

**ISSUE:** Recently interest has increased in the beneficial use of fine-grained material dredged from navigation channels to create offshore underwater berms to absorb wave energy and to act as buffers against wave attack in areas in the lee of the berms. It is important to the design process to forecast the degree of wave damping for a berm of given dimensions and mud rheology.

**RESEARCH:** The mud/wave domain and fluid mud were defined and the equations identified that describe generation and erosion of fluid mud. Water waves over mud and water-column dynamics were modeled. Model simulations were compared with laboratory and field data.

**SUMMARY:** As its title indicates, the report presents a short review of iterative procedures and simple modeling approaches for studying the basics of the interaction between progressive water waves and a compliant mud bed in the shallow coastal environment. Laboratory and field data and model simulations are discussed; an appendix briefly summarizes additional modeling studies.

**AVAILABILITY OF REPORT:** The report is available through the Interlibrary Loan Service from the U.S. Army Engineer Waterways Experiment Station (WES) Library, telephone number (601) 634-2355. National Technical Information Service (NTIS) report numbers may be requested from WES Librarians. To purchase a copy of the report, call NTIS at (703) 487-4780.

DTIC QUALITY INSPECTED 3

**About the Authors:** Dr. Ashish J. Mehta is a major professor and Say-Chong Lee and Yigong Li are graduate students in the Coastal and Oceanographic Engineering Department of the University of Florida, Gainesville, FL.

**Point of Contact:** Mr. Allen M. Teeter, Hydraulics Laboratory, WES, was Principal Investigator for this work unit. For information about the DRP, contact Mr. E. Clark McNair, Jr., Manager, DRP, at (601) 634-2070.

# Fluid Mud and Water Waves: A Brief Review of Interactive Processes and Simple Modeling Approaches

by Ashish J. Mehta, Say-Chong Lee, Yigong Li  
Coastal and Oceanographic Engineering Department  
University of Florida  
Gainesville, FL 32611

Accession For	
NTIS CRA&I	<input checked="" type="checkbox"/>
DTIC TAB	<input type="checkbox"/>
Unannounced	<input type="checkbox"/>
Justification	
By	
Distribution/	
Availability Codes	
Dist	Avail and/or Special
A-1	

Final report

Approved for public release; distribution is unlimited

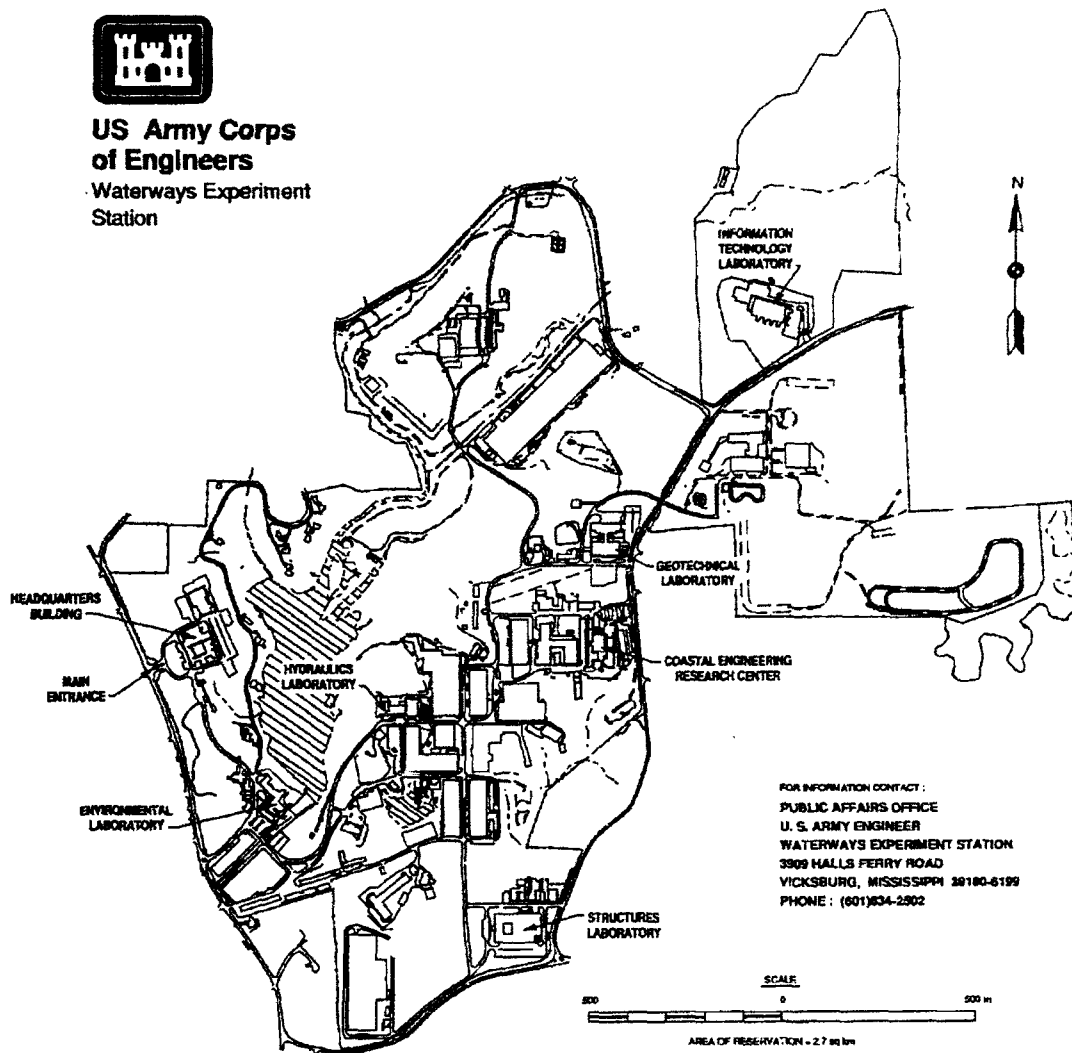
Prepared for U.S. Army Corps of Engineers  
Washington, DC 20314-1000

Under Work Unit 32590

Monitored by U.S. Army Engineer Waterways Experiment Station  
3909 Halls Ferry Road, Vicksburg, MS 39180-6199



**US Army Corps  
of Engineers**  
Waterways Experiment  
Station



FOR INFORMATION CONTACT :  
PUBLIC AFFAIRS OFFICE  
U. S. ARMY ENGINEER  
WATERWAYS EXPERIMENT STATION  
3309 HALLS FERRY ROAD  
VICKSBURG, MISSISSIPPI 39180-6199  
PHONE : (601)834-2902

### Waterways Experiment Station Cataloging-in-Publication Data

Mehta, A. J. (Ashish Jayant), 1914-

Fluid mud and water waves : A brief review of interactive processes and simple modeling approaches / by Ashish J. Mehta, Say-Chong Lee, Yigong Li ; prepared for Department of the Army, U.S. Army Corps of Engineers ; monitored by U.S. Army Engineer Waterways Experiment Station.

92 p. : ill. ; 28 cm. -- (Contract report ; DRP-94-4)

Includes bibliographical references.

1. Sediment transport -- Mathematical models 2. Marine sediments. 3. Rheology. 4. Fluid dynamics -- Mathematical models. I. Lee, Say-Chong. II. Li, Yigong. III. United States. Army. Corps of Engineers. IV. U.S. Army Engineer Waterways Experiment Station. V. Dredging Research Program. VI. Title. VII. Title: A brief review of interactive processes and simple modeling approaches. VIII. Series: Contract report (U.S. Army Engineer Waterways Experiment Station) ; DRP-94-4. TA7 W34c no.DRP-94-4

## TABLE OF CONTENTS

PREFACE .....	xi
SUMMARY .....	xii
INTRODUCTION .....	1
1.1 MUD-WAVE DYNAMICS IN ENGINEERING AND SCIENTIFIC APPLICATIONS .....	1
1.2 PROCESSES AND FEEDBACKS .....	1
MUD-WAVE DOMAIN .....	4
2.1 DEFINITIONS .....	4
2.2 FLUID MUD .....	5
GENERATION AND EROSION OF FLUID MUD .....	10
3.1 FLUIDIZATION .....	10
3.2 ESTIMATION OF FLUIDIZATION THICKNESS .....	16
3.3 SURFACE EROSION .....	19
3.4 BED RECOVERY .....	21
ENERGY DISSIPATION AND ELEMENTS OF MODELING .....	23
4.1 WAVE ENERGY DISSIPATION OVER NON-RIGID BEDS .....	23
4.2 A MODELING PERSPECTIVE .....	23
4.3 BASIC CONSERVATION EQUATIONS .....	25
4.4 CONSTITUTIVE EQUATIONS .....	26
4.4.1 <i>Fluid (incompressible)</i> .....	26
4.4.2 <i>Elastic Material</i> .....	26
4.4.3 <i>Viscoelastic Material</i> .....	26
4.5 MODELS FOR WATER WAVES OVER MUD (X-Z PLANE) .....	28
4.5.1 <i>Inviscid, Shallow Water over Mud</i> .....	28
4.5.2 <i>Viscid Fluid (Water) over Viscid/Viscoelastic Mud</i> .....	32
4.6 MODELING WATER COLUMN SEDIMENT DYNAMICS .....	34
LABORATORY/FIELD DATA AND MODEL SIMULATIONS .....	40
5.1 INTRODUCTION .....	40
5.2 WAVE FLUME RESULTS .....	40
5.2.1 <i>Test Facility, Experiments and Modeling Approaches</i> .....	40
5.2.2 <i>Wave Attenuation and Mud Motion</i> .....	43
5.2.3 <i>Bed/Interface Erosion</i> .....	48
5.3 LAKE OKEECHOBEE, FLORIDA .....	51
5.3.1 <i>Setting</i> .....	51
5.3.2 <i>Mud Motion</i> .....	52
5.3.3 <i>Resuspension</i> .....	54
5.4 SOUTHWEST COAST OF INDIA .....	54
5.5 MOBILE BERM, ALABAMA .....	57
BIBLIOGRAPHY .....	62
APPENDICES	
A EXPLANATORY NOTES FOR TABLE 7 .....	69
B A SUMMARY OF SOME WAVE-MUD MODELING STUDIES .....	76

## LIST OF FIGURES

Figure		Page
1	Schematic description of the processes and feedbacks related to the response of mud bed to water waves. Box with dashed line represents the mud-water system, inverted triangle represents forcing, rectangles are components of the mud-water system, ellipses are process transfer functions and circles represent manifested responses (adapted from Maa and Mehta, 1989).	1
2	Schematic diagram showing the vertical variation of the density of mud-water mixture in the wave environment. MWL = mean water level	6
3	a) Settling flux variation with excess density for sediment from the Severn Estuary, United Kingdom. Laboratory column data reported by Odd and Rodger (1986); b) An instantaneous excess density profile showing a marked lutocline in the Severn Estuary, United Kingdom (data reported by Odd and Rodger, 1986)	6
4	Shear rigidity modulus versus solids volume fraction for sediment S1 (after James et al., 1988)	8
5	Schematic of time-variation of pore pressure under wave action	10
6	Schematic of instantaneous stress profiles in a water-mud system	11
7	Time-variation of effective stress at three elevations (above flume bottom) in a clay bed (kaolinite + attapulgite) subjected to 1 Hz progressive waves of 4 cm amplitude (after Feng, 1992)	11
8	Time-variation of the depth of fluidization in three tests with different wave amplitudes and consolidation periods. Data points from Feng (1992)	13
9	Development of a fluid mud layer starting with a "bed" of Hillsboro Bay mud (Run 1; see Ross and Mehta, 1990). $d_f$ is the vertical distance between the lutocline and the $\sigma' = 1$ Pa level. Note the occurrence of an initial, 1.1 cm thick layer of fluid mud over the bed, as a result of a local disturbance of the bed prior to test initiation. The observed initial increase in the lutocline elevation is attributed to advection of fluid mud to the measurement site	13
10	Mud density profiles from Run 1 (Fig. 9). Arrows indicate bed level ( $\sigma' = 1$ Pa) at different times at test initiation (level 1), and following test initiation (after Ross and Mehta, 1990)	15
11	Time-variation of relative shear wave velocity in a bed of attapulgite + kaolinite of 20 hr consolidation subjected to a 1 Hz progressive water wave of 2 cm forcing amplitude (after Williams and Williams, 1992)	15
12	Storage modulus, $G'(\bullet)$ , and loss modulus $G''(\circ)$ , versus strain amplitude, $\gamma$ , for K2 kaolin at a salinity of 35 ppt and a solids concentration of 41%. $\omega = 1.5$ rad/s. Lines are drawn to enhance data trends (after Chou, 1989)	17
13	Contours of storage modulus, $G'$ in (a) and loss modulus, $G''$ , in (b) for K1 kaolin at a salinity of 35 ppt (after Chou, 1989)	17

14	A four-layer viscoelastic model (adapted from Chou, 1989) . . . . .	18
15	Thickness of fluid mud (for a clayey sediment) as a function of wave height, H, assuming a water depth of 5 m, a wave frequency of 0.1 Hz (adapted from Chou, 1989) . . . . .	18
16	Influence of waves on shear resistance to erosion of kaolinite beds in flumes (after Mehta, 1989) . . . . .	21
17	Normalized rate of erosion versus normalized excess shear stress for a bay mud (after Maa and Mehta, 1987) . . . . .	22
18	Three-element viscoelastic models: a) Voigt element (represented by $2\mu_2, 2G_2$ ) modulated by additional elasticity; b) Maxwell element (represented by $2\mu_2, 2G_2$ ) constrained by elastic modulus represented by $2G_1$ . . . . .	29
19	Water-mud system in the x-z plane . . . . .	29
20	Variation of $\hat{\beta}$ with normalized time, $\hat{t}$ (after Cervantes, 1987). . . . .	35
21	Wave-mud interaction flume (after Maa, 1986) . . . . .	35
22	Diffusion flux, $F_d$ , as a function of $\partial\rho_D/\partial z$ for $\alpha_6=2$ and $\beta_6=4.17$ (modified from Ross, 1988) . . . . .	38
23	Settling velocity (and flux) variation with $\rho_D$ . Data points obtained from tests using a lake (Okeechobee, Florida) sediment in a laboratory column (after Hwang, 1989) . . . . .	39
24	Settling velocity versus $\rho_D$ data using a bay (Townsville, Australia) sediment under two conditions: quiescent water and water agitated by vertically oscillating rings (adapted from Wolanski et al., 1992) . . . . .	39
25	a) Time-variation of the bottom mud density profile during an erosion experiment (Run 1) using mud from Cedar Key, Florida (after Maa, 1986); b) Uniform density profile of a mixture of an attapulgite and a kaolinite (after Jiang, 1993) . . . . .	41
26	Magnitude of equivalent dynamic viscosity (applicable to the viscoelastic model of Fig. 18a) as a function of wave forcing frequency and mud volume fraction, $\phi$ , for MB mud . . . . .	43
27	Wave spectra from synchronous wave stations 22, 11 and 4 km offshore, showing loss of wave energy and change in the shape of the spectrum over a fluid-like mud bottom along the central Surinam coast. $H_{rms}$ = root mean square wave height, T = wave period and h = water depth (after Wells and Kemp, 1986) . . . . .	44
28	Wave attenuation coefficient against frequency for two AK mud ( $\phi=0.16$ ) depths, 12 cm and 18 cm. Water depth was 16 cm. The input wave amplitude was 1.3 cm. Circles are data; lines are simulations based on the model of Jiang (1993) . . . . .	45
29	Comparison between measured and model-calculated profiles of the amplitude of horizontal acceleration in a water-mud (AK) system. The water depth was 16 cm, mud thickness 18 cm, water surface forcing wave amplitude 0.5 cm, wave frequency 1 Hz and $\phi=0.12$ (after Jiang, 1993) . . . . .	45

30	Mass transport velocity in AK mud. Wave amplitude 2 cm, frequency 1 Hz, $h_1 = 14$ cm and mud thickness $h_2 = 17$ cm (after Jiang, 1993) . . . . .	47
31	a) Horizontal and vertical velocity amplitudes in water and CK mud; b) Dynamic pressure amplitude profile corresponding to Fig. 31a. Smooth profiles have been drawn based on spatially discretized calculations (after Maa and Mehta, 1987; Maa, 1986) . . . . .	47
32	Time-variation of normalized dry density (concentration), $\hat{\rho}_D(t) = \bar{\rho}_D(t)/\bar{\rho}_{DS}$ , for CK mud, during test T-1. Mud depth ( $h_2$ ) was 16 cm, water depth ( $h_1$ ) was 17 cm, forcing wave amplitude ( $a_0$ ) was 3 cm and frequency ( $f$ ) was 1 Hz (after Cervantes, 1987) . . . . .	49
33	Phases in the time-variation of $\bar{\rho}_D(t)$ , such as in Fig. 32 (after Cervantes, 1987) . . . . .	49
34	Measured and model-calculated dry density (concentration) profiles during erosion of Hillsboro Bay mud (HB). Water depth ( $h_1$ ) 31 cm, mud depth ( $h_2$ ) 12 cm, forcing wave amplitude, $a_0 = 3$ cm and wave frequency, $f = 1$ Hz (after Ross, 1988) . . . . .	50
35	Vertical suspended sediment dry density (concentration) profiles obtained before, during, and after the passage of a winter cold front at a coastal site in Louisiana. Times are relative to time of measurement of the pre-frontal profile 1 (adapted from Kemp and Wells, 1987) . . . . .	50
36	Mud thickness contour map of Lake Okeechobee, Florida (after Kirby et al., 1989). . . . .	51
37	Typical mud bottom density profile based on vibrocore data from two nearby sampling sites (after Hwang, 1989). . . . .	52
38	<i>Data and model application, Lake Okeechobee, Florida:</i> a) Measured water wave spectrum; b) Comparison between measured and simulated water velocity spectra; c) Comparison between measured and simulated mud acceleration spectra (after Jiang, 1993) . . . . .	53
39	a) Simulated time-evolution of suspension profile due to 0.9 m high, 4 s waves in a 4.6 m deep water column; b) Settling of sediment once waves cease 11 hr from start of wave action (after Hwang, 1989). . . . .	55
40	Coastal site off Alleppey in Kerala, India, where monsoonal, mudbanks occur. The pier is 300 m long (after Mathew, 1992). . . . .	56
41	Schematic profile of mudbank off the coast of Kerala, India (after Nair, 1988) . . . . .	56
42	Offshore and inshore wave spectra off Alleppey: a) without mudbank; b) with mudbank (after Mathew, 1992) . . . . .	57
43	Comparison between measured and model-simulated inshore wave spectra off Alleppey in Kerala, India: a) fair weather condition (mudbank absent); b) monsoonal condition (mudbank present) . . . . .	58
44	Construction site (2,750 m long corridor for dredged material placement) for the Mobile berm, and offshore/inshore sites of wave measurement (after McLellan et al., 1990) . . . . .	59

45 Offshore and inshore wave spectra at the Mobile berm site for two different wave conditions at the offshore site characterized by the maximum wave height,  $H_{max}$ :  
a)  $H_{max} = 0.9$  m; b)  $H_{max} = 1.5$  m (after McLellan et al., 1990) . . . . . 60

46 Comparison between measured and model-simulated inshore wave spectra at the Mobile berm site corresponding to two offshore wave conditions: a)  $H_{max} = 0.9$  m (see Fig. 45a);  
b)  $H_{max} = 1.5$  m (see Fig. 45b). Measured offshore spectra have been included for reference . 61

## LIST OF TABLES

Table		Page
1	Some issues in which application of knowledge of mud-wave dynamics plays an important role . . . . .	2
2	Selected definitions of mud . . . . .	4
3	Fluid mud density and corresponding solids volume fraction ranges . . . . .	8
4	Fluidization depth related parameters . . . . .	12
5	Laboratory based, wave-induced mud erosion rates . . . . .	20
6	Bed recovery in Test No. 9 of Feng (1992) . . . . .	22
7	Some energy dissipation rate expressions due to non-rigid bed mechanisms . . . . .	24
8	Test parameters including wave frequency $\omega$ and nominal wave amplitude, $a_0$ , and coefficients $\beta_0$ , $\beta_4$ and $\delta_1$ for empirical-fit equation in Fig. 20 . . . . .	35
9	Coefficients of Eq. 75 for MB mud . . . . .	43

# Preface

---

This study was authorized as part of the Dredging Research Program (DRP) of the Headquarters, U.S. Army Corps of Engineers (HQUSACE), and was performed under the DRP Work Unit 32590, "Cohesive Sediment Processes." This work unit is part of DRP Technical Area 1 (TA1), Analysis of Dredged Material Placed in Open Water. Messrs. David B. Mathis, Barry Holliday, John H. Lockhart, Jr., Gerald E. Greener, M. K. Miles, and John Sanda were Technical Monitors from HQUSACE during the preparation and publication of this report. Mr. E. Clark McNair, Jr., Coastal Engineering Research Center (CERC), U.S. Army Engineer Waterways Experiment Station (WES), was DRP Program Manager (PM), and Dr. Lyndell Z. Hales, CERC, was Assistant PM. Dr. Billy H. Johnson, Hydraulics Laboratory (HL), WES, is the Technical Manager for TA1.

This study was conducted under Contract No. DACW39-90-K-0010 with the Coastal and Oceanographic Engineering Department, University of Florida, Gainesville. The contract was managed for CERC by the Work Unit Principal Investigator, Mr. Allen M. Teeter, Estuarine Processes Branch (EPB), Estuaries Division (ED), HL, under the direct supervision of Messrs. George M. Fisackerly, Chief, EPB; and William H. McAnally, Jr., Chief, ED; and under the general supervision of Messrs. Frank A. Herrmann, Director, HL; and Richard A. Sager, Assistant Director, HL.

At the time of publication of this report, Director of WES was Dr. Robert W. Whalin. Commander was COL Bruce K. Howard, EN.

For further information on this report or on the Dredging Research Program, contact Mr. E. Clark McNair, Jr., Program Manager, at (601) 634-2070 or Mr. Allen M. Teeter, Principal Investigator, at (601) 634-2820.

*The contents of this report are not to be used for advertising, publication, or promotional purposes. Citation of trade names does not constitute an official endorsement or approval of the use of such commercial products.*

# Summary

---

The basics of the interaction between progressive water waves and a compliant mud bed in the shallow coastal environment have been briefly reviewed. A key feature of the interactive process is the ability of waves to fluidize bottom mud and sustain it in that state as long as wave action continues. Compliant or fluid mud is a highly viscous medium that can oscillate as waves pass over and cause wave heights to attenuate significantly. At the same time, given a high enough fluid stress at the mud-water interface, particulate entrainment can occur, thus increasing water column turbidity.

The wave-mud interaction problem, involving the prediction of surface wave attenuation, bottom mud motion, and interfacial entrainment or erosion, is simply treated here as one concerned primarily with vertical exchanges of momentum and sediment mass. A dichotomy inherent in such a treatment arises from the need to assume mud to be a continuum when simulating wave attenuation and mud motion, while considering the vertical transport of sediment in the water column to be a two-phased problem amenable to classical approaches in sediment transport.

At the center of the continuum approach is the requirement to describe the constitutive relations characterizing mud rheology. Depending on the properties of the constituent sediment and the ambient fluid, mud in general can range from being a highly rigid and weakly viscous material to one that can be approximated as a purely viscous fluid. In that context, fluid mud is better defined as fluidlike mud, since it is not always wholly devoid of rigidity.

As wave action proceeds, the viscoelastic (or poroelastic) properties of mud tend to change with time over scales that can be two to three orders longer than the typical wave period. The resulting feedbacks in terms of the influence of this change on wave propagation are not always easy to quantify. Yet, over the past three to four decades simple hydrodynamic models have been developed to simulate wave attenuation, mud motion, and interfacial erosion in the prototype environment with an acceptable degree of accuracy.

Conventionally, model applications have dealt mainly with investigations of natural phenomena including predictions of coastal wave heights and turbidity generation for understanding beach erosion and flooding, planning of port and harbor facilities including safe navigation channels, and design of offshore structures where bottom stability may be a problem. In recent years

applications have been extended to problems of water quality and benthic biota, since both can be influenced by mud motion and associated constituent fluxes. Most recently, engineering interest has grown in beneficially using dredged fine-grained material from navigation channels to create offshore underwater berms that can absorb wave energy and thus act as buffers against wave attack in areas in the lee of the berms. To that end, applications of wave-mud interaction modeling have been carried out to simulate the degree of wave damping that will occur for a berm of given dimensions and mud rheology. Thus, in turn this type of modeling can be potentially useful in developing guidelines for designing wave energy absorbing berms in future.

## INTRODUCTION

### 1.1 MUD-WAVE DYNAMICS IN ENGINEERING AND SCIENTIFIC APPLICATIONS

Advancements in numerous scientific and engineering applications in the shallow marine environment are contingent upon a better understanding of the physical processes and associated feedback mechanisms that are inherent in the dynamical response of a muddy bottom subjected to wave action. Some relevant areas and their descriptions are briefly noted in Table 1. They highlight the wide ranging scientific and engineering concerns in which mud dynamics plays a key role, including coastal fisheries and agriculture, shore and channel protection, oil and gas exploration, water quality, shallow marine habitats and so on. Despite the diversity and complexity of the physical, physicochemical and biological processes involved in these situations, in most cases the processes and feedbacks related to the physics of mud-wave interaction can be identified in a simplified manner, and is the focus of this report.

### 1.2 PROCESSES AND FEEDBACKS

The response of a mud bed to wave forcing is schematized in Fig. 1. A brief description of the numbered pathways is as follows: 1,2) water waves determine the flow field; 3,4) flow field and bed properties together govern the character and the dynamics of the interface; 5,6) wave loading, consolidation, fluidization and thixotropy

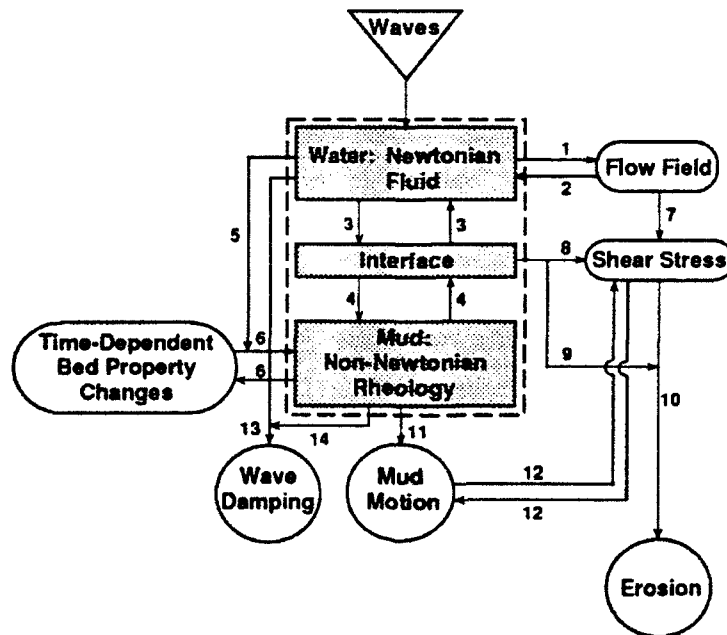


Figure 1. Schematic description of the processes and feedbacks related to the response of mud bed to water waves. Box with dashed line represents the mud-water system, inverted triangle represents forcing, rectangles are components of the mud-water system, ellipses are process transfer functions and circles represent manifested responses (adapted from Maa and Mehta, 1989).

Table 1. Some issues in which application of knowledge of mud-wave dynamics plays an important role

Problem Area	Description
Fisheries	Natural coastal mud banks provide a relatively wave-free environment and where, due to nutrient-rich mud, fish catch is often high, e.g. off Surinam and India (Wells, 1983; Nair, 1988; Mathew, 1992).
Shore protection	Engineered underwater berms in the nearshore region can substantially reduce wave height as waves pass over the berm towards the shore or a navigable channel, e.g. off Mobile Bay, Alabama (McLellan et al., 1990; Dredging Research Technical Notes, 1992).
Agriculture	Coastal mud levees and dikes are designed to reclaim land for agricultural purposes, e.g. in Hangzhou Bay, China (Wang and Xue, 1990).
Oil and gas exploration	Offshore platforms must be designed to withstand failure due to episodic mud slides and mud fluidization, e.g. in the Mississippi Delta area (Sterling and Strohbeck, 1973).
Port navigation	Channel depth based on the "nautical depth" concept, in which underkeel clearance is determined on the basis of mud resistance to ship motion (Migniot and Hamm, 1990). Design of underwater sills to prevent port channel shoaling (Tsuruya et al., 1990).
Eutrophication and other water quality issues	In these problems in lakes, reservoirs and coastal waters, it is desirable to understand/control turbidity generation due to bottom mud resuspension (Somlyódy et al., 1983; Mehta, 1991a). Scavenging of water-borne contaminants by suspended fine-grained sediment and its ultimate deposition in quiescent areas can, in fact, lead to an improvement in water quality. In such a case, wave-induced turbidity can therefore be generated, at least in principle, to accomplish contaminant scavenging, as often occurs naturally in bays and estuaries (e.g. Krone, 1979).
Habitat protection, restoration and enhancement	Design of stable habitats may be accomplished by appropriately shaping the bank to afford greatest protection against wave action, a desirable feature in coastal wetland creation (e.g. Connors et al., 1990; National Research Council, 1994).
Oil spill	Tracking the fate of coastal oil spills requires predictive process models for the entrainment of oil emulsion in mud and release of oil from mud into wave-generated waters (National Research Council, 1989).

erosion; 11,12) shear (and normal) stresses together with mud properties determine mud motion; 13,14) mud change mud properties with time; 7,8) flow field and interfacial character determine the interfacial shear stress; 9,10) interfacial shear stress and interfacial properties determine the rate of particle entrainment, or interfacial properties largely determine the rate of surface wave damping or attenuation.

In this report we will examine the inter-relationship between forcing and responses identified in Fig. 1, and in so doing inherently highlight significant feedbacks represented by some of the numbered pathways. Feedbacks shown tend to be time-dependent, typically varying the behavior of the system gradually in comparison with the

forcing period, as the mud properties change under continued wave action. Thus, predictive approaches for determining wave attenuation, mud motion and erosion are dependent on a knowledge of the constitutive properties of mud, which themselves vary widely depending on the mineralogical composition of mud, and modulation of inorganic properties by biochemical and biophysical influences. Consequently, a few important tests for characterizing mud properties and transport, e.g. erodibility, must accompany any predictive effort. However, notwithstanding site-specificity that is inherent in every problem, an attempt has been made in the report to emphasize those physical principles that are common to most problems.

The degree of importance of a particular response of the mud-water system evidently depends on the problem area and the application sought. Thus, for example, wave attenuation is of primary significance for mitigation of shoreline erosion and coastal flooding. Mud motion determines bottom stability, hence the integrity of structural foundation. It also controls the intake and release of nutrients and contaminants across the mud-water interface. Finally, coastal and estuarine turbidity due to wave action is the result of particulate entrainment at the mud/water interface. In any event, as a first step it is essential to introduce basic definitions related to the physical state of mud in the wave field. This aspect is considered next.

## MUD-WAVE DOMAIN

### 2.1 DEFINITIONS

Three previous definitions of mud are given in Table 2, two ocean science related and the third from coastal engineering. From the present standpoint, the coastal engineering description is perhaps more relevant than the other two because it refers to the state of mud (fluid-to-plastic) as opposed to composition alone. In that context it is noteworthy that wave attenuation and mud motion are both dependent on the constitutive relations characterizing mud rheology, which in turn depends on the physical state of mud. On the other hand, particle entrainment at the interface largely depends on the structure of the particulate aggregate network, which is specified by sediment composition for a given composition of the fluid (ionic species in water, their concentration, and pH). Mud that is predominantly composed of particles smaller than about 20  $\mu\text{m}$  is much more cohesive than one in which the particles are coarser (Mehta and Lee, 1994). Where it is essential to make this distinction, we will refer to the former as cohesive mud.

Table 2. Selected definitions of mud

Source	Field	Definition
Hunt and Groves (1965)	Ocean science	Pelagic or terrigenous detrital material consisting of particles smaller than sand, i.e., an undifferentiated sediment made up of particles mostly within the silt-clay range smaller than 0.0625 mm.
Allen (1972)	Coastal engineering	A fluid-to-plastic mixture of finely divided particles of solid material and water.
Tver (1979)	Ocean science	Pelagic or terrigenous detrital material consisting mostly of silt and clay-sized particles (less than 0.06 mm), but often containing varying amounts of sand and/or organic materials. It is a general term applied to any sticky fine-grained sediment whose exact size classification has not been determined.

The forcing frequency ( $f$ ) of common interest relative to gravity waves ranges widely, from about 10 Hz to  $10^{-5}$  Hz. The former corresponds to the transition whereby surface tension becomes increasingly important as a restoring force with increasing frequency, while the latter is representative of the frequency of the astronomical tide. It should be added, however, that frequencies that are lower than tidal, especially those corresponding to sub-tidal oscillations having periods on the order of days, can also be important in some situations, for example with regard to long term erosion or accretion of fine-grained sediments in wind-forced bays.

Given water depth,  $h$ , and particle settling velocity,  $w_s$ , two characteristic, frequency dependent numbers that together characterize the primary nature of wave forcing and bottom response are  $h\omega^2/g$  and  $h\omega/w_s$ , where  $\omega = 2\pi f$

and  $g$  is the acceleration due to gravity. When the first number is less than 0.3, fluid pressure is practically hydrostatic, and the celerity of the shallow water wave,  $\zeta=(gh)^{1/2}$ . As  $h\omega^2/g$  exceeds 0.3, dynamic pressure effects become increasingly important with increasing water depth, or frequency. The second number scales the water depth in relation to the settling velocity for a given frequency. For fine-grained sediment, selecting  $w_s=10^{-4}$  m/s,  $h=10$  m and  $\omega=1$  rad/s as characteristic values yields  $h\omega/w_s=10^5$ , which is up to two orders of magnitude greater than the corresponding value for a sandy bed, for example. A manifestation of this difference is related to the vertical structure of density, which assumes considerable importance when the sediment is fine-grained. Sediment-induced stratification characteristically occurs in this case irrespective of the value of  $h\omega^2/g$ , as long as the wave is not in deep water ( $h\omega/\zeta > \pi$ ), since in the latter case wave-bottom mud interaction ceases.

Other parametric approaches have also been proposed for characterizing the wave-mud environment in contrast to wave-sand environment. For example, McCave (1971) has defined a "wave effectiveness parameter" as the product of the theoretical instantaneous sediment transport rate times wave frequency. In the southern North Sea area examined, relatively low values of this parameter correlated with the occurrence of mud.

## 2.2 FLUID MUD

A simple description of the mud-wave system is given in Fig. 2, in which  $u_m$  is the amplitude of the horizontal wave orbital velocity. The (bulk) density of the water-mud mixture,  $\rho$ , varies from  $\rho_u$  at the surface to  $\rho_b$  at the bottom. The quantity  $\rho_w$  is water density. A sharp density gradient, or lutocline (Parker and Kirby, 1982), separates the upper column suspension from fluidized, compliant mud below. At the bottom of the mobile suspension the density rises from  $\rho_u$  to  $\rho_t$ , which is the range over which fluid mud is considered to occur. The bed below fluid mud can undergo deformation. This deformation in fact may eventually break the inter-particle or inter-aggregate bonds, and thus change the bed, possessing a structured matrix, to fluid mud. Below the level at which the depth of penetration of the wave orbit practically ends the bed remains uninfluenced by wave motion.

Fluid mud characterizing densities,  $\rho_u$  and  $\rho_t$ , are operationally defined as follows. The flux of sediment settling within the mobile suspension,  $F_s = w_s \rho_s \phi$ , where  $\phi = (\rho - \rho_w) / (\rho_s - \rho_w)$  is the solids volume fraction ( $= 1 - n$ , where  $n$  is the porosity) and  $\rho_s =$  granular density of the sediment. In Fig. 3a, data from a laboratory settling column using sediment from the Severn Estuary in the United Kingdom have been used to plot  $F_s$  against the excess density,  $\Delta\rho = \rho - \rho_w$  (adapted from Odd and Rodger, 1986). The peak value of  $F_s = F_{sm} = 40$  g/m<sup>2</sup>·s corresponds to the onset of hindered settling, under which  $F_s$  decreases with increasing  $\Delta\rho$  (Mehta, 1990). Hindered settling begins at  $\Delta\rho_m = \rho_m - \rho_w = 9$  kg/m<sup>3</sup>, where  $\rho_m$  is the value of  $\rho$  when  $F_s = F_{sm}$ . We further note that at the peak flux,  $\partial F_s / \partial \Delta\rho = 0$ . Furthermore, given  $z$  as the vertical coordinate,  $\partial F_s / \partial \Delta\rho = (\partial F_s / \partial z) / (\partial \Delta\rho / \partial z)$ . Thus, since at the lutocline  $\partial \Delta\rho / \partial z$  tends to infinity the condition,  $\partial F_s / \partial \Delta\rho = 0$ , is satisfied there (horizontal line in Fig. 2), irrespective of the value of  $\partial F_s / \partial z$ . Thus, in reality  $\Delta\rho_m$  practically coincides with  $\Delta\rho_u = \rho_u - \rho_w$ . In Fig. 3b the correspondence between the lutocline elevation,  $z_u$ , and  $\Delta\rho_u$  is shown for a measured density profile from the Severn. Note that the sediment remains suspended in this estuary largely as a result of tidal flow, as opposed to wave action. Where waves predominate, the essential description should remain unchanged, however.

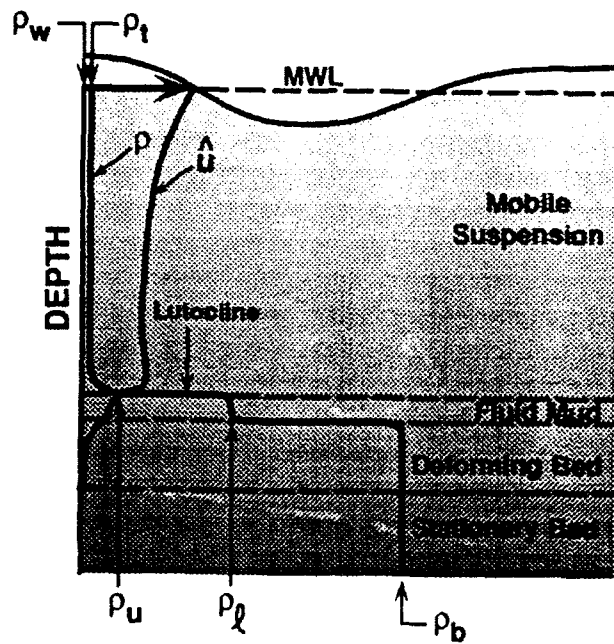


Figure 2. Schematic diagram showing the vertical variation of the density of mud-water mixture in the wave environment. MWL = mean water level.

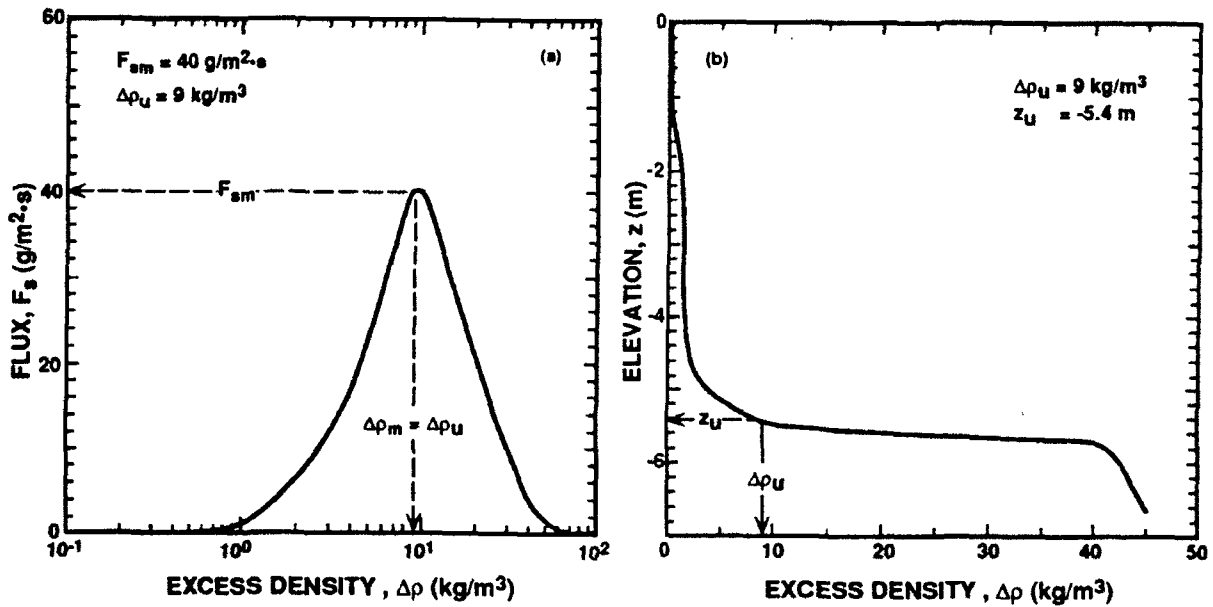


Fig. 3. a) Settling flux variation with excess density for sediment from the Severn Estuary, United Kingdom. Laboratory column data reported by Odd and Rodger (1986); b) An instantaneous excess density profile showing a marked lutocline in the Severn Estuary, United Kingdom (data reported by Odd and Rodger, 1986).

Lutoclines have been found to persist even under fairly drastic wave-induced agitation, as a result of the significant negative buoyancy of bottom mud. However, under highly eroding conditions,  $\rho_u$  may decrease measurably below  $\rho_m$  (Ross and Mehta, 1989) and, in fact, the equality between  $\rho_m$  and  $\rho_u$  is valid only for conditions under which the sediment settles without resuspension or upward diffusion. It holds reasonably well for weakly eroding conditions, however.

Fluid mud is better described as "fluid-like" mud, in which the particles are largely (but not always solely) fluid-supported (Smith and Kirby, 1989). Thus, in general, it is a "quasi-suspension". Since the bed below it is essentially particle-supported the density,  $\rho_t$ , is the value of  $\rho$  below which inter-granular contact is marginal. Since if left at rest fluid mud will dewater to form a bed, its existence in the present case is dependent on wave agitation, which prevents a reduction in the pore pressure, and thereby, in turn, prevents the constituent particles from developing permanent electro-chemical bonds. In many shallow, wave-dominated environments, continued wave action causes the top layer of mud to remain fluidized. For instance, in Lake Okeechobee, Florida wind waves persistently sustain the top 5-20 cm thick, organic-rich mud in the fluidized state (Kirby et al., 1989; Hwang, 1989).

Since the fluid mud/bed boundary is typically very dynamic, and pore pressures difficult to measure in the field, practical definitions have been used to determine  $\rho_t$ . One such definition is based on the approximate empirical relationship between the vane shear strength of the soil,  $\tau_v$ , and  $\rho$  or, equivalently the solids volume fraction,  $\phi$ :  $\tau_v = \alpha_0(\phi - \phi_t)^{\beta_0}$ , where  $\phi_t$  is solids volume fraction corresponding to  $\rho_t$ , and  $\alpha_0$  and  $\beta_0$  are sediment-specific coefficients that must be determined experimentally. Thus, when  $\phi = \phi_t$ ,  $\tau_v = 0$ , and shearometric evidence has been used to characterize  $\phi_t$  as the critical, space-filling solids volume fraction (James et al., 1988). For the mud from Lake Okeechobee, Hwang (1989) obtained (given  $\tau_v$  in Pa)  $\alpha_0 = 22.6$ ,  $\beta_0 = 1$  and  $\phi_t = 0.06$ ; the latter corresponding to  $\rho_t = 1,065 \text{ kg/m}^3$ . Other definitions of a similar nature, but ones in which  $\tau_v$  is substituted by the upper Bingham yield stress,  $\tau_y$ , which is obtained for the typically pseudoplastic stress-rate of strain curve for mud at low rates of strain, have also been used widely. See Mehta (1991b) for a brief review of these definitions. In recent years a revised interpretation of  $\tau_y$  as the critical stress at which plastic yield occurs in a creep test has been proposed (James et al., 1988; Jiang, 1993). This test, which must be conducted in a controlled-stress rheometer, provides a direct measure of  $\tau_y$ , thus obviating approximations inherent in the estimation of  $\tau_v$ .

The most commonly considered values of  $\rho_u$  and  $\rho_t$  are 1,030 and 1,300  $\text{kg/m}^3$ , respectively, although other ranges have been reported, as noted in Table 3 (amended from Ross et al., 1987). The main reason for the observed variations in  $\rho_u$  and  $\rho_t$  is that they were determined under different hydrodynamic conditions and for different muds.

Cohesive muds having concentrations  $\phi > \phi_t$  tend to exhibit a measurable viscoelastic response to wave forcing of stresses below the critical stress for plastic yield. The viscosity,  $\mu$ , and shear modulus of elasticity, or the rigidity modulus,  $G$ , of typical surficial muds found in the shallow marine environment range from  $O(10^1)$  to  $O(10^4)$  Pa.s and Pa, respectively. These ranges indicate that such muds tend to be highly viscous but only weakly to moderately elastic.

By way of an elaborate but also theoretically more accurate definition than stated above, Foda et al. (1993) consider the bed to be an elastic medium, and "fluid" mud to incorporate a transitional viscoelastic layer between

Table 3. Fluid mud density and corresponding solids volume fraction ranges

Investigator(s)	$\rho_u^a$ (kg/m <sup>3</sup> )	$\phi_u^a$	$\rho_r^a$ (kg/m <sup>3</sup> )	$\phi_r^a$
Inglis and Allen (1957)	1,030	0.018	1,300	0.182
Krone (1962) <sup>b</sup>	1,010	0.0061	1,110	0.067
Wells (1983)	1,030	0.018	1,300	0.182
Nichols (1985)	1,003	0.0018	1,200	0.121
Kendrick and Derbyshire (1985)	1,120	0.073	1,250	0.152
Hwang (1989)	1,002	0.047	1,065	0.060

<sup>a</sup>Conversion between density and solids volume fraction by using sediment granular density,  $\rho_s = 2,650$  kg/m<sup>3</sup>, and water density = 1,000 kg/m<sup>3</sup>, except for Hwang (1989), in which case  $\rho_s = 2,140$  kg/m<sup>3</sup>.

<sup>b</sup>Exclusively based on laboratory data. The other definitions rely on field evidence, although they are not necessarily based solely on field data.

the bed and a viscous layer above. Returning however to the more simple definition, as shown in Fig. 4, typical shearometric data suggest  $\phi_r$  to be in the range of 0.05 to 0.1, below which  $G$  is comparatively small (James et al., 1988).  $\phi_r$  values in Table 3 on the other hand are generally higher, with the exception of Krone's (0.067) and Hwang's (0.060), both of which are based on laboratory data. The other four are field-based, and technically somewhat arbitrary. At the same time however, any definition of  $\phi_r$  based on  $G$  (Fig. 4) would also be somewhat arbitrary, unless it is contingent upon a quantitative criterion concerning the magnitude of  $G$  for defining  $\phi_r$ .

Since the dissipative role of mud is largely confined to the top compliant layer (Foda, 1989), predictive hydrodynamic models that assume cohesive mud to be a purely viscous fluid seem to yield simulations of surface wave attenuation of acceptable accuracy for field application (Jiang and Mehta, 1992). In other simulations an elastic

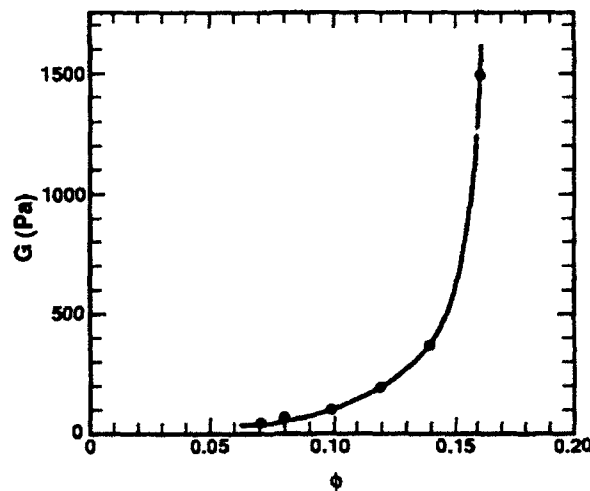


Figure 4. Shear rigidity modulus versus solids volume fraction for sediment S1 (after James et al., 1988).

component has been added (Jiang, 1993). Less dissipative and more elastic silty, "fluid-like" muds have been considered to be poroelastic (Yamamoto, 1983). In any event, it is essential to estimate the thickness of the fluid (or fluid-like) mud layer as a precursor to hydrodynamic modeling. The simplest way to identify layer thickness is in terms of densities  $\rho_b$  and  $\rho_t$ . However, this very approximate approach does not explicitly account for the dynamic nature of the fluid mud boundaries, dependent as they are on the nature of wave forcing. Processes contributing to the generation of fluid mud from bed, and the scour of the fluid mud-water interface leading to its entrainment are briefly considered next.

## GENERATION AND EROSION OF FLUID MUD

### 3.1 FLUIDIZATION

Under progressive waves that are not in deep water, gradients in pore pressure can cause the pore fluid to flow relative to the soil skeleton, which may eventually lead to rupturing of the inter-particle cohesive bonds, hence a loss of effective stress. Starting with a bed at rest, the increase in (wave-averaged) pore pressure,  $u_w$ , with time at a fixed position is shown schematically in Fig. 5, in which  $\sigma_h$  = hydrostatic pressure and  $\Delta u$  = wave-averaged excess pore pressure. This wave-averaged effective (normal) stress,  $\sigma'$ , decreases with a buildup of excess pore pressure until soil liquefaction occurs when the total stress,  $\sigma = u_w = \Delta u + \sigma_h$ , and  $\sigma' = 0$  (see, e.g. Lamb and Whitman, 1969). The wave-averaged portrayal of pore water variation is an evident approximation of a phenomenon that actually occurs within a two-phased medium, in which properties of the sedimentary matrix vary spatially at the micro-fabric scale, even when the medium is of uniform bulk density and composition. In fact, careful measurements of pore pressure oscillations under wave-forcing in silty soils suggest that transitional, resonant amplification of the pressure amplitude accompanies an episodic increase in the wave-mean pore pressure at preferential sites (cavities) within the soil mass (Foda et al., 1991). A somewhat similar occurrence is reported in a clayey soil (Feng, 1992). An important implication of this observation is that at the micro-fabric scale, soil liquefaction is initiated in a spatially and temporally inhomogeneous manner.

An instantaneous view of the stress profiles in the mud-water system is shown schematically in Fig. 6. When the initial bed matrix is disturbed by wave motion, the general manner in which fluidization, when considered synonymous with liquefaction, occurs depends on several factors, an important one being the thickness and the degree of consolidation of the mud layer. When the thickness is small and the mud is unconsolidated or partially consolidated, mud displacement tends to be greater near the rigid bottom below compliant mud, than near the surface. In this case fluidization can conceivably proceed from the rigid bottom up. In a comparatively deep mud layer, or a consolidated thinner layer, the displacement is greatest at the top and decreases with depth; hence in this

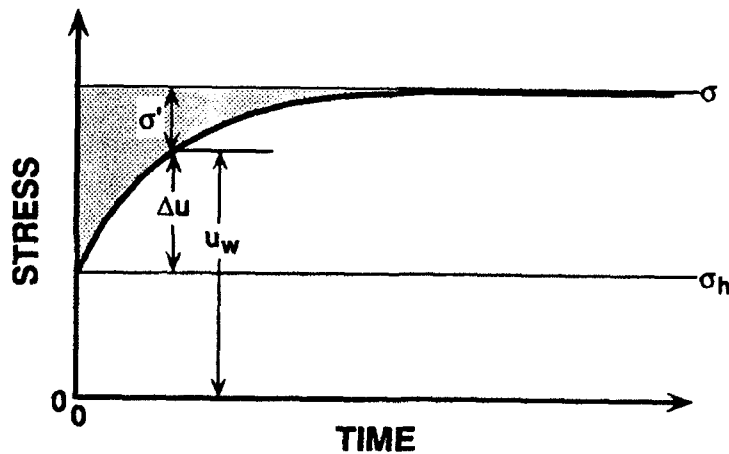


Figure 5. Schematic of time-variation of pore pressure under wave action.

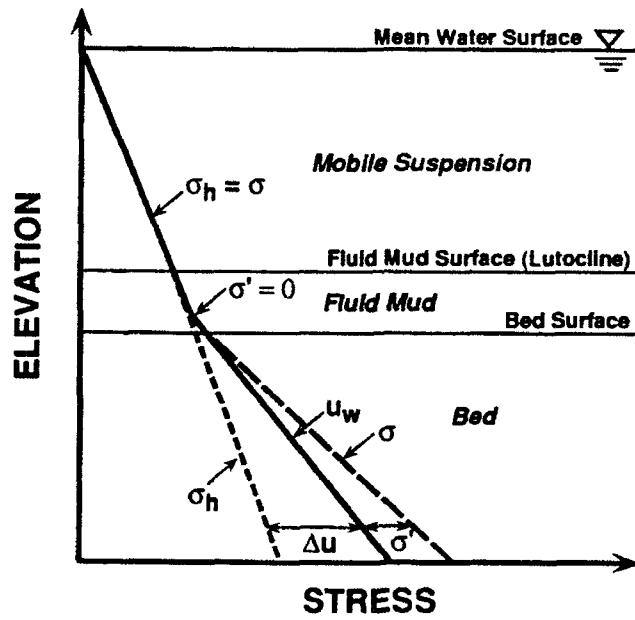


Figure 6. Schematic of instantaneous stress profiles in a water-mud system.

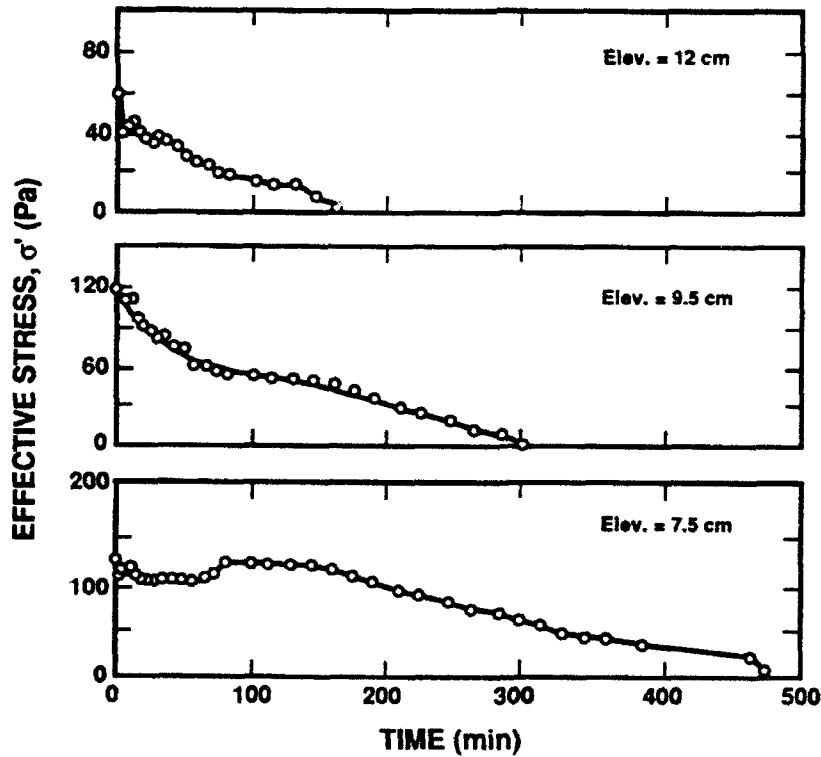


Figure 7. Time-variation of effective stress at three elevations (above flume bottom) in a clay bed (kaolinite + attapulgite) subjected to 1 Hz progressive waves of 4 cm amplitude (after Feng, 1992).

case fluidization tends to proceed from the top (Chou, 1989). Formally then it appears that the manner in which fluidization occurs characteristically depends on the relative water depth,  $kh_1$ , and the wave Reynolds number in mud,  $\omega h_2^2/\nu_2$ , where  $k$  = wave number,  $\omega$  = wave frequency,  $h_1$  = water depth,  $h_2$  = mud depth and  $\nu_2$  = kinematic viscosity of mud. For small values of  $kh_1$  and  $\omega h_2^2/\nu_2$  bottom-up fluidization should be favored. For relatively large values of these parameters, the reverse process should be facilitated, provided there is sufficient wave energy input to initiate and sustain fluidization. Imposing a non-uniform bed density gradient, with density increasing with depth, should further enhance the likelihood of fluidization occurring from top, since in this case the dynamic pressure gradient tends to decrease rather markedly with depth (Maa and Mehta, 1987).

When fluidization proceeds downward from the mud/water interface an equilibrium thickness of the fluid mud layer is attained. In Fig. 7 the fall in the wave-averaged effective stress with time at three selected elevations where time-series of total and pore pressures were measured below the interface is shown from a preliminary test (No. 10; see Feng, 1992) in a wave flume. The 16 cm thick bed was composed of an aqueous mixture of a kaolinite and an attapulgite in equal proportions by weight, having a mean density of 1,170 kg/m<sup>3</sup>. The water depth was 19 cm, and the 1 Hz forcing wave had an amplitude of 4 cm. The bed was allowed to consolidate for 85 hours before test initiation. Notice the increasing time required for fluidization with depth below the interface.

The thickness of the fluid mud layer,  $d_f(t)$ , in general can be expressed as

$$d_f = d_{fe} \cdot f(t) \quad (1)$$

where  $d_{fe}$  is the equilibrium value of  $d_f$ , such that the function  $f(t) \rightarrow 1$ , as  $t \rightarrow \infty$ . Data such as those shown in Fig. 7 were used to determine the increase in  $d_f$  with time in Fig. 8 from three tests (Nos. 8, 9 and 10) summarized in Table 4. The comparatively short durations of these tests were insufficient for the attainment of equilibrium depths,  $d_{fe}$ . In any event, selecting the following empirical equation for fitting the data points,

$$d_f = M_1 \left[ 1 - e^{-\alpha_f t^{1/2}} \right]^{2.5} \quad (2)$$

Table 4. Fluidization depth related parameters

Test No.	Wave Amplitude (cm)	Consolidation Period (hr)	$M_1$ (cm)
8	2.0	240	18
9	2.8	65	50
10	4.0	85	35

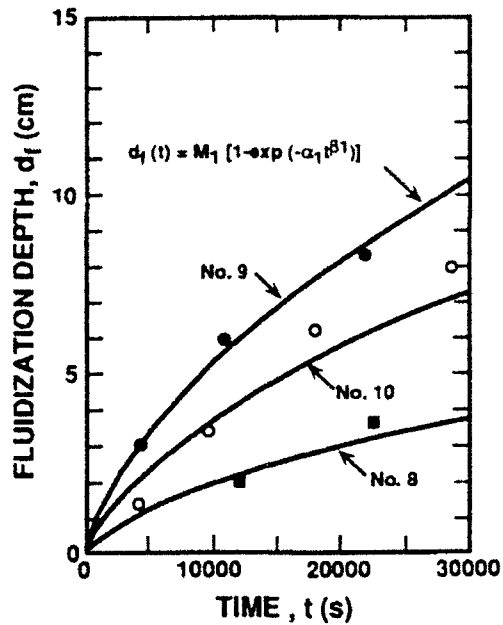


Figure 8. Time-variation of the depth of fluidization in three tests with different wave amplitudes and consolidation periods. Data points from Feng (1992).

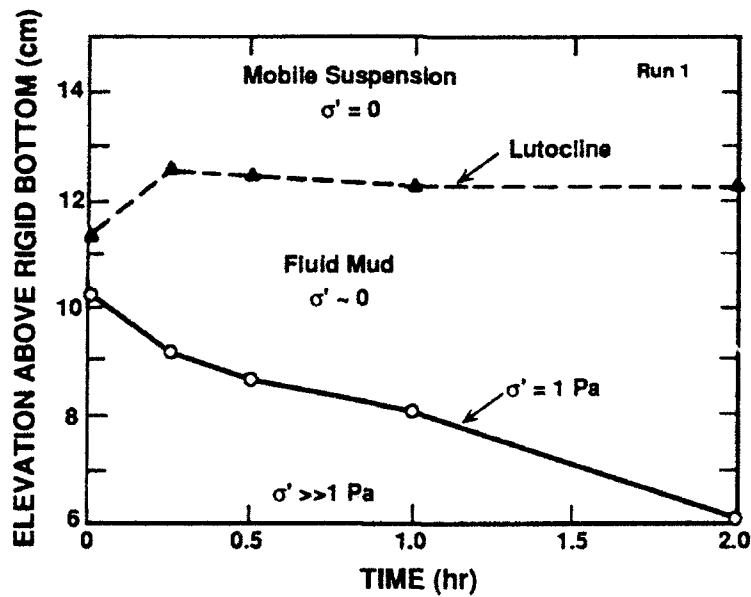


Figure 9. Development of a fluid mud layer starting with a "bed" of Hillsboro Bay mud (Run 1; see Ross and Mehta, 1990).  $d_f$  is the vertical distance between the lutocline and the  $\sigma' = 1$  Pa level. Note the occurrence of an initial, 1.1 cm thick layer of fluid mud over the bed, as a result of a local disturbance of the bed prior to test initiation. The observed initial increase in the lutocline elevation is attributed to advection of fluid mud to the measurement site.

we note that the curves drawn are obtained by retaining constant values of the coefficients  $\alpha_1 (=0.0216)$  and  $\beta_1 (=0.346)$  for the time-dependent function  $\{f(t)\}$  within the brackets, while varying  $M_1$  (Table 4). Thus the influences of wave amplitude and bed consolidation period are contained wholly in  $M_1$ . Since both the amplitude and the consolidation period were varied in each test their individual effects cannot be gleaned; however we note that the trend of increasing rate of fluidization corresponds with decreasing bed consolidation. Thus the initial state of the bed seems to have had a dominant influence on the rate of fluidization in these particular tests. Note that according to the form of Eq. 2,  $M_1 = d_{fc}$ ; yet, because  $d_{fc}$  was not actually attained,  $M_1$  should preferably not be set equal to  $d_{fc}$ , and the applicability of Eq. 2 should be restricted to the experimental durations only.

A difficulty with tracking wave-induced fluidization by means other than pore pressures, such as by measuring accompanying changes in bed density, is that conventional methods for measuring density, e.g. by collecting mud samples for subsequent gravimetric analysis, are often too coarse for the degree of resolution required to detect the necessary changes. In fact, there may be no "significant" change, as in the case of the fluidization test shown in Fig. 9, in which the time-variation of  $d_t$  is shown for a bed composed of a predominantly montmorillonitic estuarine mud (from Hillsboro Bay, Florida). The water depth was 31 cm and the nominal mud thickness 12 cm. The bed, which was prepared 168 hr before test initiation, was forced by a 1 Hz wave of 3 cm amplitude. The boundary between the fluid mud layer and the cohesive bed is defined by the locus of the elevation corresponding to  $\sigma' = 1$  Pa, a very small value. During the first hour, vertical profiles of mud density were measured (by gravimetric analysis of samples withdrawn from the side of the experimental flume via tubes), as shown in Fig. 10. Arrows 1 through 4 mark the positions of the  $\sigma' = 1$  Pa boundary in Fig. 9. Note that between levels 1 and 4 no measurable change in density occurred (Ross and Mehta, 1990).

Sensitive measures of "soil softening" by waves include such lumped parameters as the undrained shear strength and the shear modulus or rigidity modulus,  $G$ , of the bed (Thiers and Seed, 1968; Schuckman and Yamamoto, 1982). Within the bed of kaolinite and attapulgite mentioned earlier, and having a pre-test consolidation period of 20 hr, a specially designed, miniature shearometer was installed to record the change in  $G$  with time under continued wave action (Williams and Williams, 1992). The device measured the speed of propagation,  $V$ , of a 1.8 kHz shear wave generated and detected by transducers incorporating piezo-ceramic "bimorph" elements bonded to miniature steel plates which served as the generating/detecting surfaces (length 12 mm; width 4 mm; thickness 100  $\mu\text{m}$ ). At this high shear wave frequency,  $V$  was practically instantaneous in terms of its variation over the experimental time scale. Given the initial speed  $V(0)$ , the corresponding ratio,  $V(t)/V(0)$ , is plotted against time in Fig. 11. Notice the "exponential" fall in the speed, which is commensurate with a corresponding increase in  $d_t$  such as that observed in Fig. 8. The best fit equation is

$$\frac{V(t)}{V(0)} = e^{-\alpha_2 t^{\beta_2}} \quad (3)$$

where  $\alpha_2 = 0.0216$  and  $\beta_2 = 0.346$ . Recognizing that the forms of the time-dependent terms in Eqs. 2 and 3 are analogous, and that, perhaps fortuitously,  $\alpha_1 = \alpha_2$  and  $\beta_1 = \beta_2$ , eliminating time between the two equations leads to

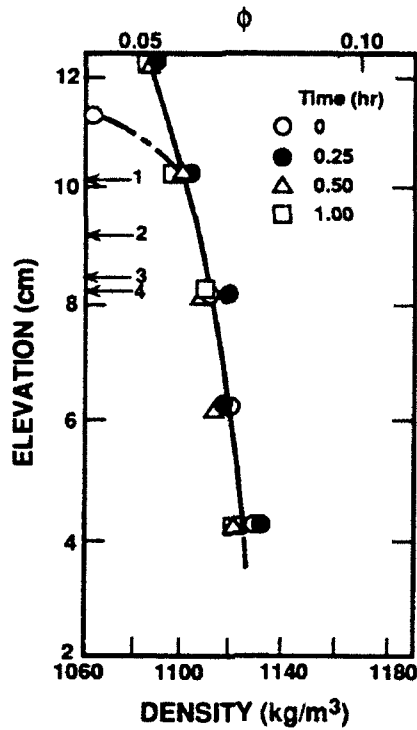


Figure 10. Mud density profiles from Run 1 (Fig. 9). Arrows indicate bed level ( $\sigma' = 1$  Pa) at different times at test initiation (level 1), and following test initiation (after Ross and Mehta, 1990).

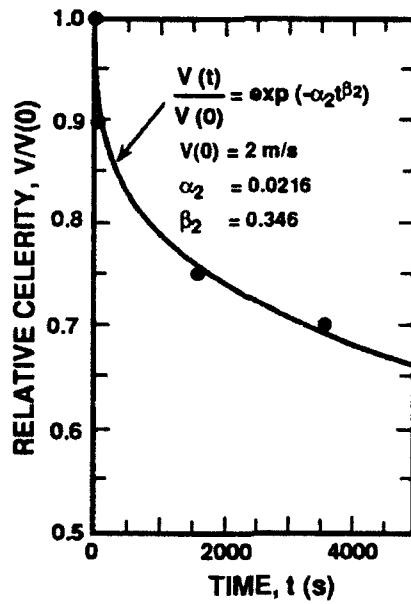


Figure 11. Time-variation of relative shear wave velocity in a bed of attapulgite + kaolinite of 20 hr consolidation subjected to a 1 Hz progressive water wave of 2 cm forcing amplitude (after Williams and Williams, 1992).

$$d_r = M_1 \left[ 1 - \frac{V(t)}{V(0)} \right]^{2.5} \quad (4)$$

which indicates a seemingly unique dependence of  $d_r$  on  $V$  for a given bed. For a given shear wave forcing frequency,  $G$  depends on  $V$  as well as on the phase angle between the shear stress amplitude and the resulting amplitude of strain (Williams and Williams, 1992). Thus the coefficient  $M_1$  essentially contains the influence of the phase angle in an unquantifiable way. Nevertheless, Eq. 4 demonstrates the dependence of  $d_r$  on a soil dynamical parameter that intrinsically reflects the physical state of mud.

### 3.2 ESTIMATION OF FLUIDIZATION THICKNESS

Research on the estimation of the fluidization thickness apparently has largely focussed on the equilibrium value,  $d_{fc}$ , as opposed to  $d_f(t)$ . Thus, for example, the linkage between mud rheology and  $d_{fc}$  was explored by Chou (1989), by considering bottom mud to be generally viscoelastic. Onset of fluidization was defined in terms of critical values of shear strain related to elastic and viscous responses of the bed. This criterion is mathematically different from that for liquefaction (i.e.  $\sigma' = 0$ ). Yet, the two characterize the same phenomenon. As noted in Section 4.4.3, the constitutive equation for a viscoelastic material is,  $T_{ij} = G^* E_{ij}$ , where  $T_{ij}$  = deviatoric component of stress,  $E_{ij}$  = deviatoric component of strain, subscripts  $i, j$  denote directions and  $G^*$  is the complex shear modulus. By definition,  $G^* = G' - iG''$ , where  $G'$  = storage modulus (associated with the elastic component) and  $G''$  = loss modulus (associated with the viscous component). For a Voigt material,  $G' = G$  and  $G'' = \mu\omega$ , where  $\mu$  = viscosity,  $G$  = shear modulus of elasticity and  $\omega$  = forcing frequency (Barnes et al., 1989).

The behaviors of  $G'$  and  $G''$  as functions of the amplitude of applied oscillatory strain,  $\gamma^o$ , were examined by Chou (1989) in a controlled-strain rheometer. Figure 12 shows the results for a kaolin. Note the importance of elasticity at low strains when viscous loss was practically nil. With increasing strain the clay behaved increasingly as a viscous material. Results such as these were used to develop the nomograms of Figs. 13a,b for  $G'$  and  $G''$  as functions of strain amplitude,  $\gamma^o$  and relative mud density ( $\rho/\rho_w$ ). The forcing frequency was held constant at 1.5 rad/s. However, in experimenting with changing the forcing frequency it was found that the influence of  $\gamma^o$  was much more pronounced than that of  $\omega$  in controlling  $G'$  and  $G''$ . Depending on the value of  $\gamma^o$ , the domain is seen to be subdivided into three regimes - viscous, viscoelastic and elastic;  $\gamma_v$  and  $\gamma_e$  are values of the strain,  $\gamma$ , that define the appropriate boundaries.

The  $G'$ ,  $G''$  nomograms enable an empirical determination of the thicknesses of the viscous and viscoelastic layers in an otherwise elastic bed. Chou (1989) considered the water-mud system shown schematically in Fig. 14, and calculated the equilibrium thicknesses of the fluid-like viscous layer and the soft viscoelastic layer as functions of the wave height  $H = 2a$ , where  $a$  is the forcing wave amplitude. The procedure involved the use of a wave-mud interaction model in conjunction with the  $G'$ ,  $G''$  nomograms. For a Voigt viscoelastic mud the model becomes analogous to that of Maa (1986). The model was used iteratively to calculate strain amplitudes at different depths

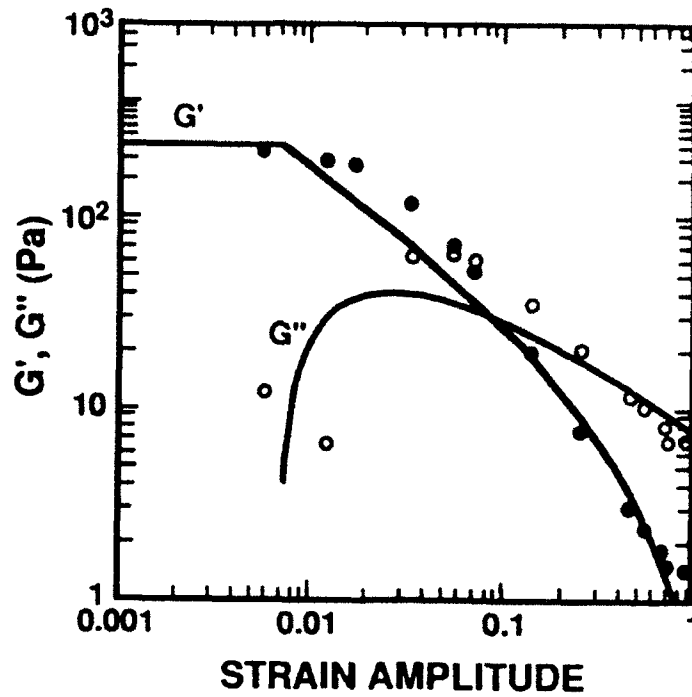


Figure 12. Storage modulus,  $G'$  (•), and loss modulus  $G''$  (○), versus strain amplitude,  $\gamma^0$ , for K2 kaolin at a salinity of 35 ppt and a solids concentration of 41%.  $\omega = 1.5$  rad/s. Lines are drawn to enhance data trends (after Chou, 1989).

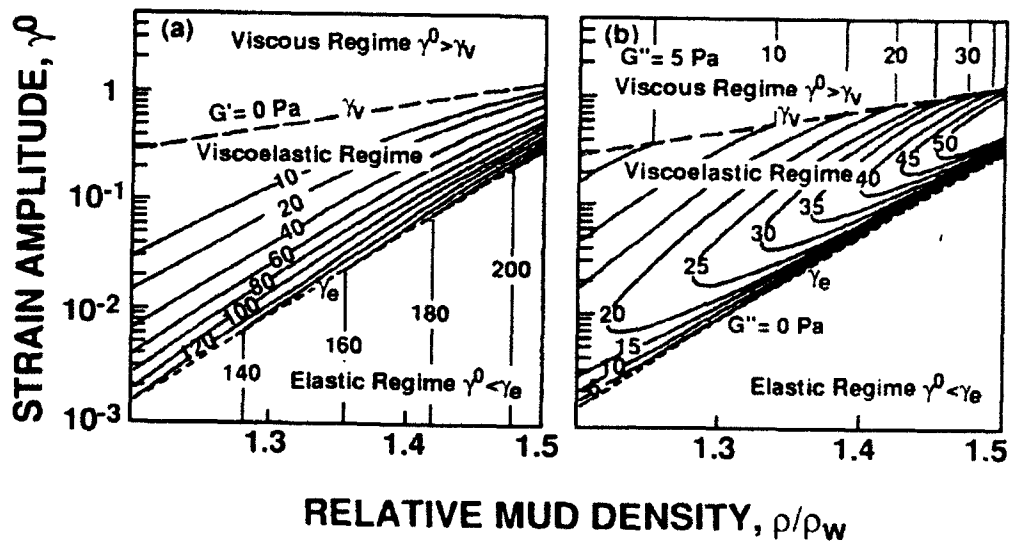


Figure 13. Contours of storage modulus,  $G'$  in (a) and loss modulus,  $G''$ , in (b) for K1 kaolin at a salinity of 35 ppt (after Chou, 1989).

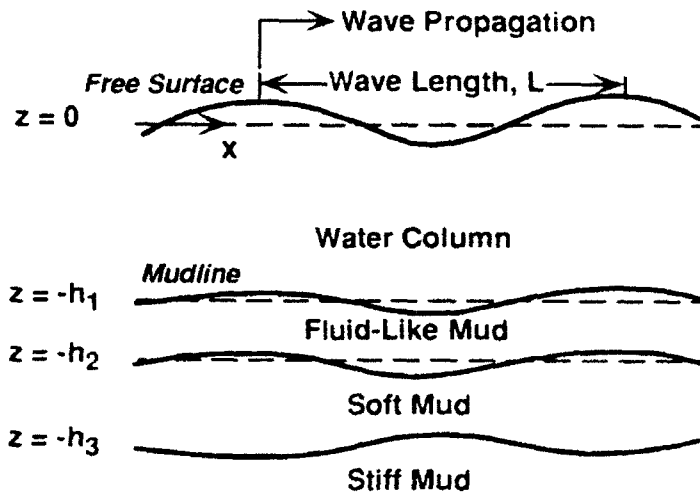


Figure 14. A four-layer viscoelastic model (adapted from Chou, 1989).

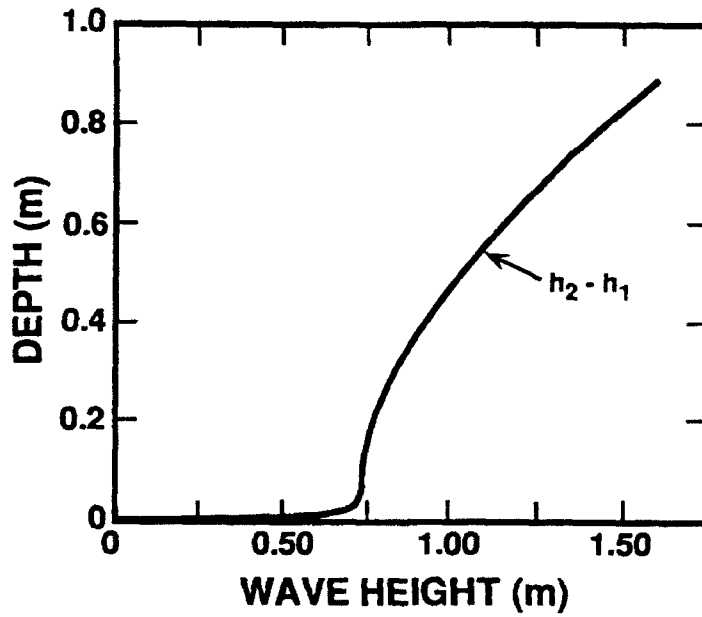


Figure 15. Thickness of fluid mud (for a clayey sediment) as a function of wave height,  $H$ , assuming a water depth of 5 m, a wave frequency of 0.1 Hz (adapted from Chou, 1989).

as functions of the wave amplitude, and hence the depths  $h_1$  and  $h_2$ . An example of the fluidized or fluid-like layer thickness,  $h_2-h_1$ , as a function of wave height is shown in Fig. 15.

### 3.3 SURFACE EROSION

Since the action of waves over a cohesive bed leads to a fairly rapid development of the fluidized mud layer, and since fluidization can be considered to be a mode of entrainment, it is sometimes reasonable to consider the interface between fluid mud and the bed to be the appropriate bed "surface". This assumption however becomes increasingly tenuous with increasing thickness of the fluid mud layer. Accurate models for sediment transport must therefore consider bed fluidization as a process that is distinct from mud surface erosion. Nevertheless, in a large number of practical applications the use of stress-based equations for the rate of bottom erosion, akin to those obtained for uni-directional flow situations, seems to yield acceptable answers with regard to the entrainment of particles into the water column.

Expressions for the rate of erosion have been derived almost exclusively from laboratory studies. Exceptions include "back calculated" rates using field data and numerical models for suspended sediment transport (e.g. Sheng et al., 1986). Some laboratory erosion rate expressions are listed in Table 5. The expression of Alishahi and Krone (1964) is based on data on the time-variation of the depth-mean suspension concentration during erosion reported by the investigators. Experimental data, in general, typically conform to the relationship

$$\dot{e} = M_2 \left[ \frac{\tau_b}{\tau_R} - 1 \right]^{\alpha_3} \quad (5)$$

where  $\dot{e}$  = rate of erosion,  $\tau_b$  = peak value of the cyclic bed shear stress,  $M_2$  = erosion rate constant,  $\tau_R$  = erosion resistance and  $\alpha_3$  = empirical constant. Values of  $\alpha_3$  in Table 5 range from 0.95 to 1.82. When  $\alpha_3=1$ , Eq. 5 becomes analogous to the corresponding expression for cohesive bed erosion under steady or quasi-steady flows (see e.g. Mehta, 1988):

$$\dot{e} = M_3 \left[ \frac{\tau_b}{\tau_s} - 1 \right] \quad (6)$$

where  $M_3$  is the rate constant and  $\tau_s$  is defined as the erosion shear strength. In the laboratory setting,  $\tau_s$  can be determined as a function of depth below the bed surface via a procedure involving layer-by-layer erosion of the bed (Parchure and Mehta, 1985). Maa (1986) used a similar procedure to determine  $\tau_R$ , and thus, in a sense, established a correspondence between  $\tau_s$  and  $\tau_R$ . Furthermore, the range of 0.15 to 0.39 Pa reported for  $\tau_R$  in Table 5 is generally of the same order of magnitude as that for  $\tau_s$  (see e.g. Mehta, 1988). However, it must also be recognized that the time-change in the properties of the bottom mud due to wave action tends to influence  $\tau_R$  in a significant way (Maa, 1986). Thus the value of  $\tau_R$  used in solving Eq. 5 must be inherently a characteristic time-mean value, unless the variation of  $\tau_R$  with time is explicitly included. However, given the usual paucity of data on  $\tau_R$  and

Table 5. Laboratory based, wave-induced mud erosion rates

Investigator(s)	Mode of Wave Generation	Sediment Type	Parameter Ranges <sup>a</sup> a (cm); $\omega$ (rad/s)	Parameter Values in Erosion Rate Expression <sup>b</sup> $\dot{e} = M_2 \left[ \frac{\tau_b}{\tau_R} - 1 \right]^{\alpha_3}$
Alishahi and Krone (1964)	Wind	Bay mud	$0.9 \leq a \leq 3.4$ $11.6 \leq \omega \leq 17.5$	Test 1: $M_2 = 0.00048$ ; $\tau_R = 0.29$ ; $\alpha_3 = 1.72$ Test 2: $M_2 = 0.0112$ ; $\tau_R = 0.39$ ; $\alpha_3 = 1.15$
Thimakorn (1980, 1984)	Mechanical	River-mouth mud	$(0.16 < ak < 1.60)$ $3.1 \leq \omega \leq 12.6$	$M_2 = \bar{U} \delta_b \tau_b / 2 \tau_R$ ; $\tau_R = \text{variable}$ ; $\alpha_3 = 1.00$
Maa and Mehta (1987)	Mechanical	Commercial clay, Bay mud	$1.4 \leq a \leq 3.7$ $3.3 \leq \omega \leq 6.3$	Commercial clay: $M_2 = 0.131$ ; $\tau_R = f(z)$ ; $\alpha_3 = 1.15$ Bay mud: $M_2 = 0.030$ ; $\tau_R = f(z)$ ; $\alpha_3 = 0.95$
Mimura (1993)	Mechanical	Commercial clay	$0.6 \leq a \leq 6.9$ $4.8 \leq \omega \leq 8.2$	$M_2 = 0.00027$ ; $\tau_R = 0.15$ ; $\alpha_3 = 1.82$

<sup>a</sup>a = wave amplitude;  $\omega$  = wave frequency; k = wave number.

<sup>b</sup> $\dot{e}$  = erosion rate ( $\text{kg/m}^2\text{s}$ );  $\tau_b$  = peak value of the cyclic bed shear stress (Pa);  $M_2$  = erosion rate constant ( $\text{kg/m}^2\text{s}$ );  $\tau_R$  = erosion resistance (Pa);  $\alpha_3$  = empirical constant;  $\bar{U} = a\omega/\sinh(kh_1)$  is the amplitude of the bottom oscillatory velocity, where k = wave number and  $h_1$  = water depth;  $\delta_b = (\nu/2\omega)^{1/2}$  is the wave boundary layer thickness where  $\nu$  = kinematic viscosity of water;  $f(z)$  = bed shear strength as a function of depth (z); Test 2 (148 hr) had a longer consolidation period than Test 1 (38 hr).

unquantifiable effects of bed changes on particulate entrainment, the use of time-varying  $\tau_R$  is generally not warranted. It is also noteworthy that, depending on the way in which waves influence the bed,  $\tau_R$  may be lower or higher than  $\tau_c$  (Mimura, 1993). In Fig. 16,  $\tau_R$  is observed to be lower than  $\tau_c$  for a bed of kaolinite.

In Fig. 17, a typical relationship in the form of Eq. 5 based on flume measurements is shown (Maa and Mehta, 1987). Data smearing of the degree observed is typical of such plots, and is at least in part due to the uncertainty in estimating  $\tau_R$ . Furthermore, it is rather self-evident that plots such as these mask influences that may depend on multiple causes and associated feedbacks. For example, Jackson (1973), who conducted laboratory tests on wave resuspension of a mixture of silt, clay and some fine sand on a sloping beach, observed rapidly increasing suspended sediment concentration in the first hour, reaching a maximum after the second hour and decreasing subsequently. A possible explanation for the decrease in concentration is that the bed became less rigid with time under wave action, which in turn resulted in greater energy dissipation and reduced the shear stress at the interface. Jackson also noted that for relatively small orbital velocities (12-15 cm/s), there was very little erosion, whereas for velocities greater than about 20 cm/s the surface erosion process was replaced by mass erosion, with comparatively much larger rates of sediment entrainment, a behavior also observed under steady flows (Mehta, 1991c).

### 3.4 BED RECOVERY

Since the experimental data presented in Section 3.2 suggest that the loss of effective stress is primarily due to the rupturing of inter-particle bonds without a significant change in the density or void ratio, it follows that bed recovery should be comparatively rapid in the laboratory setting after wave action ceases. In test No. 9 of Feng (1992) mentioned earlier, wave action was maintained for 7.5 hr, following which effective stresses at different elevations above the flume bottom were determined from pore pressure profiles 4 hr later. Observe in Table 6 that the percent recovery, as defined, varied from 0 to 77, with a mean of 36. The non-uniformity in percentages

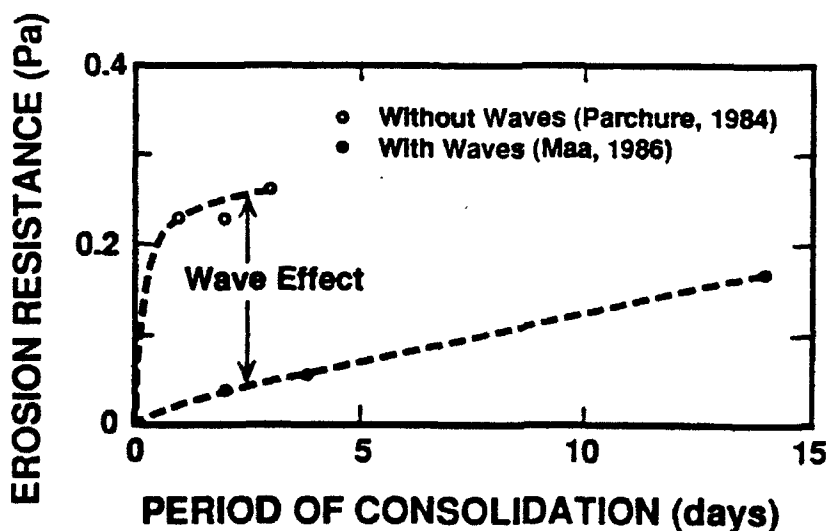


Figure 16. Influence of waves on shear resistance to erosion of kaolinite beds in flumes (after Mehta, 1989).

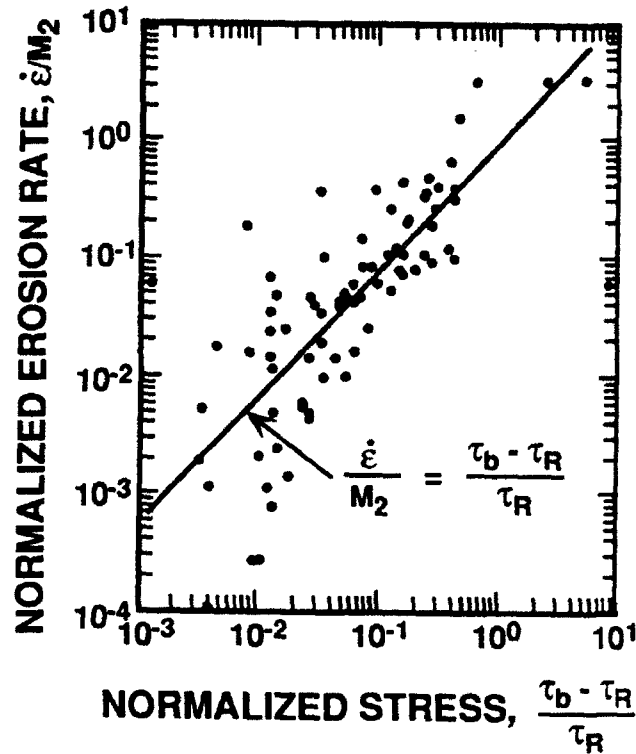


Figure 17. Normalized rate of erosion versus normalized excess shear stress for a bay mud (after Maa and Mehta, 1987).

Table 6. Bed recovery in Test No. 9 of Feng (1992)

Elevation (cm)	$\sigma'$ (Pa)			Recovery [[ $(\sigma'_{11.5} - \sigma'_{7.5}) / (\sigma'_0 - \sigma'_{7.5})$ ]] x 100
	t=0	t=7.5 hr	t=11.5 hr	
12.0	39	8	8	0
9.5	53	0	41	77
7.5	67	7	35	47
5.1	83	53	59	20

presumably reflects local variability in the mud properties at the sites of pressure measurements. In general, however, with the exception of the data point at 12 cm (4 cm below the interface), recovery is observed to slow down with increasing depth. Overall, since the attapulgite + kaolinite mixture was thixotropic, the rate of recovery is likely to be related in some way to the rate of gelling. Thus, for example, Day and Ripple (1966) reported a recovery period of 14 hr for an initially sheared K-montmorillonite based on the measurement of suction in a tensiometer. Typically, gelling is complete in about a day.

## ENERGY DISSIPATION AND ELEMENTS OF MODELING

### 4.1 WAVE ENERGY DISSIPATION OVER NON-RIGID BEDS

The conservation equation for wave energy within the water column is:

$$\frac{\partial E}{\partial t} + \nabla_h \cdot (\bar{C}_g E) + \epsilon_D = 0 \quad (7)$$

where  $E$  = mean wave energy per unit surface area,  $\nabla_h$  = horizontal gradient operator,  $\bar{C}_g$  = wave group velocity and  $\epsilon_D$  = rate of dissipation of wave-mean energy per unit area. Constitutive models proposed for the rate of energy dissipation within mud generally fall into two groups: 1) models which are specific to the assumed description of mud rheology, and, 2) models which are non-specific with regard to rheology. Some of the proposed expressions for  $\epsilon_D$  are listed in Table 7. In the first group, cohesive mud has been considered either as a viscous fluid, or as a viscoelastic or poroelastic medium. Some investigators, e.g. Shibayama et al. (1990), have also considered cohesive mud to be a Bingham viscoplastic in which, at stresses less than the yield value, the material is treated as a viscoelastic, whereas at higher stresses it is a fluid. Silty muds, considered to be poroelastic, incorporate energy loss by Coulomb friction between clay particles (e.g. Yamamoto and Takahashi, 1985).

In the second group, the expression of Tubman and Suhayda (1976) requires coefficients  $M$  and  $\phi$  which depend on the character of the water pressure wave near the mud surface and that of the induced mud surface wave. Since these waves depend on the solution of the hydrodynamic problem with an assumed constitutive relationship for mud,  $M$  and  $\phi$  must be measured directly, or obtained indirectly via model calibration using experimental data. Likewise, the expression of Schreuder et al. (1986) involves the mean shear strain rate as an explicit input parameter. Appendix A provides additional information on the bases of the  $\epsilon_D$  expressions.

### 4.2 A MODELING PERSPECTIVE

The response elements shown in Fig. 1, namely wave attenuation, mud motion and surface erosion, do not easily lend themselves to a unified theoretical treatment, since the first two can be examined, at least in the simplified treatment, by assuming bottom mud to be a constant density, incompressible continuum, whereas particulate entrainment at the mud-water interface requires separate consideration in terms of the change in the density of the overlying water layer due to a fluid stress-dependent vertical mass flux at the interface. Even under the most severe wave-induced agitation of bottom mud, the lack of a competent diffusive mechanism to transport the sediment mass from the bottom to the top of the water column usually precludes the development of high suspension concentrations in the surficial waters; most of the material remains close to the bed, approximately within the wave boundary layer. In turn, the depth of scour of bottom mud is typically sufficiently small to make it practicable, at least to first order accuracy, to assume water and mud thicknesses to be time-independent. Under

Table 7. Some energy dissipation rate expressions due to non-rigid bed mechanisms

Mud property <sup>a</sup>	Expression <sup>b</sup>	Investigator(s)
<i>Group 1</i>		
Mud as viscous fluid <sup>1</sup>	$\left[ \frac{1}{4\sqrt{2}} \right] \left[ \frac{\rho_2}{\omega} \left[ \frac{2\nu_2}{\omega} \right]^{1/2} e^{2k_r h_1} (\omega^2 - gk_r)^2 a_0^2 \right]$	Dean and Dalrymple (1984)
Mud as viscous fluid <sup>2</sup>	$\epsilon_{D1} + \epsilon_{D2} + \epsilon_{D3}$	Dalrymple and Liu (1978)
Mud as viscous fluid <sup>3</sup>	$\epsilon_{D4} + \epsilon_{D5}$	Feng (1992)
Mud as Voigt body <sup>4</sup>	$\left[ \frac{1}{2} \rho_1 g \right] \left\{ \omega A_r^2 \text{Im} \left[ \frac{\omega^2 (gk \cosh kh_1 - \omega^2 \sinh kh_1)}{gk (gk \sinh kh_1 - \omega^2 \cosh kh_1)} \right] a^2 \right\}$	MacPherson (1980)
Coulomb friction in bed <sup>5</sup>	$\left[ \frac{\rho_1^2 g^2}{4} \right] \left[ \frac{\omega \delta a^2}{G k_0 \cosh^2 k_0 h_1} \right]$	Yamamoto and Takahashi (1985)
Coulomb friction in bed <sup>6</sup>	$\left[ \frac{\rho_1^2 g^2}{4} \right] \left\{ \frac{\omega \delta a^2}{G k_0 \cosh^2 k_0 h_1} \left[ \frac{1}{(1 - \omega^2/\omega_0^2)^2 + \delta^2} \right] \right\}$	Yamamoto and Takahashi (1985)
<i>Group 2</i>		
Mud wave <sup>7</sup>	$\left[ \frac{\rho_1 g}{2} \right] \left[ \frac{\omega M \sin \phi a^2}{\cosh^2 k_r h_1} \right]$	Tubman and Suhayda (1976)
Mud as viscoelastic medium <sup>8</sup>	$\left[ \frac{\pi^2}{8} \right] (\mu' < \dot{\gamma} >^2 h_2)$	Schreuder et al. (1986)

<sup>a</sup>See Appendix A for explanatory notes 1 through 8.

<sup>b</sup>Notation: 1 = water layer; 2 = mud layer;  $\rho$  = density;  $\nu$  = kinematic viscosity;  $\omega$  = wave frequency;  $k$  = complex wave number =  $k_r + ik_i$ , where  $k_i$  = wave attenuation coefficient,  $k_r$  = wave number and  $i = (-1)^{1/2}$ ;  $h$  = depth;  $g$  = acceleration due to gravity;  $a$  = local wave amplitude;  $a_0$  = reference wave amplitude;  $\epsilon_{D1}$  through  $\epsilon_{D5}$  = rate of energy dissipation terms;  $A_r$  = wave amplitude ratio;  $\text{Im}$  = imaginary part of a complex variable;  $\delta$  = Coulomb specific loss;  $G$  = dynamic shear modulus;  $k_0$  = wave number for a rigid bottom;  $\omega_0^2 = 2Gk_0^2/\rho_2$ ;  $M$  = proportionality constant between the amplitudes of the mud wave and the wave-induced bottom pressure wave;  $\phi = 180^\circ - \theta$ , where  $\theta$  = phase angle between the crest of the bottom pressure wave and the crest of the mud wave;  $\mu'$  = dynamic viscosity;  $< \dot{\gamma} >$  = average value of shear strain rate.

these assumptions, solutions developed for problems involving stratified, non-Newtonian fluid mechanics have been applied extensively to model wave-mud interaction. Some of the previous developments are summarized in Appendix B.

In what follows, the formulation of the linearized hydrodynamic problem for wave attenuation and mud motion is considered in conjunction with Newtonian viscous and linear viscoelastic descriptions of mud rheology. Progressive, non-breaking waves are treated for their propagation within shallow water and non-shallow (intermediate depth) water conditions. Following this development, simple bases for modeling erosion are discussed briefly. These presentations are for informative purposes only; for details the referenced works in Appendix B must be consulted.

#### 4.3 BASIC CONSERVATION EQUATIONS

For continuous media, the governing equation of continuity is:

$$\frac{D\rho}{Dt} + \rho \frac{\partial u_i}{\partial x_i} = 0 \quad (8)$$

where  $\rho(x_i, t)$  = density,  $u_i(x_i, t)$  = velocity and subscript  $i$  denotes direction. For an incompressible fluid  $D\rho/Dt=0$ , and the continuity equation is simplified to

$$\frac{\partial u_i}{\partial x_i} = 0 \quad (9)$$

The corresponding equation of momentum is:

$$\rho \frac{Du_i}{Dt} = \rho b_i + \frac{\partial T_{ji}}{\partial x_j} \quad (10)$$

where  $b_i(x_i)$  = body force,  $T_{ji}(x_i, t)$  = external surface stresses, and subscripts  $i$  and  $j$  denote directions in conjunction with subscript  $ji$ , which implies a second order tensor. Thus,  $j$  = direction normal to the surface and  $i$  = stress direction. Because gravity is the only body force of concern here and as we set the  $z$ -direction vertically upward, then  $b_1=b_2=0$  and  $b_3=-g$ . The stress,  $T_{ji}$ , can be expressed as the sum of the deviatoric component,  $T'_{ji}$ , and the spherical component,  $\frac{1}{3} T_{kk} \delta_{ji} = -p \delta_{ji}$ , where  $T_{kk}$  is the sum of the diagonal terms in the stress tensor,  $p$  is the mean normal pressure and  $\delta_{ji}$  = kronecker delta; for  $j=i$ ,  $\delta_{ji}=1$ , and for  $j \neq i$ ,  $\delta_{ji}=0$ . Thus,

$$\rho \frac{Du_i}{Dt} = \rho \delta_{3i} b_3 - \frac{\partial p}{\partial x_i} + \frac{\partial T'_{ji}}{\partial x_j} \quad (11)$$

## 4.4 CONSTITUTIVE EQUATIONS

### 4.4.1 Fluid (incompressible)

The constitutive equation for the fluid is:

$$T_{ji}' = 2\mu D_{ji}' \quad (12)$$

where  $\mu$  = viscosity, and the rate of strain,  $D_{ji}' = 0.5[(\partial u_j/\partial x_i) + (\partial u_i/\partial x_j)]$ . Thus, the momentum equation becomes

$$\rho \frac{Du_i}{Dt} = \rho \delta_{3i} b_3 - \frac{\partial p}{\partial x_i} + \mu \frac{\partial^2 u_i}{\partial x_j \partial x_j} \quad (13)$$

### 4.4.2 Elastic Material

The constitutive equation for elasticity is:

$$T_{ji}' = 2GE_{ji}' \quad (14)$$

where  $G$  = modulus of elasticity, and the strain  $E_{ji}' = 0.5[(\partial L_j/\partial x_i) + (\partial L_i/\partial x_j)]$ , where  $L_i, L_j$  are displacements. Thus the momentum equation becomes

$$\rho \frac{Du_i}{Dt} = \rho \frac{D^2 L_i}{Dt^2} = \rho \delta_{3i} b_3 - \frac{\partial p}{\partial x_i} + G \frac{\partial^2 L_i}{\partial x_j \partial x_j} \quad (15)$$

### 4.4.3 Viscoelastic Material

The general constitutive equation for a linear viscoelastic medium is

$$\sum_{r=0}^M p_r \frac{\partial^r}{\partial t^r} (T_{ji}') = \sum_{s=0}^N q_s \frac{\partial^s}{\partial t^s} (E_{ji}') \quad (16)$$

where subscripts  $r$  and  $s$  denote orders of partial differentiation,  $p_r$  and  $q_s$  are coefficients related to the viscoelastic model, and  $M$  and  $N$  are the specified maximum differential orders of the chosen model. Under cyclic loading, we consider

$$T_{ji}' = T_0 \exp[-i(\omega t)] \quad (17)$$

$$E_{ji}' = E_0 \exp[-i(\omega t - \delta)] \quad (18)$$

where  $\omega$  = angular frequency,  $\delta$  = phase shift,  $T_0$  and  $E_0$  are amplitudes of  $T_{ji}$  and  $E_{ji}$ , respectively, and  $i = (-1)^{1/2}$ . Therefore, the relation between the deviatoric stress and the strain becomes

$$\frac{T_{ji}}{E_{ji}} = \frac{\sum_{s=0}^N q_s (-i\omega)^s}{\sum_{r=0}^M p_r (-i\omega)^r} \quad (19)$$

and the corresponding relation between the deviatoric stress and the rate of strain is:

$$\frac{\dot{T}_{ji}}{\dot{E}_{ji}} = \frac{\sum_{s=0}^N q_s (-i\omega)^s}{\sum_{r=0}^M p_r (-i\omega)^{r+1}} \quad (20)$$

After some manipulation the result is

$$\dot{T}_{ji} = (\mu' + i\mu'')\dot{E}_{ji} = \mu^* \dot{E}_{ji} \quad (21)$$

where the dot denotes time-derivative,  $\mu^* = \mu' + i\mu''$  is the complex dynamic viscosity,  $\mu'$  = real part, or the dynamic viscosity, and  $\mu''$  = imaginary part, or second viscosity. Thus the momentum equation becomes

$$\rho \frac{Du_1}{Dt} = \rho \delta_3 b_3 - \frac{\partial p}{\partial x} + (\mu' + i\mu'') \frac{\partial^2 u_1}{\partial x_j \partial x_j} \quad (22)$$

For a fluid:

$$\mu' = \mu_2 \quad ; \quad \mu'' = 0 \quad (23)$$

For an elastic material:

$$\mu' = 0 \quad ; \quad \mu'' = \frac{G}{\omega} \quad (24)$$

For a viscoelastic material - Voigt (Kelvin) model:

$$\mu' = \mu_2 \quad ; \quad \mu'' = \frac{G}{\omega} \quad (25)$$

Note that for a viscoelastic medium, from Eq. 19 we can also define  $T_{ji} = G^* E_{ji}$ , where  $G^* = G' - iG''$ , where  $G'$  is the elastic energy storage modulus and  $G''$  is the viscous energy dissipation modulus. Thus it can be shown that for the Voigt model, for example,  $G' = G$  and  $G'' = \mu_2 \omega$  (Barnes et al., 1989).

For a viscoelastic material - Maxwell model:

$$\mu' = \frac{2G \left[ \frac{G}{\mu_2} \right]}{\omega^2 + \left[ \frac{G}{\mu_2} \right]^2} ; \mu'' = \frac{2G\omega}{\omega^2 + \left[ \frac{G}{\mu_2} \right]^2} \quad (26)$$

Next, as illustrations of more complex models, for the three-element viscoelastic models, constructed from Voigt and Maxwell elements, shown in Figs. 18a,b:

Model (a):

$$\mu' = \frac{2G_1 \left[ \frac{G_1}{\mu_2} \right]}{\left[ \frac{G_1 + G_2}{\mu_2} \right]^2 + \omega^2} ; \mu'' = \frac{2G_1 \left[ \frac{(G_1 + G_2)G_2}{\mu_2^2} + \omega^2 \right]}{\left[ \frac{G_1 + G_2}{\mu_2} \right]^2 + \omega^2} \quad (27)$$

This model has been used in describing the consolidation behavior of soils (Keedwell, 1984). Jiang (1993) used it in his wave-mud interaction model described in Section 4.5.

Model (b):

$$\mu' = \frac{2G_2 \left[ \frac{G_2}{\mu_2} \right]}{\left[ \frac{G_2}{\mu_2} \right]^2 + \omega^2} ; \mu'' = \frac{\frac{2}{\omega} \left[ \frac{G_1 G_2^2}{\mu_2^2} + \omega^2 (G_1 + G_2) \right]}{\left[ \frac{G_2}{\mu_2} \right]^2 + \omega^2} \quad (28)$$

For any other (linear) viscoelastic model, the complex dynamic viscosity,  $\mu^* = \mu' + i\mu''$ , can be obtained through Eq. 20.

## 4.5 MODELS FOR WATER WAVES OVER MUD (X-Z PLANE)

### 4.5.1 *Inviscid, Shallow Water over Mud*

A general definition diagram for the wave-mud system is shown in Fig. 19. In the case considered first, water is assumed to be inviscid and mud to be viscoelastic. Under the shallow water assumption, the following analytical solution of the linearized problem is obtained based on the works of Gade (1957, 1958) and Jiang (1993).

*For water:*

The continuity Eq. 9 is integrated from the water-mud interface to the water surface:

$$\int_{-\eta_1 + \zeta_1}^{\eta_1} \left[ \frac{\partial u_1}{\partial x} + \frac{\partial w_1}{\partial z} \right] dz = 0 \quad (29)$$



From Eq. 13, omitting the viscous terms,  $\mu \partial^2 u_1 / \partial x \partial x$ , for inviscid "water", using the hydrostatic assumption for pressure,  $p = \rho_1 g(\zeta_1 - z)$ , in shallow water and omitting the non-linear terms,  $u_1 \partial u_1 / \partial x$ , the momentum equation for water (in the x-direction) becomes

$$\rho_1 \frac{\partial u_1}{\partial t} = - \frac{\partial p}{\partial x} = - \rho_1 g \frac{\partial \zeta_1}{\partial x} \quad (32)$$

For mud:

Equation 9 is integrated from the mud bottom to the water-mud interface using:

$$w|_{-h_1-h_2} = 0 \quad ; \quad w|_{-h_1-\zeta_1} = \frac{\partial \zeta_2}{\partial t} \quad (33)$$

Then the continuity equation for mud becomes

$$\int_{-(h_1+h_2)}^{-h_1-\zeta_1} \frac{\partial u_2}{\partial x} dz + \frac{\partial \zeta_2}{\partial t} = 0 \quad (34)$$

From the momentum Eq. 22, using the hydrostatic pressure assumption and omitting the non-linear terms, we obtain:

$$\rho_2 \frac{\partial u_2}{\partial t} = - \rho_1 g \frac{\partial \zeta_1}{\partial x} - (\rho_2 - \rho_1) g \frac{\partial \zeta_2}{\partial x} + \mu \frac{\partial^2 u_2}{\partial z^2} \quad (35)$$

where  $\rho_2 =$  mud density. The horizontal diffusion term,  $\mu (\partial^2 u_2 / \partial x^2)$ , has been ignored in comparison with the last term on the right hand side (in Eq. 35) corresponding to vertical diffusion. Eq. 35, in general, is applicable to small strain oscillatory forcing.

The following boundary conditions are next introduced:

At the free surface,  $z=0$ :

$$\zeta_1(0,t) = A \cos(\omega t) \quad (36)$$

where  $A =$  wave amplitude.

At water-mud interface,  $z=-h_1$ :

$$\frac{\partial u_2(x, -h_1, t)}{\partial z} = 0 \quad (37)$$

At the mud bottom,  $z=-(h_1+h_2)$ :

$$u_2(x, -(h_1+h_2), t) = 0 \quad (38)$$

Under cyclic wave loading, the following harmonic assumptions occur:

$$\zeta_1 = \hat{\zeta}_1 \exp[i(kx - \omega t)] \quad (39)$$

$$\zeta_2 = \hat{\zeta}_2 \exp[i(kx - \omega t)] \quad (40)$$

$$u_1 = \hat{u}_1 \exp[i(kx - \omega t)] \quad (41)$$

$$u_2 = \hat{u}_2(z) \exp[i(kx - \omega t)] \quad (42)$$

where the amplitudes denoted by  $\hat{\phantom{x}}$  are independent of  $x$ ,  $z$  and  $t$  except in Eq. 42, wherein  $\hat{u}_2$  varies with  $z$ . Next, substituting the boundary conditions into the governing equations (31, 32, 34, 35) and after some manipulation the following solution for the complex wave number,  $k$ , is obtained:

$$k = \frac{F_r}{h_1} \left\{ \frac{1 + \frac{h_2}{h_1} \Gamma - \left[ \left( 1 + \frac{h_2}{h_1} \Gamma \right)^2 - 4r \frac{h_2}{h_1} \Gamma \right]^{1/2}}{2r \frac{h_2}{h_1} \Gamma} \right\}^{1/2} \quad (43)$$

where  $r = (\rho_2 - \rho_1) / \rho_2$ ; Froude number,  $F_r = \omega(h_1/g)^{1/2}$ ;  $\Gamma = 1 - [\tanh(mh_2/h_1) / (mh_2/h_1)]$ ;  $m = (R_e/i)^{1/2}$  and Reynolds number,  $R_e = \omega h_1^2 / \nu^*$  ( $\nu^* = \mu^* / \rho_2$ ). Note that  $k = k_r + ik_i$ , where  $k_r$  is the wave number and  $k_i$  is the wave attenuation coefficient. Thus the wave amplitude at a distance  $x$ ,  $a_x = a_0 \exp(-k_i x)$ , where  $a_0$  is the amplitude at  $x=0$ . Solutions for the other variables are:

$$\zeta_1 = A \exp[i(kx - \omega t)] \quad (44)$$

$$\zeta_2 = A \left[ 1 - \left( \frac{kh_1}{F_r} \right)^2 \right] \exp[i(kx - \omega t)] \quad (45)$$

$$u_1 = \omega A \frac{kh_1}{F_r^2} \exp[i(kx - \omega t)] \quad (46)$$

$$u_2 = \omega A \frac{kh_1}{F_r^2} \left[ 1 - \cosh \left( m \frac{z + (h_1 + h_2)}{h_1} \right) + \tanh \left( m \frac{h_2}{h_1} \right) \sinh \left( m \frac{z + (h_1 + h_2)}{h_1} \right) \right] \left[ 1 - r \left( \frac{kh_1}{F_r} \right)^2 \right] \exp[i(kx - \omega t)] \quad (47)$$

Finally, the shear stress in the water layer, hence at the interface, is zero because of the inviscid assumption, and in mud layer the shear stress is obtained from:

$$\begin{aligned}
\tau(x,z,t) &= \mu \cdot \left[ \frac{\partial u_z}{\partial z} \right] \\
&= \left[ -\frac{m}{h_1} \sinh \left[ m \frac{z+(h_1+h_2)}{h_1} \right] + \frac{m}{h_1} \tanh \left[ m \frac{h_2}{h_1} \right] \cosh \left[ m \frac{z+(h_1+h_2)}{h_1} \right] \right] \\
&\quad \mu \cdot \omega A \frac{kh_1}{F_r^2} \left[ 1 - r \left( \frac{kh_1}{F_r^2} \right)^2 \right] \exp[i(kx - \sigma t)]
\end{aligned} \tag{48}$$

Without invoking the shallow water assumption, Hsiao and Shemdin (1980) and MacPherson (1980) independently investigated the problem of inviscid water waves propagating over a linear viscoelastic mud, and obtained analytical solutions in which the wave number is implicitly expressed. Suhayda (1986) extended MacPherson's results to a non-linear viscoelastic bed, while Mei and Liu (1987) considered a viscoplastic bed. Foda (1989) examined a stratified elastic bed and Feng (1992) and Isobe et al. (1992) set up their models considering mud to be a non-Newtonian (power-law) fluid. However, as noted, since in these models the viscosity of water was not included, the shear stress on water-mud interface, which governs particulate entrainment at the interface, was neglected.

#### 4.5.2 Viscid Fluid (Water) over Viscid/Viscoelastic Mud

Considering the viscosity of water and non-shallow water conditions, the governing equations can be set up as follows:

From Eq. 9 the continuity equation is:

$$\frac{\partial u_i}{\partial x} + \frac{\partial w_i}{\partial z} = 0 \tag{49}$$

where  $u$  and  $w$  are velocities in the  $x$ - and  $z$ -directions, respectively, and  $i=1,2$  denote the upper (water) and lower (mud) layers.

From Eq. 22 for a viscid fluid, omitting the non-linear terms, the momentum equation components are:

$$\frac{\partial u_i}{\partial t} = -\frac{1}{\rho_i} \frac{\partial P_i}{\partial x} + \nu_i \left[ \frac{\partial^2 u_i}{\partial x^2} + \frac{\partial^2 u_i}{\partial z^2} \right] \tag{50}$$

$$\frac{\partial w_i}{\partial t} = -\frac{1}{\rho_i} \frac{\partial P_i}{\partial z} + \nu_i \left[ \frac{\partial^2 w_i}{\partial x^2} + \frac{\partial^2 w_i}{\partial z^2} \right] \tag{51}$$

where the dynamic pressure,  $P_i$ , is defined as:

$$P_i = P_i^t + \rho_i g z + P_i^0 \tag{52}$$

Here,  $P_i^t$  = total pressure, and

$$P_i^0 = \begin{cases} 0, & \text{when } i=1 \\ (\rho_2 - \rho_1)gh_1, & \text{when } i=2 \end{cases} \quad (53)$$

The viscosity,  $\nu_i$ , depends on the medium; for water,  $\nu_1 = \nu_1$ , while for mud,  $\nu_1 = \nu_2 = \mu^*/\rho_2$  from Eq. 21. The complex viscosity,  $\mu^*$ , depends on the chosen constitutive model for mud rheology; see, e.g. Eqs. 23 through 28.

The following ten boundary conditions are introduced next:

At the mud bottom,  $z = -(h_1 + h_2)$

$$w_2 = 0 \quad (54)$$

$$u_2 = 0 \quad (55)$$

At the mud-water interface,  $z = -h_1 + \zeta_2$

$$w_2 = w_1 \quad (56)$$

$$u_2 = u_1 \quad (57)$$

$$w_2 = \frac{\partial \zeta_2}{\partial t} \quad (58)$$

$$P_1^i - 2\rho_1\nu_1 \frac{\partial w_1}{\partial z} - \rho_1 g \zeta_2 = P_2^i - 2\rho_2\nu_2 \frac{\partial w_2}{\partial z} - \rho_2 g \zeta_2 \quad (59)$$

$$\rho_1\nu_1 \left[ \frac{\partial u_1}{\partial z} + \frac{\partial w_1}{\partial x} \right] = \rho_2\nu_2 \left[ \frac{\partial u_2}{\partial z} + \frac{\partial w_2}{\partial x} \right] \quad (60)$$

At the free surface,  $z = \zeta_1$

$$w_1 = \frac{\partial \zeta_1}{\partial t} \quad (61)$$

$$P_1^i - 2\rho_1\nu_1 \frac{\partial w_1}{\partial z} = 0 \quad (62)$$

$$\rho_1\nu_1 \left[ \frac{\partial u_1}{\partial z} + \frac{\partial w_1}{\partial x} \right] = 0 \quad (63)$$

Under cyclic wave loading, consider:

$$\zeta_i = \hat{\zeta}_i(z) \exp[i(kx - \omega t)] \quad (64)$$

$$u_i = \hat{u}_i(z) \exp[i(kx - \omega t)] \quad (65)$$

$$w_i = \hat{w}_i(z) \exp[i(kx - \omega t)] \quad (66)$$

$$P_i = \hat{P}_i(z) \exp[i(kx - \omega t)] \quad (67)$$

and for the shear stress:

$$\begin{aligned}\tau_i &= \rho_i \nu_i \left[ \frac{\partial u_i}{\partial z} + \frac{\partial w_i}{\partial x} \right] \\ &= \rho_i \nu_i \left[ \frac{\partial \hat{u}_i(z)}{\partial z} + \hat{w}_i(z) \cdot ik \right] \exp[i(kx - \omega t)]\end{aligned}\quad (68)$$

Implicit solutions for the wave number and attenuation coefficient, velocity, pressure and shear stress are obtained (Dalrymple and Liu, 1978). Maa and Mehta (1987,1990), Chou (1989) and others extended this method to incorporate stratified mud properties. Jiang (1993) has extended the approach to include second order effects arising from finite amplitude waves.

#### 4.6 MODELING WATER COLUMN SEDIMENT DYNAMICS

Since we are focussing on vertical transport in the water column, the basic equation is the balance of sediment mass in terms of the settling and upward mass diffusion fluxes,  $F_s$  and  $F_d$ , respectively:

$$\frac{\partial \rho_D}{\partial t} + \frac{\partial}{\partial z} (F_d - F_s) = 0 \quad (69)$$

where  $\rho_D = \phi \rho_s = (\rho - \rho_w) \rho_s / (\rho_s - \rho_w)$  is the dry density or mass concentration of sediment in suspension (dry sediment mass per unit volume of suspension). We note that  $F_d = -k_s \partial \rho_D / \partial z$ , where  $k_s$  is the vertical mass diffusivity, and  $F_s = w_s \rho_D$ , where  $w_s$  is the settling velocity. Given the comparatively short wave periods in relation to the gradually varied trend in  $\rho_D$ , it is customary to consider vertical transport on a wave-average basis.

The initial condition for solving Eq. 69 is prescribed by  $\rho_D(z, 0)$ , and at the water surface,  $z=0$ , the usual no net flux condition is,  $F_d(0, t) - F_s(0, t) = 0$ . Two approaches have been used in prescribing the erosion flux condition at the mud surface,  $z = -h_1$ , as follows.

Some investigators, e.g. Thimakorn (1980; 1984) and Cervantes (1987), have prescribed  $\rho_D(-h_1, t)$ , following a similar approach commonly used in coarse-grained sediment transport. In that case a reference concentration is prescribed close to the bed at elevation  $z = -h_1 + \delta_a$ , where  $\delta_a$  is a small distance above the bed which depends on the work done by the fluid in dislodging and raising the potential energy of the surface particle elevated to  $\delta_a$  (Smith, 1977). Since, however, bed load transport does not occur when the sediment is fine-grained, especially cohesive (Partheniades, 1977), for most practical purposes it is reasonable to set  $\delta_a = 0$ . In any event, defining  $\beta(t) = \rho_D(-h_1, t) / \bar{\rho}_D(t)$ , where  $\bar{\rho}_D(t)$  is the instantaneous depth-mean value of  $\rho_D(t)$ , experimental data for  $\beta(t)$  and an empirical-fit equation are given in Fig. 20. The tests (T-1, T-2 and T-3) were performed in a wave-flume shown schematically in Fig. 21, using an estuarine mud. See Section 5.2 for a further description of the flume. The wave frequency  $\omega$ , and the nominal wave amplitude,  $a_0$ , for each test are given in Table 8. Other relevant test parameters are prescribed in Cervantes (1987). In the empirical equation of Fig. 20,  $\hat{\beta} = \beta / \beta_0$ ,  $\hat{\beta}_a = \beta_a / \beta_0 \delta_1$  and  $\hat{t} = \delta_1 t$ ; thus data fit for  $\beta(t)$  is dependent on  $\beta_0$ ,  $\beta_a$  and  $\delta_1$ . These values are given in Table 8.

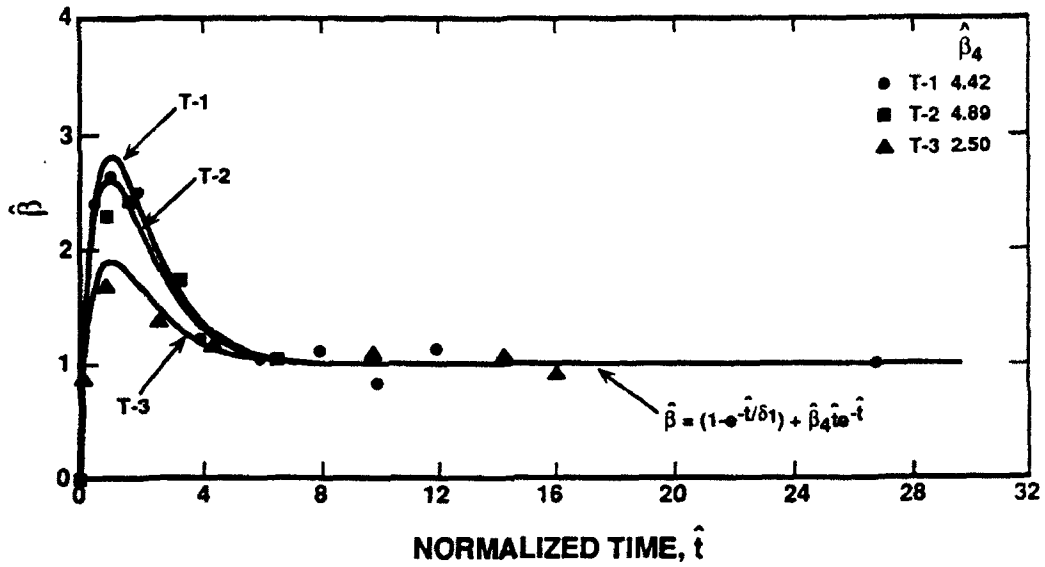


Figure 20. Variation of  $\hat{\beta}$  with normalized time,  $\hat{t}$  (after Cervantes, 1987).

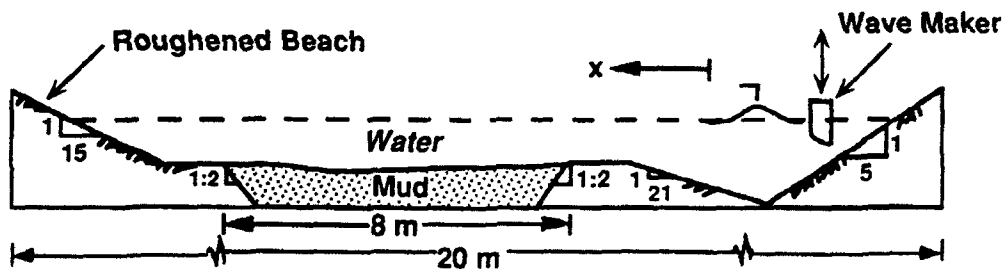


Figure 21. Wave-mud interaction flume (after Maa, 1986).

Table 8. Test parameters including wave frequency  $\omega$  and nominal wave amplitude,  $a_0$ , and coefficients  $\beta_0$ ,  $\beta_4$  and  $\delta_1$  for the empirical-fit equation in Fig. 20

Test	$\omega$ (rad/s)	$a_0$ (m)	$\beta_0$	$\beta_4$ (s <sup>-1</sup> )	$\delta_1$ (s <sup>-1</sup> )
T-1	6.3	0.030	18.5	0.045	0.00055
T-2	3.1	0.015	50.0	0.220	0.00090
T-3	6.3	0.035	48.0	0.060	0.00050

A noteworthy observation relative to Fig. 20 is that  $\hat{\beta}(t)$ , hence  $\beta(t)$ , is observed to rise rapidly initially, followed by its approach to a steady state value close to one. The initial rise represents a mass erosion-type bed failure phenomenon represented by the Mohr-Coulomb equation; see Lamb and Whitman (1969), whose effect is mainly embodied in the coefficient  $\hat{\beta}_4$ , which, for a given bed, apparently depends not only on  $\tau_b$ , but also on  $\partial\tau_b/\partial t$  (Cervantes, 1987). In Fig. 20, the trend of increasing mass erosion with increasing  $\hat{\beta}_4$  is generally evident. This characteristic response of the bed suggests that the release of fine sediment into the water column from the bed is likely to be an episodic process, with mass-eroded bottom sediment entrained perhaps by coherent bursts. The approach of  $\hat{\beta}$  to unity suggests that following the time-dependent effects associated with experimental start-up, the vertical dry density profile became uniform. This was so because  $\rho_D(-h_1, t)$  was actually measured above the lutocline. Thus, fluid mud generation is not represented in the character of  $\hat{\beta}(t)$  in Fig. 20, for which the datum,  $z=-h_1$ , was located approximately at the elevation of the lutocline. Thus, in effect  $\delta_s$  was approximately equal to the thickness of the fluid mud layer.

It can be easily shown (Cervantes, 1987) that by specifying  $\beta(t)$ , and introducing it in Eq. 69 renders the problem as one of initial value, which can be solved for  $\bar{\rho}_D(t)$  given  $\bar{\rho}_D(0)$ , and it is recognized that  $\bar{\rho}_D(t)$  approaches a constant value,  $\bar{\rho}_{DS}$ , as  $t \rightarrow \infty$ . The vertical distribution of  $\rho_D$  is not obtained by this method.

In low energy environments where significant fluid mud generation usually does not occur,  $\beta=1$  is not an unreasonable assumption. Elsewhere, however, in general wave-generated fluid mud must be treated explicitly as an eroded sediment mass, especially since in this state mud is relatively easily transported horizontally by currents. Process models for fluid mud generation have been developed (e.g. Chou, 1989; Foda et al., 1993) to calculate the fluid mud thickness (see Section 3.2).

Erosion of the fluid mud-water interface occurs as a process involving shear-induced warping of the interface, which leads to its destabilization and mixing (Scarlato and Mehta, 1993; Adams et al., 1993). This process is mainly dependent on the Richardson number and also the settling velocity of the particles being entrained. Experiments under uni-directional shear flows have yielded the following expression:

$$\dot{\epsilon} = \frac{\rho_1 \Delta b U}{g} \left[ \frac{A}{\text{Ri}} + \frac{B}{\text{Pe}^{1/2}} - D \text{Ri} \right] \quad (70)$$

where  $\rho_1$  = mean upper (mixed) layer density,  $b$  = buoyancy =  $g(\rho_2 - \rho_w)/\rho_w$ ,  $\rho_2$  = fluid mud density,  $\rho_w$  = water density,  $\Delta b$  = buoyancy jump across the fluid mud-water interface,  $\text{Ri}$  = Richardson number =  $h_1 \Delta b / U^2$ ,  $U$  = mean velocity of the upper layer,  $\text{Pe}$  = Peclet number =  $U h_1 / k_m$ ,  $k_m$  = molecular diffusivity and  $A, B, D$  are empirical constants (Mehta and Srinivas, 1993). The coefficient  $D$  depends on the settling velocity; thus, a non-settling constituent such as salt  $D=0$ , and Eq. 70 becomes applicable for example to salt entrainment. Note that the Peclet number dependent term is important only at very high values of  $\text{Ri}$  when the flow becomes viscous. For most practical applications it is appropriate to set  $B=0$ . The applicability of Eq. 70 under a wave field remains to be demonstrated, however.

The second approach with respect to the erosion flux involves the specification of  $\partial\rho_D(-h_1,t)/\partial t$  (Ross and Mehta, 1989). Thus, from Table 5,

$$\frac{\partial\rho_D(-h_1,t)}{\partial t} = \frac{M_2}{h_1} \left[ \frac{\tau_b}{\tau_R(t)} - 1 \right] \quad (71)$$

in which  $\tau_R(t)$  is obtained from  $\tau_R(z)$  via the continuity-based z-t transformation

$$\frac{\partial z}{\partial t} = \frac{h_1}{\rho_2(z)} \frac{\partial \bar{\rho}_D(t)}{\partial t} \quad (72)$$

where  $\rho_2(z)$  is the depth-varying bottom mud density. In the difference form, Eq. 72 can be written as  $\Delta t = \Delta z / \{ [h_1/\rho_2(z)] [\partial \bar{\rho}_D(t)/\partial t] \}$ . Thus, a change in  $\tau_R$  over the differential scour depth,  $\Delta z$ , can be interpreted in terms of the corresponding change in  $\tau_R$  over  $\Delta t$ . Note that, since  $\tau_R$  typically increases with  $\rho$ , by virtue of Eq. 71 scour is arrested when the condition,  $\tau_R = \tau_b$ , is attained at a particular depth.

The datum,  $z = -h_1$ , can be conveniently located at the level between the bed and fluid mud. In this way fluid mud can be treated in an approximate way as a suspension formed by bed erosion specified by Eq. 71. This equation must be "calibrated" by adjusting the value of  $M_2$  to account for the rate of generation of fluid mud, as well as its entrainment into the water column above the lutocline.

In high energy environments wherein a considerable amount of sediment is resuspended, the influence of the negative buoyancy and turbulence damping characteristic of the sediment-water mixture can be substantial, and tend to retard upward mass diffusion (Wolanski et al., 1988). It is therefore essential to amend the commonly chosen neutral diffusivity,  $k_0$ , by the damping function  $\Phi = 1 + \alpha_6 z/L$ , where  $\alpha_6$  is an empirical coefficient, and  $L$  is the Monin-Obukov length scale. Thus,  $k_1 = k_0 \Phi$ , and a common empirical form for  $\Phi$  is:  $\Phi = (1 + \beta_6 Ri_g)^{-\alpha_6}$ , where the gradient Richardson number,  $Ri_g = (g/\rho)(d\rho/dz)/(du/dz)^2$ ,  $\rho$  is the density of the sediment-water mixture and  $u(z)$  is the horizontal flow velocity. We therefore have the diffusion flux,  $F_d = -k_0(1 + \beta_6 Ri_g)^{-\alpha_6} \partial \rho_D / \partial z$ , which is plotted in Fig. 22 against  $\partial \rho_D / \partial z$  for stable and unstable stratifications, given  $\alpha_6 = 2$ ,  $\beta_6 = 4.17$  and other relevant parameters based on the work of Ross (1988). See, e.g. Horikawa (1978) for a discussion on the choice of  $k_0$  and Ross (1988) for  $\alpha_6$  and  $\beta_6$  values.

The settling velocity,  $w_s$ , in general varies with  $\rho_D$ . Defining  $\rho_{D1}$  such that for all  $\rho_D < \rho_{D1}$ , settling is free, i.e. the inter-particle collision frequency is so low that particles or aggregates settle essentially independently of each other, the following expressions can be used:

For  $\rho_D < \rho_{D1}$ ,

$$w_s = \text{contant (i.e. independent of } \rho_D) \quad (73a)$$

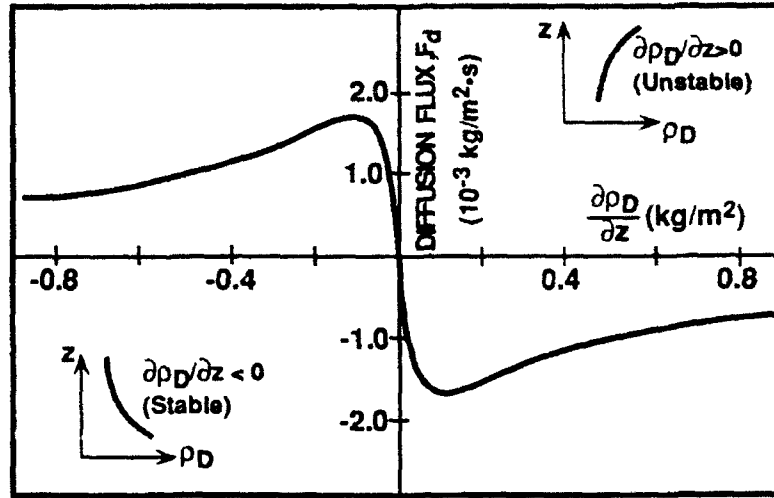


Figure 22. Diffusion flux,  $F_d$ , as a function of  $\partial \rho_D / \partial z$  for  $\alpha_6=2$  and  $\beta_6=4.17$  (modified from Ross, 1988).

For  $\rho_D > \rho_{D1}$ ,

$$w_s = \frac{a \rho_D^n}{(\rho_D^2 + b^2)^m} \quad (73b)$$

where coefficients  $a$ ,  $b$ ,  $m$  and  $n$  depend on sediment properties. In addition, as noted later, they also depend on the degree of agitation in the water column. In Eq. 73b, for relatively low values of  $\rho_D$ ,  $b^2 \gg \rho_D^2$ , hence  $w_s = ab^{-2m} \rho_D^n$ . This is called flocculation settling in which  $w_s$  increases with  $\rho_D$  due to a corresponding increase in the inter-particle collision frequency. At high values of  $\rho_D$ ,  $b^2 \ll \rho_D^2$ , hence  $w_s \approx a / \rho_D^{2m-n}$ . In this case  $w_s$  decreases ( $m > n/2$ ) with increasing  $\rho_D$  due to hindered settling.

Settling velocity data that approximately conform with Eq. 73b are shown in Fig. 23 with  $a=33.38$ ,  $b=2.537$ ,  $n=1.83$  and  $m=1.89$ . The settling flux,  $F_s$ , is obtained from

$$F_s = \frac{a \rho_D^{n+1}}{(\rho_D^2 + b^2)^m} \quad (4.68)$$

The quantity  $\rho_{D1}$  is somewhat arbitrarily prescribed in Fig. 23 as 0.1 g/l,  $\rho_{D2} = 2.46$  g/l is the value of  $\rho_D$  at which the settling velocity peak occurs, and  $\rho_{D3} = 4.38$  g/l corresponds to the peak value of  $F_s$ . A lutocline occurs when  $\rho_D$  exceeds  $\rho_{D3} = [(\rho_s - \rho_w) / (\rho_s / \rho_w)]$ .

For a given sediment, the coefficients  $a$ ,  $b$ ,  $m$  and  $n$  are found to be sensitive to the degree of agitation, or turbulence, in water. As observed from Fig. 24, agitation by vertically oscillating rings in a laboratory column caused the particulate aggregates to rupture and consequently settle more slowly than under quiescent conditions (Wolanski et al., 1992).

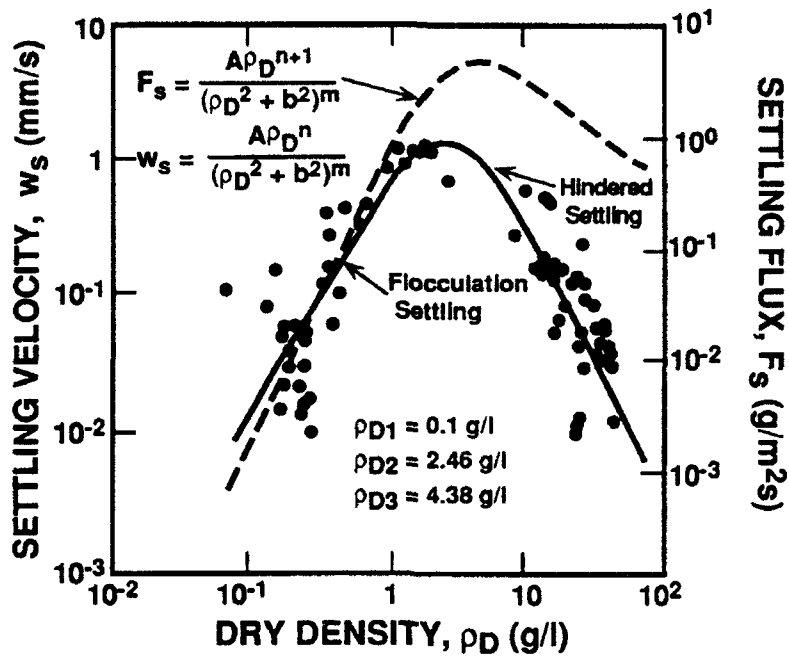


Figure 23. Settling velocity (and flux) variation with  $\rho_D$ . Data points obtained from tests using a lake (Okeechobee, Florida) sediment in a laboratory column (after Hwang, 1989).

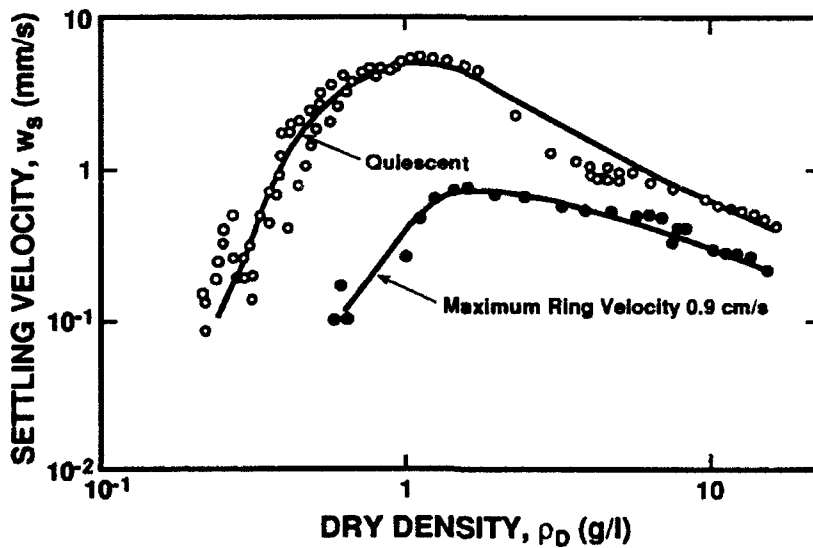


Figure 24. Settling velocity versus  $\rho_D$  data using a bay (Townsville, Australia) sediment under two conditions: quiescent water and water agitated by vertically oscillating rings (adapted from Wolanski et al., 1992).

## LABORATORY/FIELD DATA AND MODEL SIMULATIONS

### 5.1 INTRODUCTION

As noted, given the compliant and highly dissipative nature of bottom mud, wave-induced water motion is significantly contingent upon the choice of the constitutive relationship describing mud rheology. For illustrative purposes we will consider mud to be viscoelastic, a special case of which is mud as a viscous fluid. Note that mud motion under typical conditions, both in the laboratory and in the field, is sufficiently damped by the high viscosity of mud, which tends to be order of  $10^3$  to  $10^4$  times greater than water. Thus, turbulence within mud can be ignored in most practical applications, even though it does occur to some degree below the lutocline, and contributes towards the entrainment of fluid mud (Wolanski et al., 1988). Laboratory applications are described first, followed by field.

### 5.2 WAVE FLUME RESULTS

#### 5.2.1 Test Facility, Experiments and Modeling Approaches

Experiments were conducted in a 20 m long, 46 cm wide and 45 cm high plexiglass flume shown in Fig. 21. Progressive waves were generated by a programmable, plunging-type generator. Mud was contained in a 16 cm deep, 8 m long trench with end slopes as shown. The down-wave end of the flume beach was artificially roughened to absorb wave energy and thus minimize reflection. Details of flume description are found in Ross (1988). Muds of different composition, degree of consolidation and vertical density structure were tested. Figure 25a shows the time-variation of stratified density profiles of a consolidating mud from Cedar Key, Florida (designated CK) prepared by depositing the sediment from an initially formed suspension in the flume. Note that, in general, in such experiments the time-scale of measurable density variation is considerably greater, on the order of tens of minutes, than the typical wave period and, therefore, consolidation does not measurably contaminate the wave-averaging process usually inherent in modeling. In contrast to Fig. 25a, Fig. 25b, shows a practically uniform clayey mixture composed of an attapulgite and a kaolinite (designated AK) in equal proportions by weight. The bed was prepared by pouring a pre-mixed sediment slurry over the flume bottom.

All experiments were conducted with a nominally constant mud thickness, a constant water depth, and monochromatic, progressive waves of selected frequency and forcing amplitude. Measurements in general included density profiles from the water surface to the flume bottom, wave height decay over the length of the trench, mud elevations along the trench, water velocity, mud velocity and acceleration, and vertical total and pore pressure profiles. For the types of transducers and measurement techniques used see Maa (1986), Ross (1988) and Jiang (1993).

The presented experimental results encompass three categories: wave attenuation, water and mud dynamics and bed/interface erosion, in consonance with Fig. 1. With respect to wave attenuation and mud dynamics the data are compared with simulations using the models of Maa (1986) and Jiang (1993). Both consider water to be Newtonian and mud to be a viscoelastic continuum. The equations for continuity and the horizontal and vertical components of motion for these models are given by Eqs. 49, 50 and 51, respectively. The basic problem formulation for both

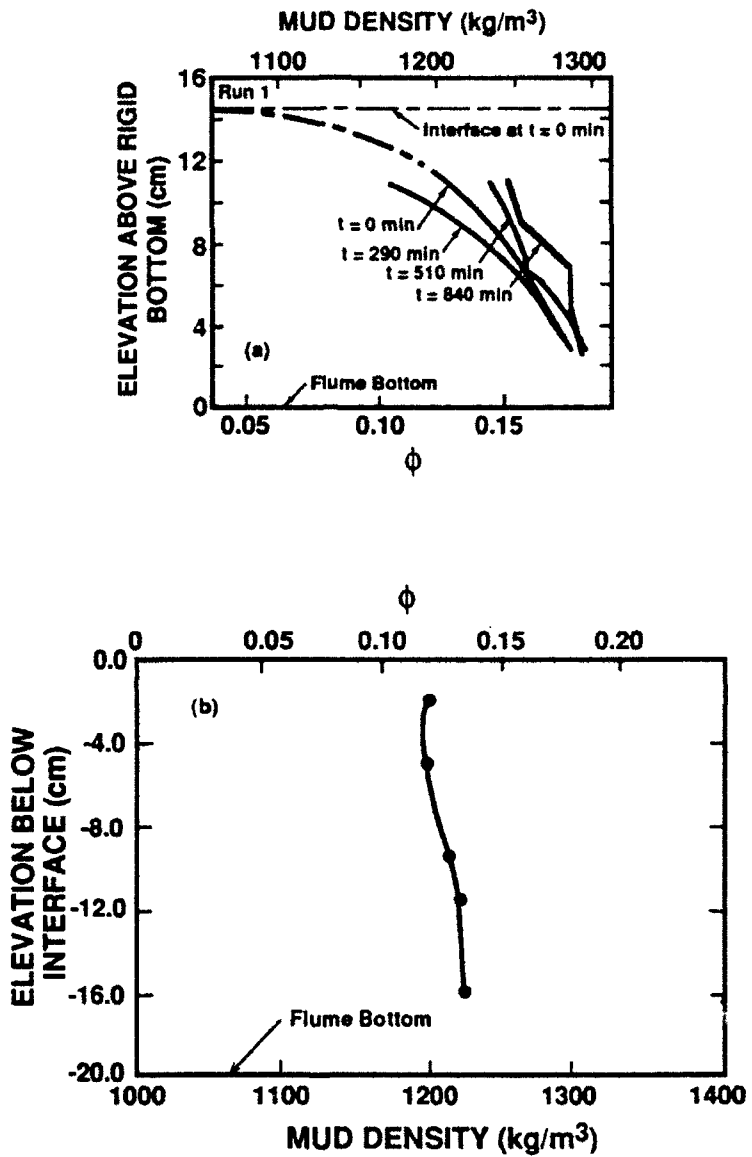


Figure 25. a) Time-variation of the bottom mud density profile during an erosion experiment (Run 1) using mud from Cedar Key, Florida (after Maa, 1986); b) Uniform density profile of a mixture of an attapulgite and a kaolinite (after Jiang, 1993).

models is given in Section 4.5.2. Differences between the two models are as follows: The small amplitude solution of Maa (1986) is based on linearized boundary conditions. In Jiang (1993), the non-linear, finite amplitude solution is carried out to second order using the perturbation expansion technique. In Maa (1986), bottom mud can be subdivided into as many layers as desired, each specified by the density and the two viscoelastic constants for the Voigt constitutive model (Eq. 25). Thus stratified mud, such as shown in Fig. 25a, can be parameterized in this model. In Jiang (1993) the bed properties are vertically uniform, such as represented by the density profile in Fig. 25b, and the viscoelastic model is given by Eq. 27, which is more general, and approaches the Voigt model at frequencies greater than about 10 Hz. Neither model includes interfacial erosion; hence the bottom mud mass is conserved.

The viscoelastic assumption causes the kinematic viscosity,  $\nu_2$ , in the equations of motion (Eqs. 50 and 51) for mud to be a complex number,  $\mu^*/\rho_2$ , the form of which depends on the choice of the constitutive model, as noted earlier. In general, for a given mud and temperature,  $\mu^*$  varies with the forcing amplitude, frequency and mud density (Jiang, 1993). As noted in Section 3.2, in a controlled-strain rheometer, Chou (1989) found the strain amplitude to be an important parameter in determining mud response (viscous, viscoelastic or elastic), and frequency to be of secondary importance within the range of frequencies examined. In a controlled-stress rheometer Jiang (1993) examined mud response to oscillatory stress amplitude as well as forcing frequency. Several muds were tested, the stress amplitude was varied from 0.3 to 25 Pa, and frequency from 0.02 to 4.5 Hz. Typically, for stress amplitudes ranging from 0.6 to 10 Pa, the response was found to be relatively weakly dependent on the amplitude. On the other hand, frequency dependence was more significant. As an example, in Fig. 26, the magnitude of the equivalent viscosity,  $|\mu^*| = |\rho_2 \nu^*| = \rho_2(\mu'^2 + \mu''^2)^{1/2}$ , is plotted against frequency,  $f$ , for a mud from offshore of Mobile Bay, Alabama (designated MB), the site of a dredged material deposit from the bay (Mehta and Jiang, 1993). The strong dependence of  $|\mu^*|$  on  $f$  is believed to be due to the thermodynamic process associated with the vibratory response of mud to cyclic forcing; at low frequencies the process is probably isothermal, while at high frequencies it tends to become adiabatic (Krizek, 1971; Schreuder et al., 1986). This change evidently has the overall effect of decreasing  $|\mu^*|$  with increasing  $f$ . Increasing  $\phi$  in turn increases the stiffness and the effective viscosity.

The effective viscosity magnitude in Fig. 26 has been determined for the viscoelastic model shown in Fig. 18a, and is thus defined by  $\mu$ ,  $G_1$  and  $G_2$ . These three parameters were experimentally found to depend on  $f$  according to:

$$\mu, G_1 \text{ or } G_2 = \exp(\epsilon) f^\Delta \quad (75)$$

where values of the coefficients  $\epsilon$  and  $\Delta$  are given in Table 9 (Mehta and Jiang, 1993). Relationships such as the ones in Fig. 26 inherently suggest that, for example, as waves pass over mudbanks the wave spectral shape may be drastically altered due to frequency-selective attenuation, as observed for example off Surinam in Fig. 27 (Wells and Kemp, 1986).

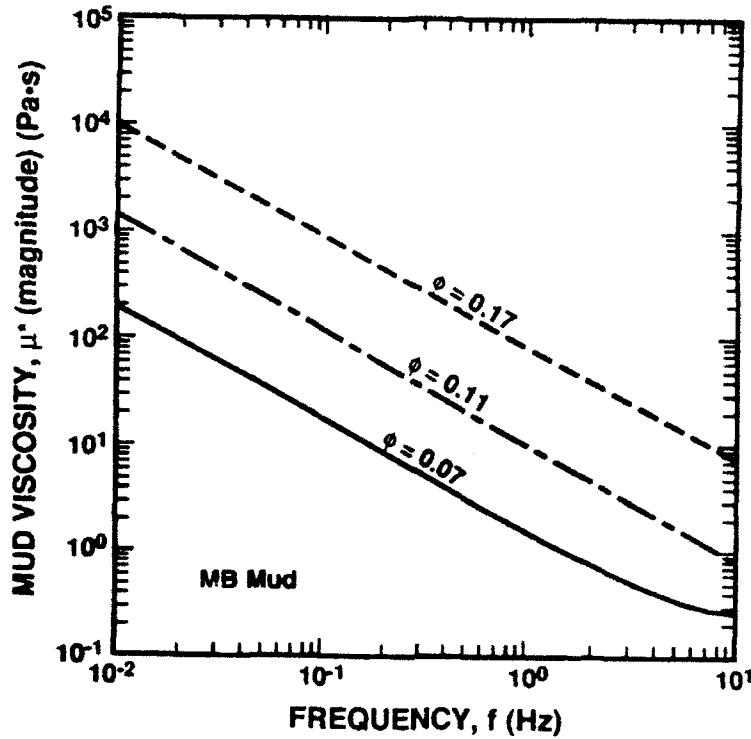


Figure 26. Magnitude of equivalent dynamic viscosity (applicable to the viscoelastic model of Fig. 18a) as a function of wave forcing frequency and mud volume fraction,  $\phi$ , for MB mud.

Table 9. Coefficients of Eq. 5.1 for MB mud

$\phi$	$G_1(\text{Pa})$		$G_2(\text{Pa})$		$\mu(\text{Pa}\cdot\text{s})$	
	$\epsilon$	$\Delta$	$\epsilon$	$\Delta$	$\epsilon$	$\Delta$
0.07	3.659	-0.030	-1.439	-0.975	3.165	-0.975
0.11	6.352	0.075	2.139	-0.745	6.695	-0.745
0.17	8.274	0.108	3.864	-0.696	8.374	-0.696

Wave-induced erosion is separately examined in Section 5.2.3 via the approaches described in Section 4.6, following wave attenuation and associated mud dynamics. The first approach yields the time-variation of the depth-averaged suspended sediment concentration or dry density,  $\bar{\rho}_D(t)$ , during erosion, while the second gives the time-variation of the vertical profile of concentration,  $\rho_D(z,t)$ . Some relevant laboratory results are considered next.

### 5.2.2 Wave Attenuation and Mud Motion

In Fig. 28 the wave attenuation coefficient,  $k_1 = -(1/\chi)\ln(a_x/a_0)$ , measured over a distance approximately equal to the length of the mud trench (Fig. 21), has been plotted against wave frequency,  $\omega$ , for AK mud. The depth of

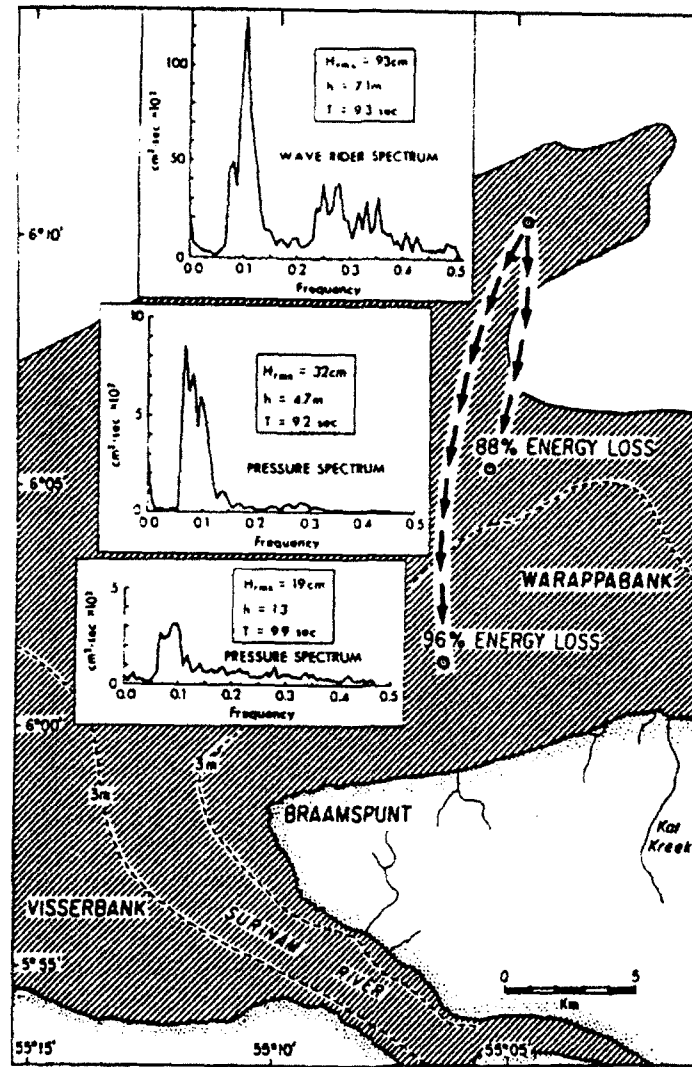


Figure 27. Wave spectra from synchronous wave stations 22, 11 and 4 km offshore, showing loss of wave energy and change in the shape of the spectrum over a fluid-like mud bottom along the central Surinam coast.  $H_{rms}$  = root mean square wave height,  $T$  = wave period and  $h$  = water depth (after Wells and Kemp, 1986).

water ( $h_1$ ) in these tests was 16 cm, while the mud depth ( $h_2$ ) was varied. The input wave amplitude ( $=a_0$ ) was 1.3 cm. In addition to the effect of water depth on the degree of attenuation, the maximum in the  $k_1$ - $\omega$  curve is an interesting and characteristic feature that requires an explanation. In the special case of shallow water and viscous mud (see Section 4.5), Jiang and Mehta (1992) showed that the degree of attenuation, as reflected by  $k_1$ , depends on the ratio,  $h_2/\delta_m$ , where  $\delta_m = (2\nu_2/\omega)^{1/2}$  represents the viscous mud boundary layer thickness. The depth-mean value of the velocity gradient,  $\partial u/\partial z$ , and in turn the rate of wave energy dissipation in mud, is maximum when  $h_2/\delta_m$  is equal to or is close to one, and decreases as  $h_2/\delta_m$  increases above one or decreases below one. This criterion is modulated when mud rigidity is measurable. Thus, MacPherson (1980) showed that the peak wave

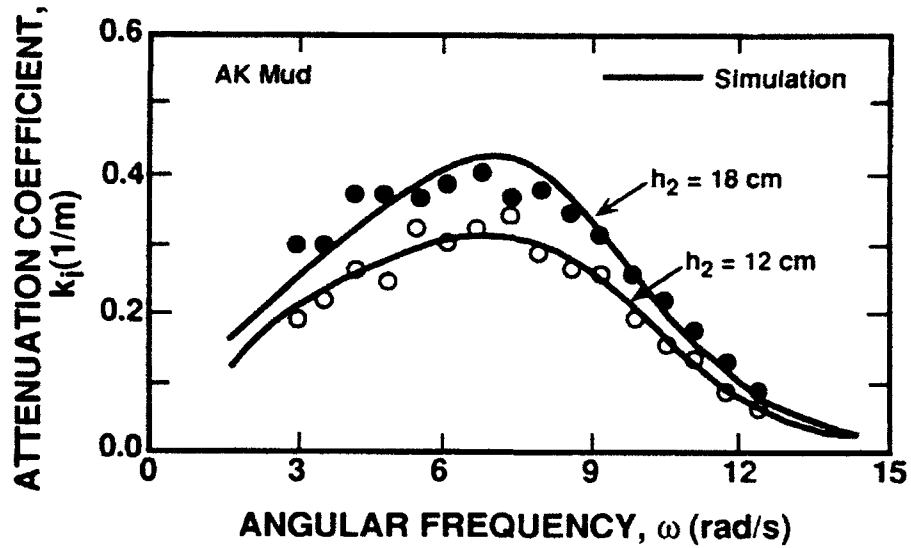


Figure 28. Wave attenuation coefficient against frequency for two AK mud ( $\phi = 0.16$ ) depths, 12 cm and 18 cm. Water depth was 16 cm. The input wave amplitude was 1.3 cm. Circles are data; lines are simulations based on the model of Jiang (1993).

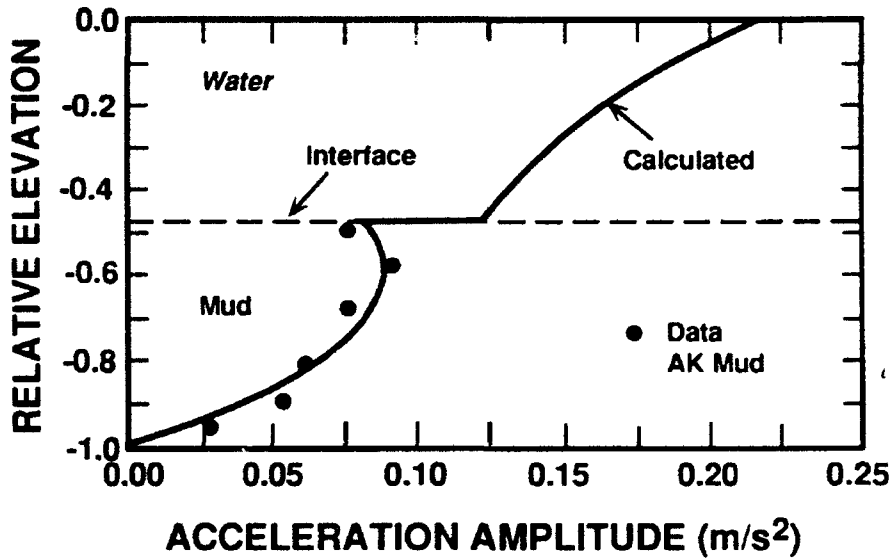


Figure 29. Comparison between measured and model-calculated profiles of the amplitude of horizontal acceleration in a water-mud (AK) system. The water depth was 16 cm, mud thickness 18 cm, water surface forcing wave amplitude 0.5 cm, wave frequency 1 Hz and  $\phi = 0.12$  (after Jiang, 1993).

attenuation rate occurs when  $\bar{\nu} = \nu_2 / (gh_1^3)^{1/2}$  and  $\tilde{G} = G / \rho_2 gh_1$  are of the same order of magnitude. In any event it is evident and noteworthy that, as a result of the strong dependence of  $k_1$  on  $\omega$ , the mode of change in the wave spectral shape as the waves pass over a mudbank will critically depend on the character of the input spectrum, mud viscosity and mud depth.

Based on the results from another test using the same mud (AK), a comparison between the measured and model-calculated amplitude of the horizontal acceleration,  $\ddot{u}_2$ , within mud is shown in Fig. 29. Note the drastic reduction in mud acceleration relative to that in the water column due to the dissipative nature of the bottom medium.

A noteworthy feature of bottom mud subjected to non-linear waves is residual mud mass transport, which in a large number of situations is a significant factor leading to sedimentation, e.g. in port channels and basins. The Lagrangian mean particle drift, or Stokes' drift,  $\bar{u}_L$ , associated with "non-closed" trajectories of mud particles must therefore be calculated. In general, the velocity of a particular particle with a mean position of  $(x_1, z_1)$  is  $u(x_1 + \zeta', z_1 + \xi')$ , where  $\zeta'$  and  $\xi'$  are instantaneous position coordinates along the particle trajectory. Based on Taylor series expansion, we have (Sakakiyama and Bijker, 1989; Jiang, 1993):

$$\bar{u}_L(x_1 + \zeta', z_1 + \xi') = \bar{u}_2(x_1, z_1) + \overline{\frac{\partial u_2}{\partial x} \int_0^t u_2(x_1, z_1) dt} + \overline{\frac{\partial u_2}{\partial z} \int_0^t w_2(x_1, z_1) dt} \quad (76)$$

where overbars denote time-averaging over the wave period and  $\bar{u}_2$  is the Eulerian mass transport velocity. To obtain  $\bar{u}_L$  theoretically, the wave-averaged integrals and derivatives on the right hand side of Eq. 76 must be obtained through an appropriate hydrodynamic model. In Fig. 30a comparison is made between measurement and prediction for AK mud, using the model of Jiang (1993). The measurements were made by observing the horizontal displacement of an initially vertically injected dye streak adjacent to the flume side wall made of plexiglass. Two sources of error are noteworthy in terms of the observed discrepancy between the data points and the model-calculated profile. Firstly, the data points incorporate the effects of drag close to the side wall and, secondly, the calculated mass transport velocity profile is approximate due to analytical limitations (Jiang, 1993). Nevertheless, the overall trends do compare favorably. Accurate field information on mass transport velocity is apparently sparse; however, the model was applied to predict the rate of mass transport of transient mudbanks (of KI mud) off the coast of Kerala (India). The predicted 0.22 km/d shoreward transport rate at the onset of monsoon at least appears to be of the correct order of magnitude (Mathew, 1992; Jiang, 1993).

From an experiment meant to investigate mud dynamics, measured and predicted profiles of velocity and dynamic pressure are compared in Fig. 31a,b for CK mud. The calculations are based on the model of Maa (1986), in which the mud bottom was subdivided into four layers of thicknesses indicated, each characterized by density, viscosity and shear modulus of elasticity. The dynamic pressure at first decreases, then increases with depth below the interface. This variation has been explained by Maa (1986) in terms of the relative influences of the effective viscous term and the pressure term in the equation of motion. Note that the model predicts an interfacial shear stress

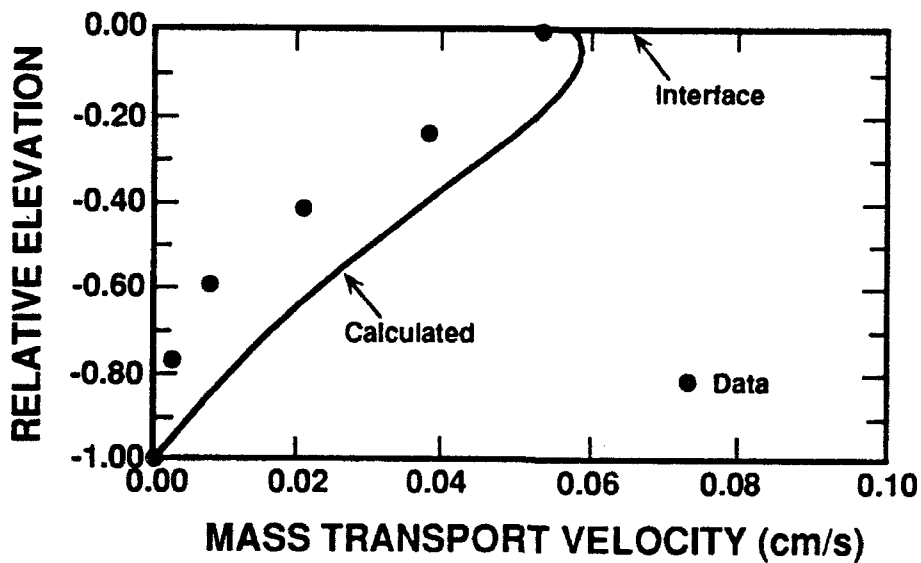


Figure 30. Mass transport velocity in AK mud. Wave amplitude 2 cm, frequency 1 Hz,  $h_1 = 14$  cm and mud thickness  $h_2 = 17$  cm (after Jiang, 1993).

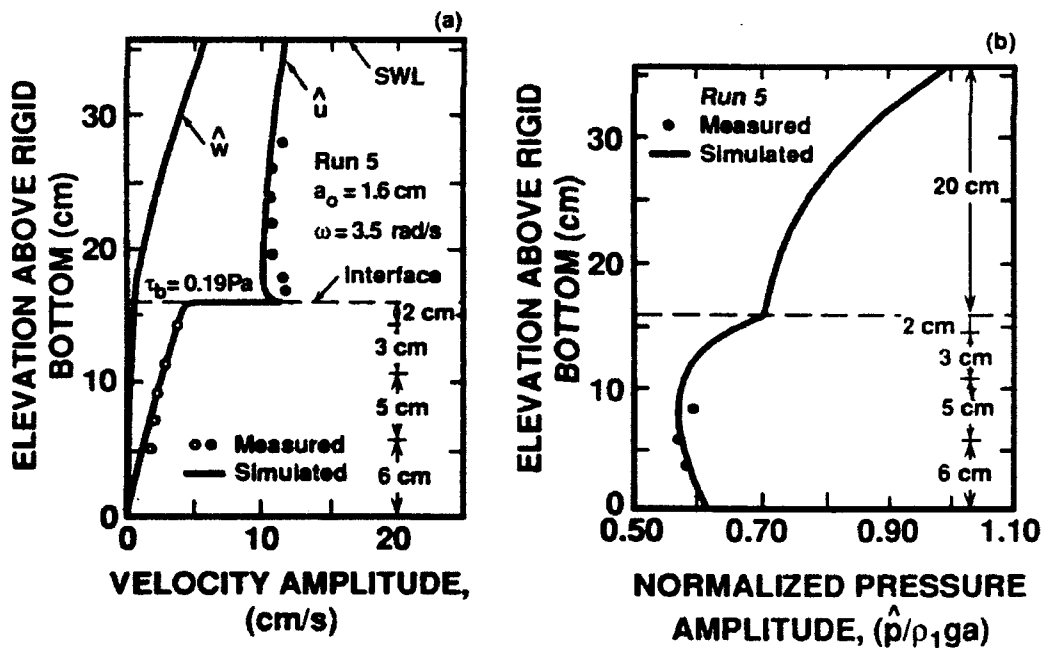


Figure 31. a) Horizontal and vertical velocity amplitudes in water and CK mud; b) Dynamic pressure amplitude profile corresponding to Fig. 31a. Smooth profiles have been drawn based on spatially discretized calculations (after Maa and Mehta, 1987; Maa, 1986).

(amplitude,  $\tau_b$ ) of 0.19 Pa, which was too small to cause a substantial amount of interfacial erosion during the experiment. Yet the bottom mud showed a measurable horizontal oscillation driven by the pressure gradient. This type of a situation is likely to be ubiquitous in nature, with the result that under typically gentle, fair weather wave action mud may oscillate, even while the upper water column is relatively free of turbidity, since the interfacial stress is insufficient to cause significant mud scour. Thus, for example, in Lake Okeechobee, Florida, daily wave-induced mud oscillation tends to retain the top 5-20 cm layer of bottom mud in a fluid-like state, which in turn presumably facilitates the transport of nutrients across the mud-water interface, and influences the trophic state of this large and shallow lake (Jiang and Mehta, 1992).

### 5.2.3 Bed/Interface Erosion

The time-variation of the wave-mean and depth-mean dry density (concentration) of suspended sediment of a bed of CK mud is shown in Fig. 32 in test T-1 of Cervantes (1987) mentioned in Section 4.6. The normalized parameters are: dry density,  $\bar{\rho}_D = \bar{\rho}_D / \bar{\rho}_{DS}$ , and time,  $\theta = (w_s/h_1)t$ . Note the almost instantaneous rise of the normalized dry density to 0.86, followed by a drop and subsequent attainment of a steady state ( $\bar{\rho}_D \rightarrow 1$ ). The peculiar nature of the curve reflects the corresponding variation of  $\hat{\beta}$  with normalized time ( $\hat{t}$ ) shown in Fig. 20. The function given in the inset of Fig. 20 has two components, the first of which reflects surface erosion and the second is attributed to Mohr-Coulomb type bed failure or mass erosion. Initially the influence of the second term is dominant in Fig. 32 and, as steady state approaches surface erosion (first term) becomes the main contributor. Thus, qualitatively the response curve, i.e. the time-variation of  $\bar{\rho}_D$ , can be divided into the three phases shown in Fig. 33. In phase P-I mass erosion is dominant, P-II is characterized by settling, and surface erosion is dominant in P-III. The occurrence of the mass erosion peak may be of noteworthy significance in nature. Although supportive field data are apparently sparse, such peaks are probably quite common at the time of comparatively sudden onset of increased storm wave action, amounting to an episodic generation of turbidity.

The time-variation of the vertical profile of the dry density during an erosion experiment is shown in Fig. 34. The bed was composed of HB (from Hillsboro Bay, Florida) mud, and simulation is via the model of Ross (1988), which is based on the sediment transport equation given in Section 4.6. Note the rapid generation of the lutocline, similar to what occurs in the field, e.g. Fig. 35 (adapted from Kemp and Wells, 1987). Of the four instantaneous, vertical dry density profiles for suspended sediment shown in Fig. 35, one represents pre-frontal wave conditions, two were obtained during frontal passage, and the last is post-frontal. The data were obtained at a site on the eastern margin of the Louisiana chernier plain where the tidal range is less than 0.5 m (Kemp and Wells, 1987). Wave height during the winter cold front passage was on the order of 13 cm and period 7 s. Of particular interest is the development of a fluid mud layer by the frontal wind-generated waves (profiles 2 and 3), which was previously absent (profile 1). The post-frontal profile 4 further suggests that this layer may have persisted following front passage, conceivably due to the comparatively low rate at which the layer was dewatered. The suspension density in the upper water column was higher following the front than that during the front, possibly due to advection of

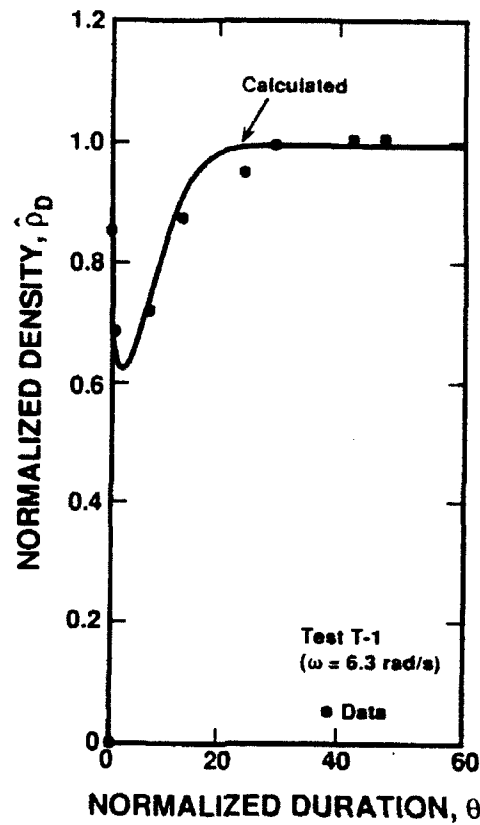


Figure 32. Time-variation of normalized dry density (concentration),  $\hat{\rho}_D(t) = \bar{\rho}_D(t)/\bar{\rho}_{DS}$ , for CK mud, during test T-1. Mud depth ( $h_2$ ) was 16 cm, water depth ( $h_1$ ) was 17 cm, forcing wave amplitude ( $a_0$ ) was 3 cm and frequency ( $f$ ) was 1 Hz (after Cervantes, 1987).

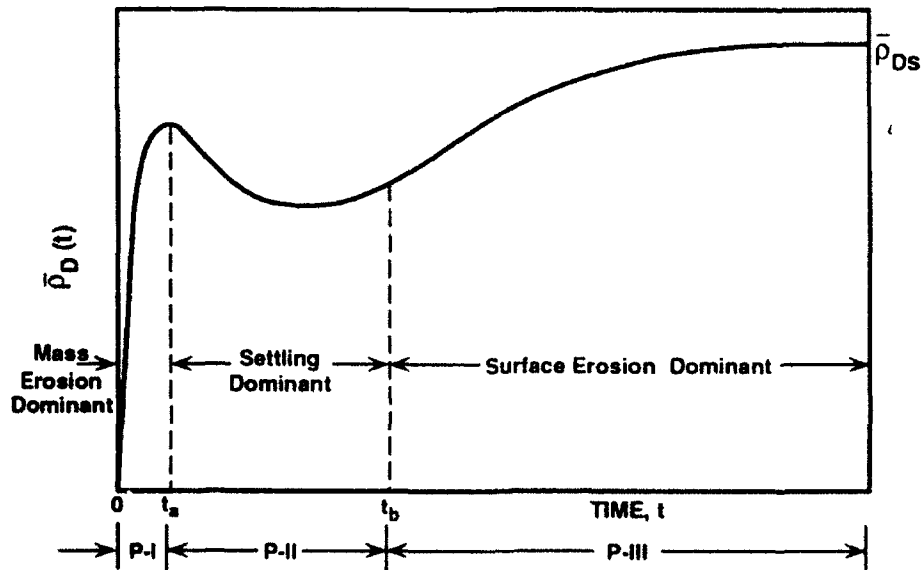


Figure 33. Phases in the time-variation of  $\bar{\rho}_D(t)$ , such as in Fig. 32 (after Cervantes, 1987).

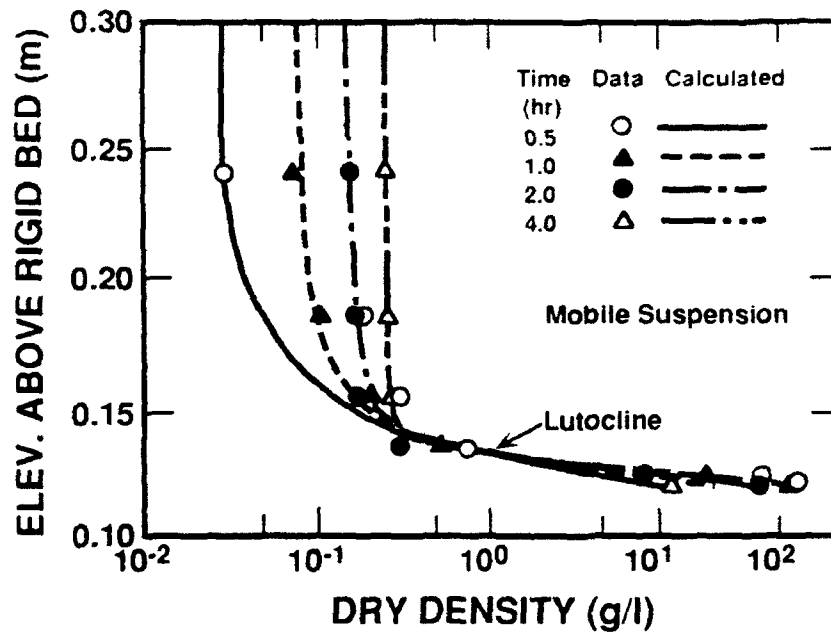


Figure 34. Measured and model-calculated dry density (concentration) profiles during erosion of Hillsboro Bay mud (HB). Water depth ( $h_1$ ) 31 cm, mud depth ( $h_2$ ) 12 cm, forcing wave amplitude,  $a_w = 3$  cm and wave frequency,  $f = 1$  Hz (after Ross, 1988).

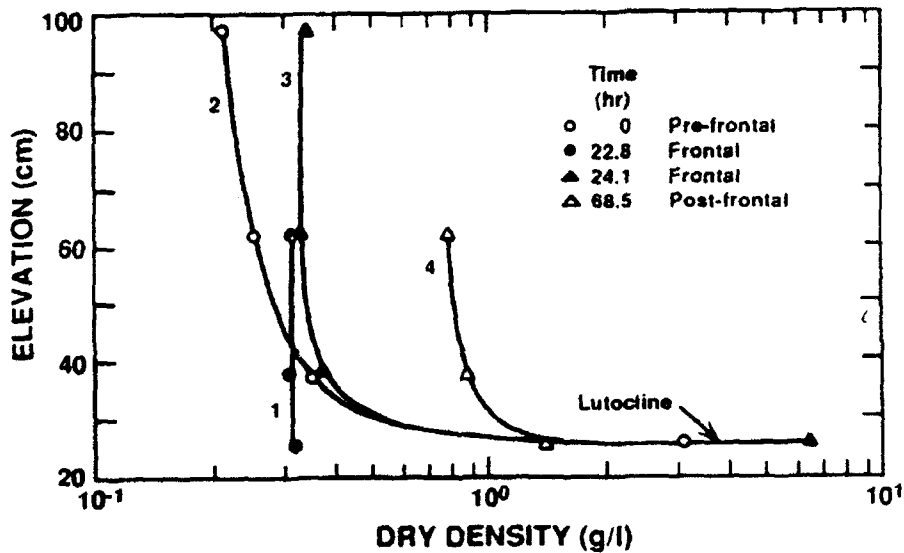


Figure 35. Vertical suspended sediment dry density (concentration) profiles obtained before, during, and after the passage of a winter cold front at a coastal site in Louisiana. Times are relative to time of measurement of the pre-frontal profile 1 (adapted from Kemp and Wells, 1987).

suspended sediment from a neighboring area of high turbidity. Also note that in Fig. 34 as well as Fig. 35, the lack of significant upward transport of sediment above the lutocline is consistent with the typically low wave-induced mass diffusivities (Sheng, 1986).

### 5.3 LAKE OKEECHOBEE, FLORIDA

#### 5.3.1 Setting

A large part of the central basin of Lake Okeechobee in southcentral Florida is overlain by a thin layer of dark, organic-rich (about 40% by weight) mud which is believed to be a significant storage for externally loaded phosphorus. Figure 36 shows the mud thickness to be 80 cm at most, generally occupying the deeper part of the lake. A typical variation of mud density with depth is shown in Fig. 37. As observed the top ~ 10 cm of the mud layer was comparatively low in density. Below this layer a rapid increase in density occurred and led to a relatively uniformly dense mud underneath. The low density structure at the top is apparently characteristic of the organic-rich mud of comparatively uniform, fluid-like consistency (Hwang, 1989).

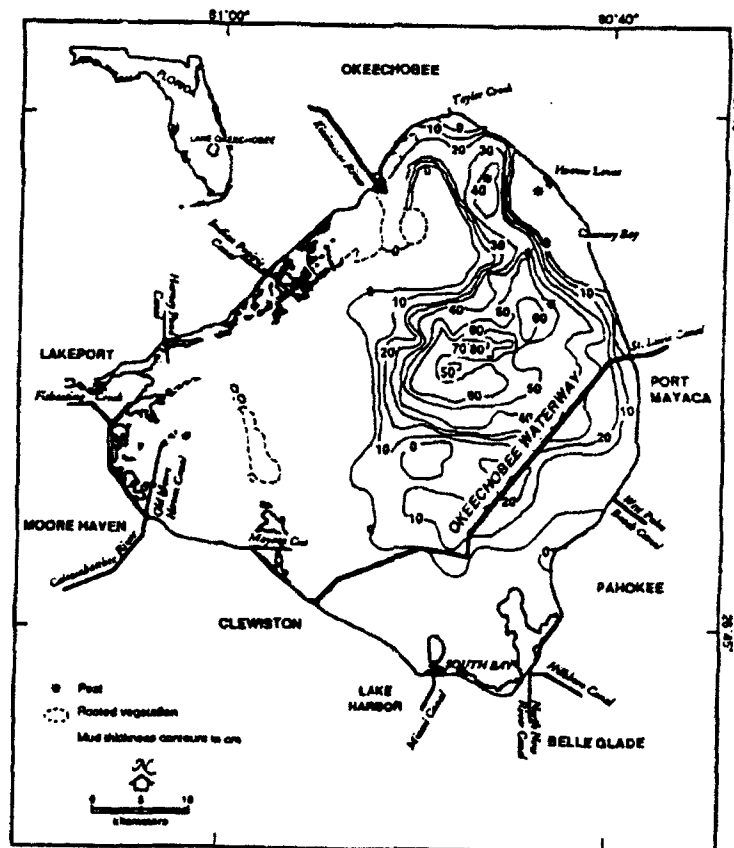


Figure 36. Mud thickness contour map of Lake Okeechobee, Florida (after Kirby et al., 1989).

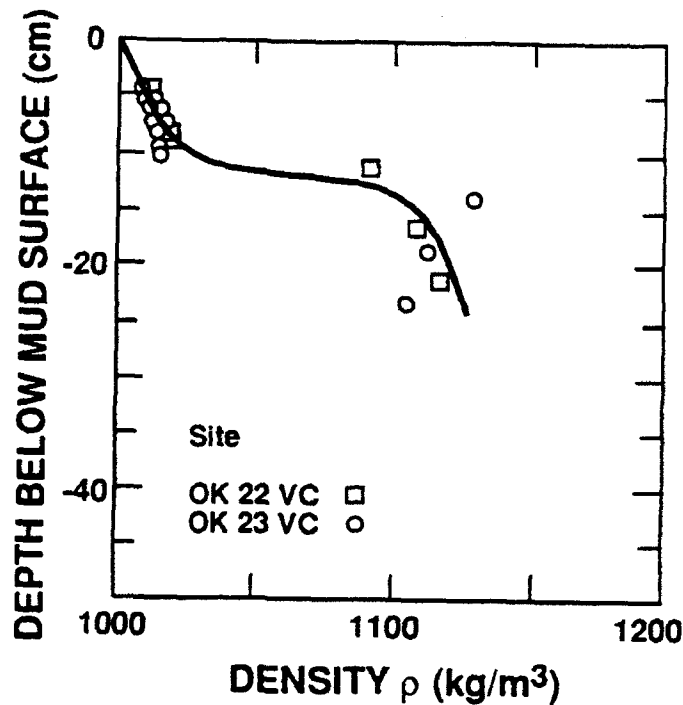


Figure 37. Typical mud bottom density profile based on vibrocore data from two nearby sampling sites (after Hwang, 1989).

### 5.3.2 Mud Motion

In order to examine the nature of mud motion induced by wave action in the lake, an instrumented tower was deployed at a site near Port Mayaca (Fig. 36). The mean water depth was 1.43 m and mud thickness 0.55 m. Water surface variation was measured with a pressure transducer, and an electromagnetic current meter was used to measure wave-induced water motion 87 cm below the mean water surface. To measure mud motion a small accelerometer was embedded 20 cm below the mud surface where the density was 1,180 kg/m<sup>3</sup>. The shallow water analytical model of Jiang (1993) described in Section 4.5.1 was used to aid in interpreting the data. In that model, the water column is considered to be inviscid, and mud is assumed to be a highly viscous fluid. Mud viscosity was measured in a rheometer; the kinematic viscosity at the density of 1,180 kg/m<sup>3</sup> was found to be  $1.76 \times 10^{-2}$  m<sup>2</sup>/s, which is very large compared to water ( $10^{-6}$  m<sup>2</sup>/s).

Figure 38a shows a typical wave spectrum obtained under moderate breeze ( $\sim 20$  km/hr) from the westerly direction. The dominant wave frequency was 0.42 Hz, with a significant height of 8 cm. It is noteworthy that calculations (Mehta and Jiang, 1990) showed that at 20 km/hr wind speed, the wave height would have been four-fold larger over an otherwise comparable rigid bottom.

In Fig. 38b the measured horizontal water velocity amplitude spectrum is compared with that simulated by the model using the wave spectrum of Fig. 38a as input. Given the model limitations, particularly with respect to the

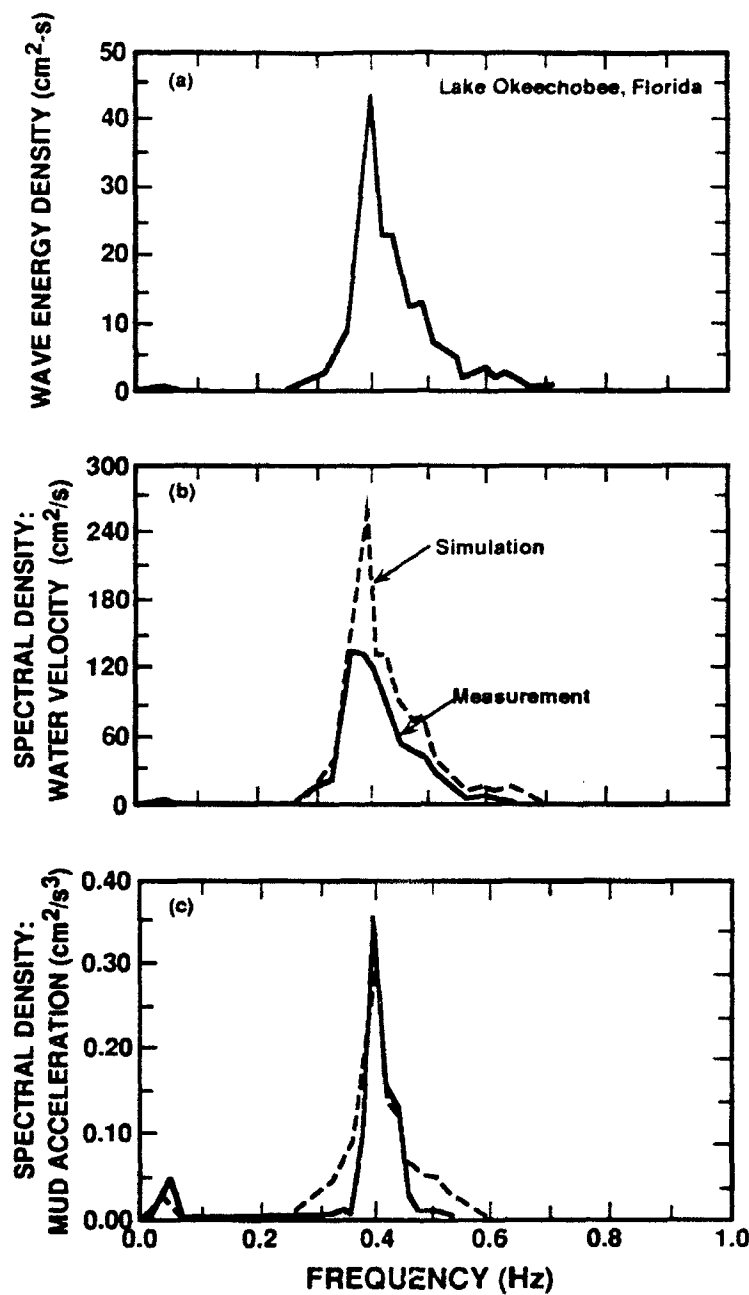


Figure 38. Data and model application, Lake Okeechobee, Florida: a) Measured water wave spectrum; b) Comparison between measured and simulated water velocity spectra; c) Comparison between measured and simulated mud acceleration spectra (after Jiang, 1993).

assumption of mud as a purely viscous fluid, and errors inherent in the data collection effort (Mehta and Jiang, 1990), the agreement between data and prediction appears to be acceptable.

Referring to Fig. 38c in which measured and simulated horizontal acceleration spectra in mud are compared, the data as well as model simulation indicate the occurrence of measurable acceleration at about 0.04 Hz. This

behavior can be attributed to a forced second order wave that results from an interaction between different frequencies of the forcing wind wave, as for example occurs in the case of surf beat over relatively flat open coast beaches (Jiang and Mehta, 1992). Note that dominant seiching in Lake Okeechobee occurs at a much lower frequency, on the order of  $10^{-4}$  Hz. While energy contribution at 0.04 Hz frequency is also found in the wave spectrum (Fig. 38a) and in the water velocity spectrum (Fig. 38b), the mud acceleration spectrum is enhanced at the 0.04 Hz in comparison with the spectrum at the 0.42 Hz forcing frequency. This relative enhancement is due to the strong frequency dependence of the wave attenuation coefficient,  $k_i$ . Model results for example yielded  $k_i = 0.0034 \text{ m}^{-1}$  at 0.42 Hz and  $0.0013 \text{ m}^{-1}$  at 0.04 Hz. Note that if the bottom were rigid,  $k_i$  would be  $0(10^{-5})\text{m}^{-1}$ , which is considerably smaller.

### 5.3.3 Resuspension

Using the vertical sediment mass transport numerical model of Ross (1988), the time-evolution of the vertical dry density (concentration) profile was simulated under selected storm wave conditions. Profiles such as the one in Fig. 37 were used to represent bed density variation with depth. For a given wave period and height, the bottom stress amplitude was calculated from:  $\tau_b = 0.5 f_w \rho_1 u(-h_1, t)^2$ , where  $f_w$  is the wave friction factor (Jonsson, 1966). The bottom velocity,  $u(-h_1, t)$ , was obtained from the linear wave theory using wave amplitude, frequency and water depth as input parameters. The neutral vertical mass diffusivity,  $k_0$ , (Section 4.6) was obtained from  $k_0 = \alpha' a^2 \omega [\sinh^2 k(z+h_1) / 2 \sinh^2 kh_1]$ , based on the work of Hwang and Wang (1982), where  $\alpha'$  is a free coefficient. The  $k_0$  value was weighted by the damping parameter  $\Phi$  (Section 4.6). Settling velocity data are given in Fig. 23.

In Fig. 39a the manner in which the suspension profile would evolve over a 48 hr period starting with a clear water column is exemplified for a 6 s ( $\omega = 1.1 \text{ rad/s}$ ) storm wave of 1 m height in a 4.6 m deep water column characteristic of the central part of the lake. Note the rather rapid formation of a fluid mud layer represented by the lutocline. The layer thickness was found to be about 7 cm at 48 hr (Hwang, 1989). Note also however, that the corresponding bed scour depth can be shown to be on the order of a centimeter only. Thus a very thin bed layer generated an order of magnitude thicker fluid mud layer. Such layers, characterized by a significant density gradient, have been observed in wave dominated environments (e.g. Fig. 35). Observe in Fig. 39a the very slow rise in the suspension density in the upper water column due to characteristically low rates of upward mass diffusion. At 48 hr the dry density at the surface rose to only about 100 mg/l, very close to 102 mg/l reported by Gleason and Stone (1975) in the southern part of the lake during a storm. If wave action were discontinued at 48 hr, the profiles of Fig. 39b would result due to sediment settling under calm conditions. At 72 hr, or 24 hr after waves ceased, most of the material is observed to have settled to the bottom, and the water column clarified.

## 5.4 SOUTHWEST COAST OF INDIA

An example of a drastic reduction in the wave energy due to wave passage over seasonal coastal mudbanks is briefly noted here. Figure 40 shows the region offshore of the town of Alleppey in State of Kerala on the southwest coast of India, where wave spectra were obtained at the two sites shown (Mathew, 1992). A schematic profile of

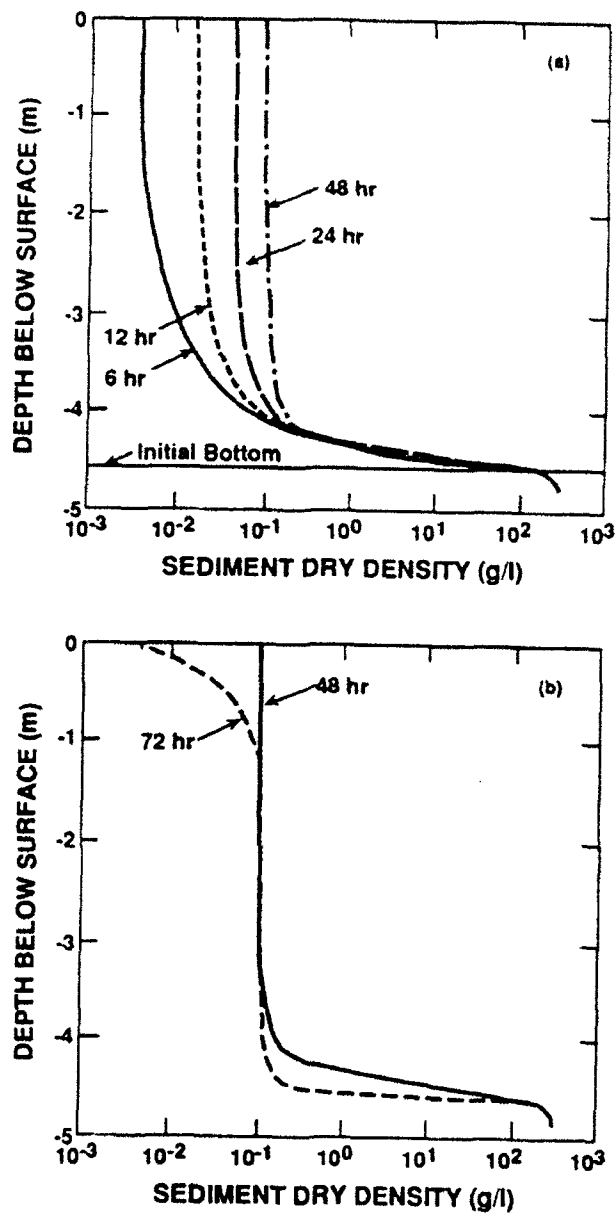


Figure 39. a) Simulated time-evolution of suspension profile due to 0.9 m high, 4 s waves in a 4.6 m deep water column; b) Settling of sediment once waves cease 11 hr from start of wave action (after Hwang, 1989).

the mudbank is shown in Fig. 41 (Nair, 1988), and the rheological characteristics of the mud (KI) are given in Fig. 26 (and Table 9). The bottom beneath the mud elsewhere in this area is sandy. Thus the subaqueous bottom mud is not always visible from the sandy beachface, even though the leading edge of the mudbank tends to occur quite close to the shoreline. The mean depth of water at the offshore site was 10 m, and at the inshore site a little over 5 m. In fair weather the mudbank was well seaward of the offshore site, in deeper water. During the monsoon the nearshore edge of the bank was shoreward of the inshore site, while the seaward edge of the bank was close to the

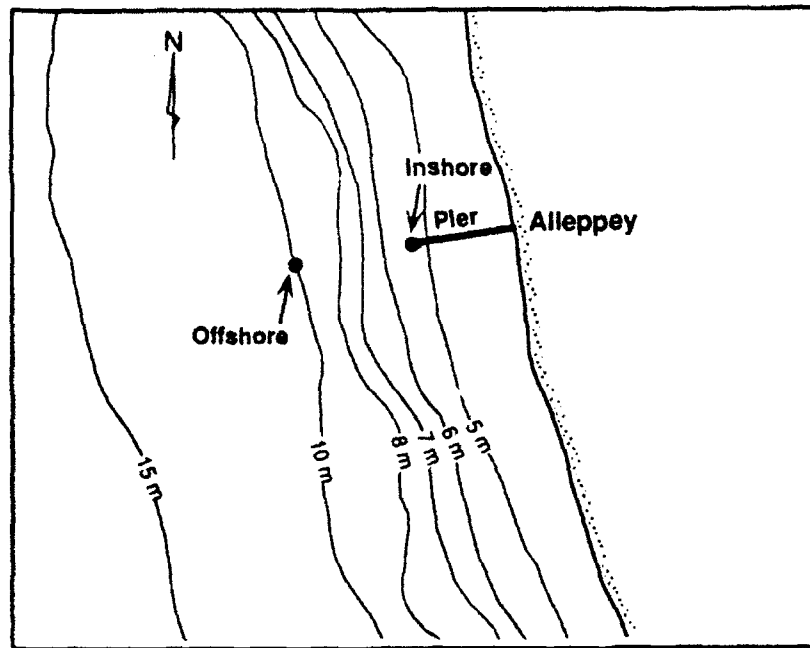


Figure 40. Coastal site off Alleppey in Kerala, India, where monsoonal, mudbanks occur. The pier is 300 m long (after Mathew, 1992).

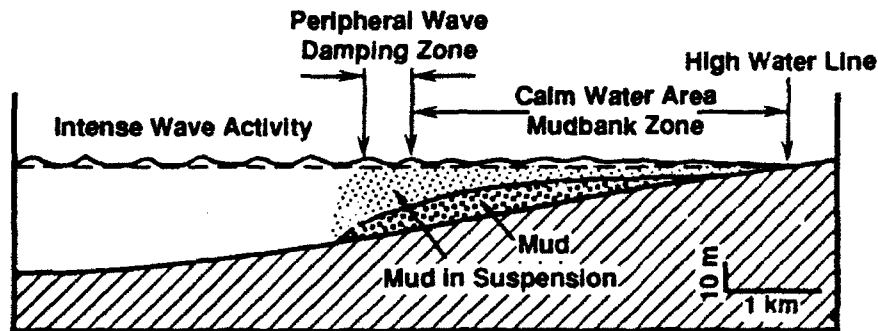


Figure 41. Schematic profile of mudbank off the coast of Kerala, India (after Nair, 1988).

offshore site. Thus the bottom at the offshore site was devoid of mud. Figures 42a,b respectively show examples of wave spectra in the absence and in the presence of 1 m thick mudbank at the inshore site. In fair weather the energy reduction is observed to have been negligible. (Note the slight phase shift of the inshore spectrum relative to offshore. This shift may be an artifact of the data analysis procedure.) In the monsoon case the energy reduction between the two stations was about 85%. In fact, as a result of the mudbank the wave energy at the inshore site was lower in monsoon than in fair weather, despite the occurrence of considerably more inclement offshore wave activity during the monsoon. Not surprisingly, monsoonal mudbanks in Kerala have served as open coast havens for small fishing vessels that would otherwise require sheltered harbors (Nair, 1988).

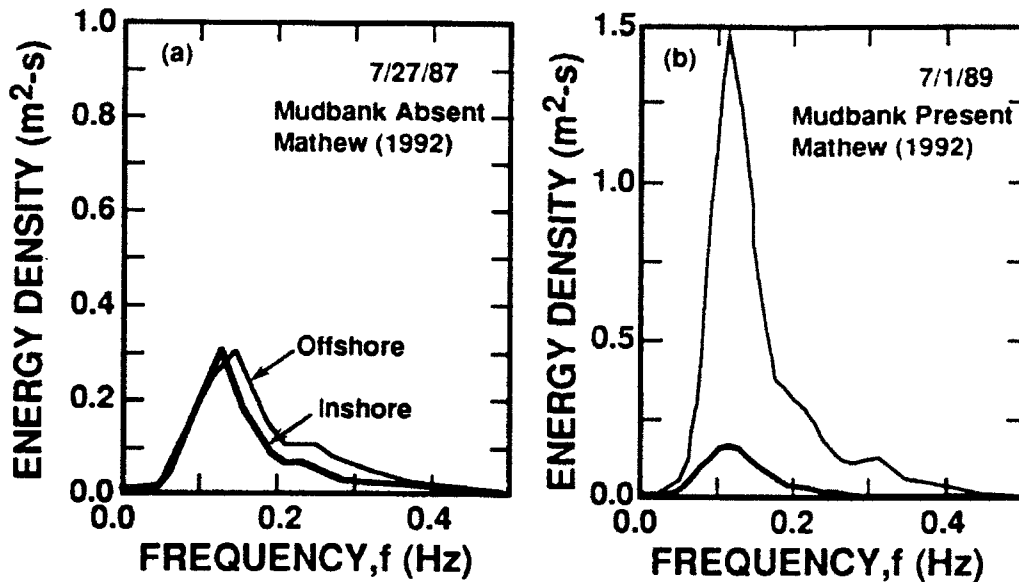


Figure 42. Offshore and inshore wave spectra off Alleppey: a) without mudbank; b) with mudbank (after Mathew, 1992).

The model of Jiang (1993) was applied to the Alleppey data on a frequency-by-frequency basis by selecting  $0.0025 \text{ m}^2/\text{s}$  for the eddy diffusivity,  $\epsilon_1$ , for the water column, a typical value (Lick, 1982), and taking the offshore wave spectrum as input at  $x=0$ . Note that in Eqs. 50 and 51,  $\nu_1 = \nu_t$  is replaced by  $\nu_1 + \epsilon_1$  to account for vertical diffusion due to turbulence in the water column in a very approximate way. The fair weather case (Fig. 42a) was treated by selecting arbitrarily high values of the rigidities  $G_1$  and  $G_2$  (applicable to Eq. 27 chosen as the constitutive model for mud rheology), in order to simulate a rigid (sandy) bottom. For the (1 m thick) mud bottom case, values of  $\mu_2(f)$ ,  $G_1(f)$  and  $G_2(f)$  for KI mud ( $\phi=0.12$ ) were inputted (Mehta and Jiang, 1993). Results shown in Figs. 43a,b indicate that the inshore wave spectra could be simulated reasonably well for the fair weather (Fig. 43a) as well as monsoon (Fig. 43b) scenarios. As noted previously the model yielded a depth-mean residual mud velocity (Stokes' drift) of 0.22 km/day, which seems to be consistent with the time-scale of mud motion at the onset of monsoon, even though no detailed mud velocity measurement are available for comparison purposes (Mathew, 1992).

### 5.5 MOBILE BERM, ALABAMA

The sediment placement site for the Mobile underwater berm off Dauphin Island in Alabama, created as a national demonstration project to highlight the beneficial role (wave height reduction in this case) of dredged material, is shown in Fig. 44. The material was derived from the ship channel within Mobile Bay (McLellan et al., 1990; Hands, 1990). Examples of offshore/inshore wave spectra are given in Figs. 45a,b under two different offshore wave conditions. Wave energy reductions were significant, 29% and 46% respectively. Using a fixed-bed hydrodynamic model McLellan et al. (1990) showed that assuming a rigid (i.e. fixed bed) berm crest produced negligible wave energy dissipation. It is believed that as a result of the shallow depth of water, on the order of

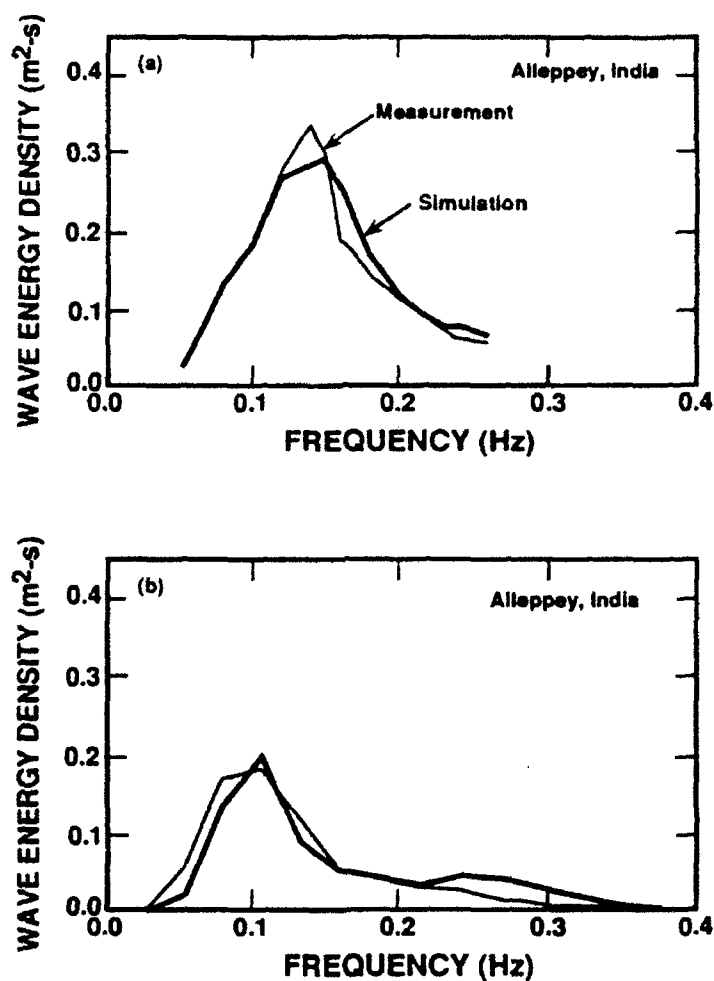


Figure 43. Comparison between measured and model-simulated inshore wave spectra off Alleppey in Kerala, India: a) fair weather condition (mudbank absent); b) monsoonal condition (mudbank present).

6.5 m over the berm, the main cause of damping is energy absorption by the deposited mud! Diver observations at the site suggested the occurrence of surface wave-forced interfacial mud waves propagating along the compliant crest (McLellan, personal communication). Such a movement can be construed as a manifestation of the participation of the bottom material in the energy dissipation process. Furthermore, the high degree of stability of the berm against displacement and deterioration pointed to the fact that wave action became sufficiently weak over the berm to prevent significant scour of the berm (Dredging Research Technical Notes, 1992).

The wave-mud interaction model of Jiang (1993) was used to simulate the inshore wave spectra at the Mobile berm site, given measured offshore spectra in Figs. 45a,b. The computations were done on a frequency-by-frequency basis. A 6 m berm height ( $=h_2$ ) and the 6.5 m water depth ( $=h_1$ ) were selected as representative vertical dimensions. In general, the effective berm width for calculating the degree of wave attenuation would depend on the direction of wave approach; for the present purpose a width of 140 m was selected, giving some allowance for

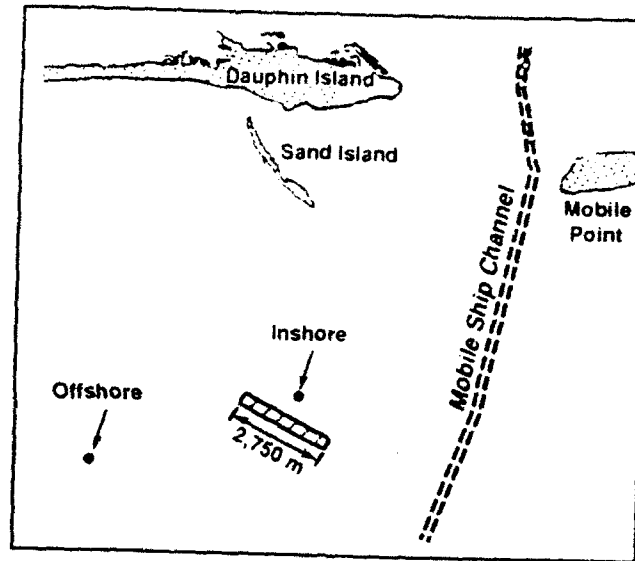


Figure 44. Construction site (2,750 m long corridor for dredged material placement) for the Mobile berm, and offshore/inshore sites of wave measurement (after McLellan et al., 1990).

the berm slopes. Thus dissipation was assumed to occur over this distance only. Rheological parameters for the mud (MB) are given in Table 9 (for  $\phi=0.11$ , corresponding to the *in situ* mud density).

Comparisons between simulated and measured inshore spectra are given in Figs. 46a,b. The simulated spectral energy is observed to be generally in agreement with the measurement at low frequencies, but is consistently lower than measured for frequencies exceeding about 0.25 Hz, i.e. periods smaller than 4 s. In that context it must be noted that, as a rule, the output spectrum from the model will have the same general shape as the offshore one, which also is the case here. Compare, for example, the measured offshore spectrum with the simulated inshore one in Fig. 46a. These two are generally similar in shape. Next compare the measured inshore spectrum with the measured offshore one in the same figure. Note that for frequencies greater than about 0.30 Hz the measured inshore wave energy was actually slightly higher than that at the offshore location. This feature suggests that the source of the high frequency inshore waves may have been at least partly different from that represented by the measured offshore spectrum. In any event, diagnostic applications such as this one provide a basis for developing design guidelines for wave absorbing berms in future. A hypothetical design example has been discussed by Mehta and Jiang (1993).

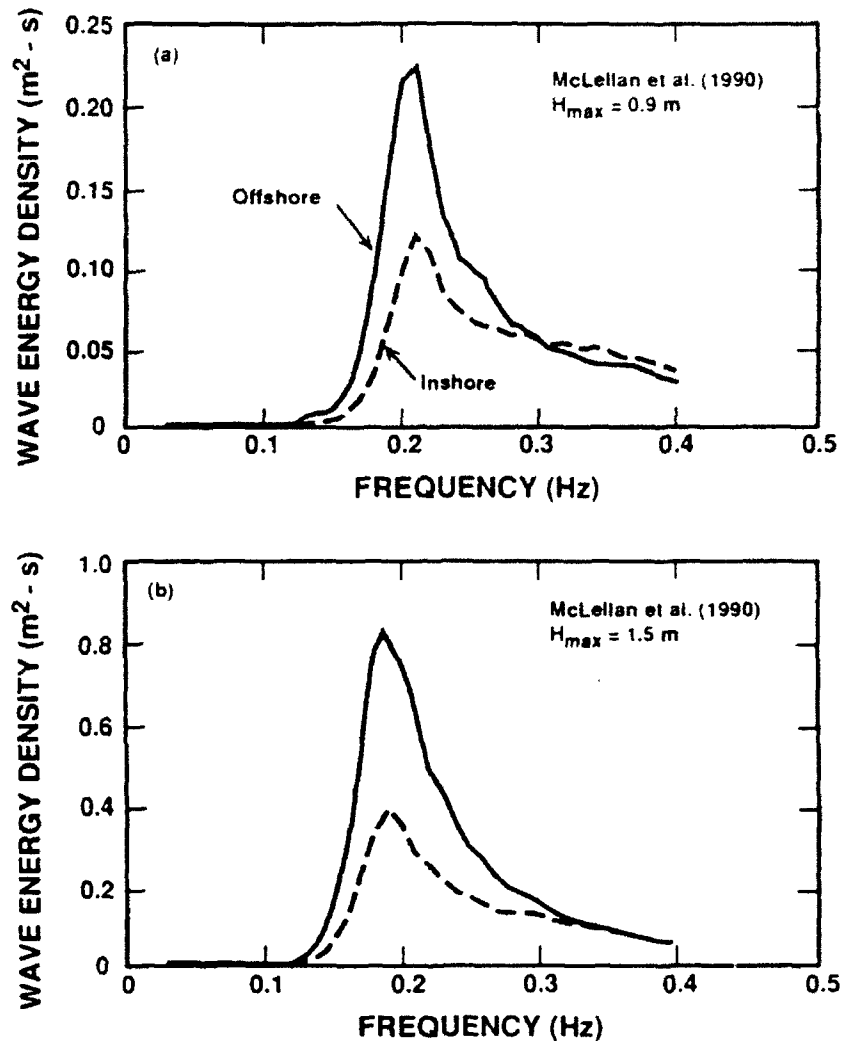


Figure 45. Offshore and inshore wave spectra at the Mobile berm site for two different wave conditions at the offshore site characterized by the maximum wave height,  $H_{max}$ : (a)  $H_{max} = 0.9$  m, and (b)  $H_{max} = 1.5$  m (after McLellan et al., 1990).

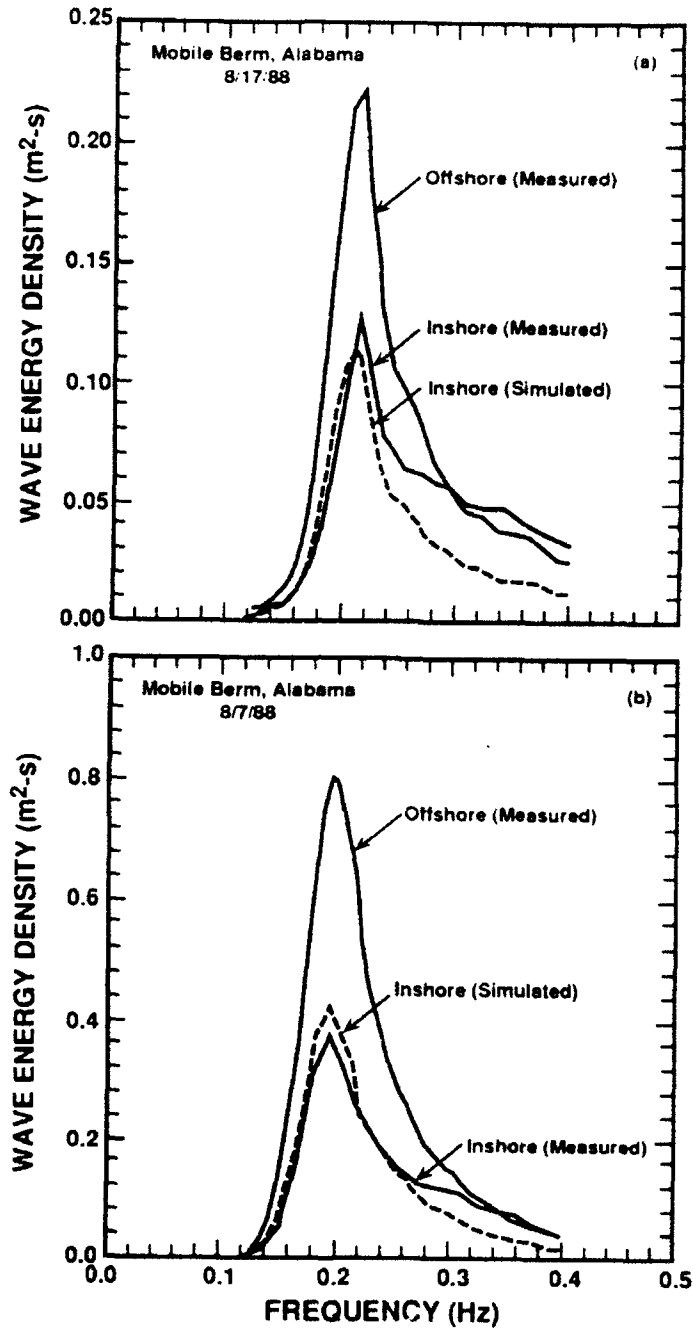


Figure 46. Comparison between measured and model-simulated inshore wave spectra at the Mobile berm site corresponding to two offshore wave conditions: (a)  $H_{max} = 0.9$  m (see Fig. 45a), and (b)  $H_{max} = 1.5$  m (see Fig. 45b). Measured offshore spectra have been included for reference.

## BIBLIOGRAPHY

- Adams C.E., Wells J.T. and Park Y.-A., 1993. Wave motions on a lutocline above a stably stratified bottom boundary layer. In.: *Nearshore and Estuarine Cohesive Sediment Transport*, A.J. Mehta ed., American Geophysical Union, Washington, DC, 393-410.
- Alishahi M.R. and R.B. Krone, 1964. Suspension of cohesive sediments by wind-generated waves. *Technical Report HEL-2-9*, Hydraulic Engineering Laboratory, University of California, Berkeley, 24p.
- Allen R.H., 1972. A glossary of coastal engineering terms. *Miscellaneous Paper 2-72*, U.S. Army Corps of Engineers Coastal Engineering Research Center, Fort Belvoir, VA, 55p.
- Barnes H.A., Hutton J.F. and Walters K., 1989. *An Introduction to Rheology*, Elsevier, Amsterdam, 208p.
- Cervantes E.E., 1987. A laboratory study of fine sediment resuspension by waves. *M.S. Thesis*, University of Florida, Gainesville, 64p.
- Chou H.T., 1989. Rheological response of cohesive sediments to water waves. *Ph.D. Dissertation*, University of California, Berkeley, 149p.
- Connors D.H., Risenberg F., Charney R.D., McEwen M.A., Krone R.B. and Tchobanoglous G., 1990. Research needs: salt marsh restoration, rehabilitation, and creation techniques for Caltrans construction projects. Report prepared for California Department of Transportation by the Civil Engineering Department, University of California, Davis, 61p.
- Cueva I.P., 1993. On the response of a muddy bottom to surface water waves. *Journal of Hydraulic Research*, 31(5), 681-696.
- Dalrymple R.A. and Liu P.L.-F., 1978. Waves over soft muds: a two-layer fluid model. *Journal of Physical Oceanography*, 8, 1121-1131.
- Dawson T.H., 1978. Wave propagation over a deformable sea floor. *Ocean Engineering*, 5, 227-234.
- Day P.R. and Ripple C.D., 1966. Effect of shear on suction in saturated clays. *Soil Society of America Proceedings*, 30, 625-679.
- Dean R.G. and Dalrymple R.A. 1984. *Water Wave Mechanics for Engineers and Scientists*, Prentice-Hall, Englewood Cliffs, NJ, 353p.
- Dredging Research Technical Notes, 1992. Monitoring Alabama berms. *DRP-1-08*, U.S. Army Engineer Waterways Experiment Station, Vicksburg, MS, 14p.
- Feng J., 1992. Laboratory experiments on cohesive soil bed fluidization by water waves. *M.S. Thesis*, University of Florida, Gainesville, 109p.
- Foda M.A., 1989. Sideband damping of water waves over a soft bed. *Journal of Fluid Mechanics*, 201, 189-201.
- Foda M.A., Tzang S.Y. and Maeno Y., 1991. Resonant soil liquefaction by water waves. *Proceedings of Geo-Coast '91*, 1, Port and Harbor Research Institute, Yokohama, Japan, 549-583.
- Foda M.A., Hunt J.R. and Chou H.-T., 1993. A non-linear model for the fluidization of marine mud by waves. *Journal of Geophysical Research*, 98(C4), 7039-7047.

- Gade H.G., 1957. Effects of a non-rigid, impermeable bottom on plane surface waves in shallow water. *M.S. Thesis*, Texas A & M University, College Station, 35p.
- Gade H.G., 1958. Effects of a non-rigid, impermeable bottom on plane surface waves in shallow water. *Journal of Marine Research*, 16(2), 61-82.
- Gleason P.J. and Stone P.A., 1975. Prehistoric trophic level status and possible cultural influences on the enrichment of Lake Okeechobee. *Unpublished Report*, South Florida Water Management District, West Palm Beach, 133p.
- Hands E.G., 1990. Results of monitoring the disposal berm at Sand Island, Alabama, report 1: construction and first year's response. *Technical Report DRP-90-2*, U.S. Army Engineer Waterways Experiment Station, Vicksburg, MS, 59p.
- Hsiao S.V. and Shemdin O.H., 1980. Interaction of ocean waves with a soft bottom. *Journal of Physical Oceanography*, 10, 605-610.
- Horikawa K., 1978. *Coastal Engineering*, Wiley, New York, 412p.
- Hunt L.M. and Groves D.G., 1965. *A Glossary of Ocean Science and Undersea Technology Terms*. Compass Publications, Arlington, VA, 180p.
- Hwang K.-N., 1989. Erodibility of fine sediment in wave-dominated environments. *M.S. Thesis*, University of Florida, Gainesville, 159p.
- Hwang P.A. and Wang H., 1982. Wave kinematics and sediment suspension at wave breaking point. *Technical Report No. 13*, Department of Civil Engineering, University of Delaware, Newark, 173p.
- Inglis C.C. and Allen F.H., 1957. The regimen of the Thames estuary as affected by currents, salinities, and river flow. *Proceedings of the Institution of Civil Engineers*, London, 7, 827-868.
- Isobe M., Huynh T.N. and Watanabe A., 1992. A study on mud mass transport under waves based on an empirical rheology model. *Proceedings of the 23rd Coastal Engineering Conference*, 3, ASCE, New York, 3093-3106.
- Jackson J.R., 1973. A model study of the effects of small amplitude waves on the resuspension of fine-grain cohesive sediments. *M.S. Thesis*, University of New Hampshire, Durham, 53p.
- James A.E., Williams D.J.A. and Williams P.R., 1988. Small strain, low shear rate rheometry of cohesive sediments. In: *Physical Processes in Estuaries*, J. Dronkers and W. van Leussen eds., Springer-Verlag, Berlin, 488-500.
- Jiang F., 1993. Bottom mud transport due to water waves. *Ph.D. Dissertation*, University of Florida, Gainesville, 222p.
- Jiang F. and Mehta A.J., 1992. Some observations on fluid mud response to water waves. In: *Dynamics and Exchanges in Estuaries and the Coastal Zone*, D. Prandle ed., American Geophysical Union, Washington, DC, 351-376.
- Jiang L. and Zhao Z., 1989. Viscous damping of solitary waves over fluid-mud seabeds. *Journal of Waterway, Port, Coastal, and Ocean Engineering*, 115(3), 345-362.

- Jiang L., Kioka W. and Ishida A., 1990. Viscous damping of cnoidal waves over fluid-mud seabed. *Journal of Waterway, Port, Coastal and Ocean Engineering*, 116(4), 470-491.
- Jonsson I.G., 1966. Wave boundary layer and friction factors. *Proceedings of the 10th Coastal Engineering Conference*, ASCE, New York, 127-148.
- Keedwell M.J., 1984. *Rheology and Soil Mechanics*. Elsevier, London, 339p.
- Kendrick M.P. and Derbyshire B.V., 1985. Monitoring of a near-bed turbid layer. *Report SR44*, Hydraulics Research, Wallingford, U.K., 20p.
- Kemp G.P. and Wells J.T., 1987. Observations of shallow-water waves over a fluid mud bottom: implications to sediment transport. *Proceedings of Coastal Sediments '87*, 1, ASCE, New York, 363-378
- Kirby R.R., Hobbs C.H. and Mehta A.J., 1989. Fine sediment regime of Lake Okeechobee, Florida. *Report UFL/COEL-89/009*, Coastal and Oceanographic Engineering Department, University of Florida, Gainesville, 77p.
- Krizek R.J., 1971. Rheological behavior of clay soils subjected to dynamic loads. *Transactions of the Society of Rheology*, 15(3), 433-489.
- Krone R.B., 1962. Flume studies of flocculation as a factor in estuarial shoaling processes. *Final Report*, Hydraulic Engineering Laboratory and Sanitary Engineering Research Laboratory, University of California, Berkeley, 118p.
- Krone R.B., 1979. Sedimentation in San Francisco Bay system. In: *The Urbanized Estuary*, California Academy of Sciences, San Francisco, 85-96.
- Lamb T.W. and Whitman R.V., 1969. *Soil Mechanics*. Wiley, New York, 563p.
- Lick W., 1982. Entrainment deposition and transport of fine-grained sediment in lakes. *Hydrobiologia*, 91, 31-40.
- Liu K.F. and Mei C.C., 1989. Effects of wave-induced friction on a muddy seabed modelled as a Bingham-plastic fluid. *Journal of Coastal Research*, 5(4), 777-789.
- Maa P.Y., 1986. Erosion of soft mud by waves. *Ph.D. Dissertation*, University of Florida, Gainesville, 296p.
- Maa, P.-Y. and Mehta A.J., 1987. Mud erosion by waves: a laboratory study. *Continental Shelf Research*, 7(11/12), 1269-1284.
- Maa P.-Y. and Mehta A.J., 1989. Considerations on soft mud response under waves. In: *Estuarine Circulation*, B.J. Neilson, A. Kuo, and J. Brubaker, eds., Humana Press, Clifton, NJ, 309-336.
- Maa P.Y. and Mehta A.J., 1990. Soft mud response to water waves. *Journal of Waterway, Port, Coastal, and Ocean Engineering*, 116(5), 634-650.
- MacPherson H., 1980. The attenuation of water waves over a non-rigid bed. *Journal of Fluid Mechanics*, 97(4), 721-742.
- Mallard W.W. and Dalrymple R.A., 1977. Water waves propagating over a deformable bottom. *Proceedings of the Offshore Technology Conference*, OTC 2895, Houston, 141-146.
- Mathew J., 1992. Wave-mud interaction in mudbanks. *Ph. D. Dissertation*, Cochin University of Science and Technology, Cochin, Kerala, India, 139p.

- McCave I.N., 1971. Wave-effectiveness at the sea bed and its relationship to bed-forms and deposition of mud. *Journal of Sedimentary Petrology*, 41(1), 89-96.
- McLellan T.N., Pope M.K. and Burke C.E., 1990. Benefits of nearshore placement. *Proceedings of the 3rd Annual National Beach Preservation Technology Conference*, Florida Shore and Beach Preservation Association, Tallahassee, 339-353.
- Mehta A.J., 1988. Laboratory studies on cohesive sediment deposition and erosion. In: *Physical Processes in Estuaries*, J. Dronkers and W. van Leussen eds., Springer-Verlag, Berlin, 427-445.
- Mehta A.J., 1989. On estuarine cohesive sediment transport. *Journal of Geophysical Research*, 94(C10), 14303-14314.
- Mehta A.J., 1990. Understanding fluid mud in a dynamic environment. *Geo-Marine Letters*, 11, 113-118.
- Mehta A.J., 1991a. Strategy for fine sediment regime investigation: Lake Okeechobee, Florida. *Proceedings of the International Conference on Coastal and Port Engineering in Developing Countries*, Mombasa, Kenya, 303-917.
- Mehta A.J., 1991b. Characterization of cohesive soil bed surface erosion, with special reference to the relationship between erosion shear strength and bed density. *Report UFL/COEL/MP-91/4*, Coastal and Oceanographic Engineering Department, University of Florida, Gainesville, 83p.
- Mehta A.J., 1991c. Review notes on cohesive sediment erosion. *Proceedings of Coastal Sediment '91*, 1, ASCE, New York, 40-53.
- Mehta A.J. and Maa P.-Y., 1986. Waves over mud: modeling erosion. *Proceedings of the Third International Symposium on River Sedimentation*, University of Mississippi, University, 588-601.
- Mehta A.J. and Srinivas R., 1993. Observations on the entrainment of fluid mud by shear flow. In: *Nearshore and Estuarine Cohesive Sediment Transport*, A.J. Mehta ed., American Geophysical Union, Washington, DC, 224-246.
- Mehta A.J. and Jiang F., 1990. Some field observations on bottom mud motion due to waves. *Report UFL/COEL-90/008*, Coastal and Oceanographic Engineering Department, University of Florida, Gainesville, 85p.
- Mehta A.J. and Jiang F., 1993. Some observations on water wave attenuation over nearshore underwater mudbanks and mud berms. *Report UFL/COEL/MP-93/01*, Coastal and Oceanographic Engineering Department, University of Florida, Gainesville, 45p.
- Mehta A.J. and Lee S.-C., 1994. Problems in linking the threshold condition for the transport of cohesionless and cohesive sediment grains. *Journal of Coastal Research* (in press).
- Mei C.C. and Liu K.F., 1987. A Bingham plastic model for muddy sea bed under long waves. *Journal of Geophysical Research*, 92(C13), 14581-14594.
- Migniot C. and Hamm, L., 1990. Consolidation and rheological properties of mud deposits. *Proceedings of the 22nd Coastal Engineering Conference*, 3, ASCE, New York, 2975-2983.

- Mimura N., 1993. Rates of erosion and deposition of cohesive sediments under wave action. In: *Nearshore and Estuarine Cohesive Sediment Transport*, A.J. Mehta, ed., American Geophysical Union, Washington, DC, 247-264.
- Mindlin R.D. and Deresiewicz H., 1953. Elastic spheres in contact under varying oblique forces. *Journal of Applied Mechanics*, 20, 327-344.
- Nair A.S.K., 1988. Mudbanks (chakara) of Kerala - a marine environment to be protected. *Proceedings of the National Seminar on Environmental Issues*, University of Kerala Golden Jubilee Seminar, Kerala, India, 76-93.
- National Research Council, 1989. *Using Oil Spill Dispersants on the Sea*. Committee on the Effectiveness of Oil Spill Dispersants, Marine Board, National Academy Press, Washington, DC, 352p.
- National Research Council, 1994. *Protecting and Restoring Marine Habitat: The Role of Engineering and Technology*. Committee on the Role of Technology in Marine Habitat Protection and Enhancement, Marine Board, National Academy Press, Washington, DC (under preparation).
- Nichols M.M., 1985. Fluid mud accumulation processes in an estuary. *Geo-Marine Letters*, 4, 171-176.
- Odd N.M.V. and Rodger J.G., 1986. An analysis of the behavior of fluid mud in estuaries. *Report SR84*, Hydraulics Research, Wallingford, U.K., 25p.
- Parchure T.M. and Mehta A.J., 1985. Erosion of soft cohesive sediment deposits. *Journal of Hydraulic Engineering*, 111(10), 1308-1326.
- Parker W.R. and Kirby R., 1982. Time dependent properties of cohesive sediment relevant to sedimentation management - a European experience. In: *Estuarine Comparisons*, V.S. Kennedy ed., Academic Press, San Diego, 573-590.
- Partheniades, E., 1977. Unified view of wash load and bed material load. *Journal of the Hydraulics Division of ASCE*, 103(9), 1037-1057.
- Ross M.A., 1988. Vertical structure of estuarine fine sediment suspensions. *Ph.D. Dissertation*, University of Florida, Gainesville, 206p.
- Ross M.A., Lin C.-P. and Mehta A.J., 1987. On the definition of fluid mud. *Proceedings of the 1987 National Conference on Hydraulic Engineering*, ASCE, New York, 231-236.
- Ross M.A. and Mehta A.J., 1989. On the mechanics of lutocline and fluid mud. *Journal of Coastal Research*, SI5, 51-61.
- Ross M.A. and Mehta A.J., 1990. Fluidization of soft estuarine mud by waves. In: *The Microstructure of Fine-Grained Sediments: From Mud to Shale*, R.H. Bennett ed., Springer-Verlag, New York, 185-191.
- Sakakiyama T. and Bijker E.W., 1989. Mass transport velocity in mud layer due to progressive waves. *Journal of Waterway, Port, Coastal, and Ocean Engineering*, 115(5), 614-633.
- Scarlato P.D. and Mehta A.J., 1993. Instability and entrainment mechanisms at the stratified fluid mud-water interface. In: *Nearshore and Estuarine Cohesive Sediment Transport*, A.J. Mehta, ed., American Geophysical Union, Washington, DC, 205-223.

- Schreuder F.W.A.M., Van Dieman A.J.G. and Stein H.N., 1986. Viscoelastic properties of concentrated suspensions. *Journal of Colloid and Interface Science*, 111(1), 35-43.
- Schuckman B. and Yamamoto T., 1982. Non-linear mechanics of sea-bed interactions part II - wave tank experiments on water wave damping by motion of clay beds. *Technical Report TR82-1*, Rosenstiel School of Marine and Atmospheric Science, University of Miami, 132p.
- Sheng Y.P., 1986. Finite-difference models for hydrodynamics of lakes and shallow seas. In: *Physics-based modeling of lakes, reservoirs and impoundments*, G. William ed., ASCE, New York, 146-228.
- Sheng Y.P., Cook V., Peene S., Eliason D., Wang P.F. and Schofield S., 1986. A field and modeling study of fine sediment transport in shallow waters. In: *Estuarine and Coastal Modeling*, M.L. Spalding ed., ASCE, New York, 113-122.
- Shibayama T., Takikawa H. and Horikawa K., 1986. Mud mass transport due to waves. *Coastal Engineering in Japan*, 29, 151-161.
- Shibayama T., Aoki T. and Sato S., 1989. Mud mass transport rate due to waves: a viscoelastic model. *Proceedings of the 23rd IAHR Congress*, Ottawa, Canada, B567-B574.
- Shibayama T., Okuno M. and Sato S., 1990. Mud transport rate in mud layer due to wave action. *Proceedings of the 22nd Coastal Engineering Conference*, 3, ASCE, New York, 3037-3049.
- Smith J.D., 1977. Modeling of sediment transport on continental shelves. In: *The Sea*, Vol. 6, E.D. Goldberg et al. eds., Wiley, New York, 539-577.
- Smith T.J. and Kirby R., 1984. Generation, stabilization and dissipation of layered fine sediment suspensions. *Journal of Coastal Research*, S15, 63-73.
- Somlyódy L., Herodek S. and Fischer J., editors, 1983. *Eutrophication of Shallow Lakes: Modeling and Management, the Lake Balaton Case Study*. International Institute for Applied Systems Analysis, Laxenburg, Austria, 377p.
- Sterling G.H. and Strohbeck E.E., 1973. The failure of the South Pass 70 "B" platform in hurricane Camile. *Proceedings of the 5th Offshore Technology Conference*, Houston TX, 719-730.
- Suhayda J.N., 1986. Interaction between surface waves and muddy bottom sediments. In: *Estuarine Cohesive Sediment Dynamics*, A.J. Mehta, ed., Springer-Verlag, Berlin, 401-428.
- Thiers G.R. and Seed H.B., 1968. Cyclic stress-strain characteristics of clays. *Journal of the Soil Mechanics and Foundations Division of ASCE*, 92(2), 555-569.
- Thimakorn P., 1980. An experiment on clay suspension under water waves. *Proceedings of the 17th Coastal Engineering Conference*, 3, ASCE, New York, 2894-2906.
- Thimakorn P., 1984. Resuspension of clays under waves. In: *Seabed Mechanics*, B. Denness ed., Graham and Trotman, London, 191-196.
- Tsuruya H., Nakano S. and Takahama J., 1987. Interactions between surface waves and a multi-layered mud bed. *Report of the Port and Harbor Research Institute*, Ministry of Transport, Japan, 26(5), 137-173.

- Tsuruya H., Murakami K. and Irie I., 1990. Numerical simulation of mud transport by a multi-layered nested grid model. *Proceedings of the 22nd Coastal Engineering Conference*, 3, ASCE, New York, 2998-3011.
- Tubman M. and Suhayda J.N., 1976. Wave action and bottom movements in fine sediments. *Proceedings of the 15th International Coastal Engineering Conference*, ASCE, New York, 1168-1183.
- Tver D.F., 1979. *Ocean and Marine Dictionary*. Cornell Maritime Press, Centerville, MD, 367p.
- Wang H. and Xue H.-C., 1990. China-U.S. joint muddy coast research, part 1, a review of hydrological and sedimentary processes in Hangzhou Bay, China. *Report UFL/COEL-90/014*, Coastal and Oceanographic Engineering Department, University of Florida, Gainesville, 60p.
- Wells J.T., 1983. Dynamics of coastal fluid muds in low-, moderate, and high-tide-range environments. *Canadian Journal of Fisheries and Aquatic Sciences*, 40(1), 130-142.
- Wells J.T. and Kemp G.P., 1986. Interaction of surface waves and cohesive sediments: field observations and geologic significance. In: *Estuarine Cohesive Sediment Transport*, A.J. Mehta ed., Springer-Verlag, Berlin, 43-65.
- Williams D.J.A. and Williams P.R., 1992. Laboratory experiments on cohesive soil bed fluidization by water waves, part II, in situ rheometry for determining the dynamic response of bed. *Report UFL/COEL-92/015*, Coastal and Oceanographic Engineering Department, University of Florida, Gainesville, 24p.
- Wolanski E., Chappell J., Ridd P. and Verbessy R., 1988. Fluidization of mud in estuaries. *Journal of Geophysical Research*, 93(C3), 2351-2361.
- Wolanski E., Gibbs R., Ridd P. and Mehta A., 1992. Settling of ocean-dumped dredged material, Townsville, Australia. *Estuarine, Coastal and Shelf Science*, 35, 473-489.
- Yamamoto T., 1982. Nonlinear mechanics of water waves interactions with sediment beds. *Applied Ocean Research*, 4(2), 99-106.
- Yamamoto T., 1983. On the response of a Coulomb-damped poroelastic bed to water waves. *Marine Technology*, 5(2), 93-130.
- Yamamoto T., Koning H.L., Sellmeijer H. and Van Hijum E., 1978. On the response of the poro-elastic bed to water wave. *Journal of Fluid Mechanics*, 87(1), 193-206.
- Yamamoto T. and Takahashi S., 1985. Wave damping by soil motion. *Journal of Waterway, Port, Coastal, and Ocean Engineering*, 111(1), 62-77.

APPENDIX A: EXPLANATORY NOTES FOR TABLE 7

*Note 1:* The solution is based on a two-fluid system consisting of an inviscid fluid overlying a lower viscous mud layer in laminar flow, which is assumed to be infinite in depth, driven by linear water waves. A boundary layer approach via prescription of a boundary layer correction to the velocity potential in the mud region is then adopted whereby mud flow is assumed inviscid except in the boundary layer region. Two wave modes emerge from the solution. The first mode,  $\omega^2 = gk$ , which is only true for infinitely deep mud layer, precludes a discontinuity of horizontal velocity across the interface and, hence, there is no boundary layer formation and no associated damping. For the second mode,  $\omega^2/gk_r = [(\rho_2/\rho_1) - 1] \tanh kh_1 / [(\rho_2/\rho_1) + \tanh kh_1]$ , the wave-mean rate of viscous energy dissipation per unit area in the boundary layer is computed from:

$$\varepsilon_D = \rho_2 \nu_2 \int_{-\infty}^{-h_1} \left[ \frac{\partial u_2}{\partial z} \right]^2 dz = \left[ \frac{1}{4\sqrt{2}} \right] \left[ \frac{\rho_2}{\omega} \left( \frac{2\nu_2}{\omega} \right)^{1/2} e^{2k_r h_1} (\omega^2 - gk_r)^2 a_0^2 \right] \quad (\text{A.1})$$

The relative dominance of the two wave modes is decided by the nature of wave generation (Dean and Dalrymple, 1984). While the first mode is more likely under the circumstance of waves propagating into a muddy region, the second mode will dominate if the waves are generated at the interface by a displacement of the mud.

*Note 2:* The solution is based on a two-layered viscous fluid system driven by linear water waves propagating in water of constant depth,  $h_1$ , overlying a viscous mud layer of thickness,  $h_2$ , with appropriate boundary layer approximation to render the solution analytical. These solutions apply when the parameters,  $\epsilon_i = (\omega^2/g)(\nu_i/\omega)^{1/2}$ ,  $i = 1, 2$ , are small whence the motion is essentially irrotational except near boundaries where the viscous boundary layer thickness is on the order of  $(2\nu_i/\omega)^{1/2}$ ,  $i = 1, 2$ . Hence, the solutions are valid for large values of  $[\omega/(2\nu_i)]^{1/2} h_i$ , i.e., the mud depth is large relative to the wave boundary layer thickness. Assuming that the free surface is uncontaminated, energy dissipation occurs only in the boundary layers, and is partitioned as follows:

$$\varepsilon_{D1} = \rho_1 \nu_1 \int_{-h_1}^{-\infty} \left[ \frac{\partial u_1}{\partial z} \right]^2 dz \quad (\text{A.2})$$

$$\varepsilon_{D2} = \rho_2 \nu_2 \int_{-\infty}^{-h_2} \left[ \frac{\partial u_2}{\partial z} \right]^2 dz \quad (\text{A.3})$$

$$\varepsilon_{D3} = \rho_2 \nu_2 \int_{(h_1-h_2)}^{-\infty} \left[ \frac{\partial u_1}{\partial z} \right]^2 dz \quad (\text{A.4})$$

where  $u_i$ ,  $i=1,2,3$  denote the rotational velocity components in the direction of wave propagation in the respective boundary layers,  $\epsilon_{D1}$  is the mean energy dissipation rate in the water boundary layer near the interface,  $\epsilon_{D2}$  is the mean energy dissipation rate in the mud boundary layer near the interface and  $\epsilon_{D3}$  is the mean energy dissipation rate in the mud boundary layer near the rigid bottom, overbar denotes time averaging and " $\pm \infty$ " implies "outside" the boundary layer. The various terms are given by:

$$u_1 = C_1 \exp\{-(1+i)[\omega/(2\nu_1)]^{1/2}(z+h_1)\} \exp[i(kx-\omega t)]$$

$$u_2 = C_2 \exp\{-(1+i)[\omega/(2\nu_2)]^{1/2}(z+h_1)\} \exp[i(kx-\omega t)]$$

$$u_3 = C_3 \exp\{-(1+i)[\omega/(2\nu_2)]^{1/2}(z+h_1+h_2)\} \exp[i(kx-\omega t)],$$

$$C_1 = \{-[gka/(\omega \sinh kh_1)] [(\rho_2/\rho_1)(\nu_2/\nu_1)^{1/2} / \{1 + (\rho_2/\rho_1)(\nu_2/\nu_1)^{1/2}\}] \{(\omega^2/gk) - [(1/2)\sinh 2kh_1] (\coth kh_1 + \coth kh_2) [(\omega^2/gk) - \tanh kh_1]\}\},$$

$$C_2 = -(\rho_1/\rho_2)(\nu_1/\nu_2)^{1/2} C_1$$

$$C_3 = \{-gka/\omega \cosh kh_1 [(\omega^2/gk) - \tanh kh_1]\} / \sinh kh_2$$

and the wave number is solved iteratively from:

$$\omega^2/gk = [-1 - (l^2 - 4mn)^{1/2}] / (2m)$$

where

$$l = -(\rho_2/\rho_1) \tanh k(h_1 + h_2) (1 + \tanh kh_1 \tanh kh_2)$$

$$m = (\rho_2/\rho_1) + \tanh kh_1 \tanh kh_2$$

$$n = [(\rho_2/\rho_1) - 1] \tanh kh_1 \tanh kh_2$$

*Note 3:* The rate of wave energy dissipation is computed by assuming mud as a viscous medium (Dean and Dalrymple, 1984):

$$\epsilon_D = \rho \nu \int_0^{h_1+h_2} \left[ 2 \left( \frac{\partial u}{\partial x} \right)^2 + \left( \frac{\partial w}{\partial x} + \frac{\partial u}{\partial z} \right)^2 \right] dz \quad (A.5)$$

where the overbar denotes wave-mean value, and  $h_1$  and  $h_2$  denote the depths of water and mud layers, respectively. A shallow water wave-mud interaction model (Jiang and Mehta, 1993), which describes a two-layered mud/water system forced by progressive surface waves of periodicity specified by wave frequency,  $\omega$ , is used to compute the required velocity gradient inputs.

Since the model assumes an inviscid upper water layer on the premise that pressure and inertial forces are typically dominant in governing water motion and an irrotational flow field is an apt description here, wave dissipation in the water layer is nil. Furthermore, by ignoring the velocity gradient in the vertical (shallow water assumption), the above equation simplifies to:

$$\epsilon_D = \rho_2 \nu_2 \int_0^{h_1} \left[ 2 \left( \frac{\partial u}{\partial x} \right)^2 + \left( \frac{\partial u}{\partial z} \right)^2 \right] dz \quad (\text{A.6})$$

which may be conveniently divided into two terms,

$$\epsilon_D = \epsilon_{D1} + \epsilon_{D2} = \rho_2 \nu_2 \int_0^{h_1} \left[ \left( \frac{\partial u}{\partial x} \right)^2 \right] dz + \rho_2 \nu_2 \int_0^{h_1} \left[ \left( \frac{\partial u}{\partial z} \right)^2 \right] dz \quad (\text{A.7})$$

The appropriate final expressions are (Feng, 1992):

$$\epsilon_{D1} = \left| \rho_2 \nu_2 h_1 \omega^2 \bar{k}^2 \left( \frac{A \bar{k}}{F_r} \right)^2 \left[ 1 - r \left( \frac{\bar{k}}{F_r} \right)^2 \right]^2 \left[ \frac{3}{2} \bar{h}_2 - \frac{1}{2} \bar{h}_2 A_0^2 + \frac{2A_0}{m} (B_0 - 1) - \frac{A_0}{2m} (B_1 - 1) - \frac{2}{m} C_0 + \frac{(1 + A_0^2)}{4m} C_1 \right] \right| \quad (\text{A.8})$$

$$\epsilon_{D2} = \left| \frac{1}{2} \rho_2 \nu_2 h_1 m^2 \omega^2 \left( \frac{A \bar{k}}{F_r} \right)^2 \left[ 1 - r \left( \frac{\bar{k}}{F_r} \right)^2 \right]^2 \left[ \frac{(A_0^2 - 1)}{2} \bar{h}_2 + \frac{(1 + A_0^2)}{4m} C_1 - \frac{1}{2m} A_0 (B_1 - 1) \right] \right| \quad (\text{A.9})$$

where  $A = a/h_1$ ,  $A_0 = \tanh(m\bar{h}_2)$ ,  $B_0 = \cosh(m\bar{h}_2)$ ,  $C_0 = \sinh(m\bar{h}_2)$ ,  $B_1 = \cosh(2m\bar{h}_2)$ ,  $C_1 = \sinh(2m\bar{h}_2)$ ,  $\bar{h}_2 = h_2/h_1$ ,  $m = (-iR_e)^{1/2}$ ,  $i = (-1)^{1/2}$ , and  $R_e = \omega h_1^2 / \nu_2$  is the wave Reynolds number.  $\bar{k} = kh_1$  is the normalized complex wave number given by:

$$\frac{\bar{k}}{F_r} = \left[ \frac{1 + \bar{h}_2 \Gamma - [(1 + \bar{h}_2 \Gamma)^2 - 4r\bar{h}_2 \Gamma]^{1/2}}{2r\bar{h}_2 \Gamma} \right]^{1/2} \quad (\text{A.10})$$

where  $k = k_r + ik_i$ ,  $k_r$  = wave number,  $k_i$  = wave attenuation coefficient,  $r = (\rho_2 - \rho_1) / \rho_2$ ,  $\Gamma = 1 - \tanh(m\bar{h}_2) / (m\bar{h}_2)$  and  $F_r = \omega(h_1/g)^{1/2}$  is the wave Froude number.

*Note 4:* The solution is based on a system consisting of linear water waves propagating over a non-rigid bed characterized as a Voigt viscoelastic body overlain by inviscid water, with appropriate assumptions to obtain an explicit expression for wave attenuation. By introducing a viscoelastic parameter,  $\nu^* = \nu_e = \nu_2 + iG/\omega\rho_2$ , where  $G$  is the shear modulus of elasticity, it is shown that the equations of motion for a viscoelastic medium can be reduced to the form of the linearized Navier-Stokes equations for a viscous fluid. The following assumptions are then introduced to render the solutions explicit:

- a) Oscillations of the bed due to the propagating waves are small in comparison with the surface waves, as in the case of an almost rigid bed, or mathematically,  $|k^2 \nu_c / \omega| \gg 1$  where  $k$  is the complex wave number defined in Note 3;
- b) Mud region is assumed to be infinite in depth;
- c) Wave length is assumed long compared to water depth.

The resulting expression for  $k$ , after ignoring higher order terms, becomes:

$$k \approx \frac{\omega}{\sqrt{gh_1}} + \frac{\rho_1 g G}{4 \rho_2^2 \omega^2 (\nu_2^2 + G^2 / \rho_2^2 \omega^2)} + \frac{i \rho_1 g \nu_2}{4 \rho_2 \omega (\nu_2^2 + G^2 / \rho_2^2 \omega^2)} \quad (\text{A.11})$$

The mean rate of energy dissipation is then computed based on the mean work done on the lower layer per unit area of the interface as:

$$\epsilon_D = \frac{1}{T} \int_0^T p_1 w_1 dt \quad (\text{A.12})$$

on  $z=\eta_2=0$  after linearizing, where  $T$  = wave period, and  $p_1$  and  $w_1$  are the pressure and vertical velocity, respectively, in water. Upon time-averaging and integration, the following expression results:

$$\epsilon_D = \left[ \frac{1}{2} \rho_1 g \right] \left\{ \omega A_r^2 \operatorname{Im} \left[ \frac{\omega^2 (gk \cosh kh_1 - \omega^2 \sinh kh_1)}{gk (gk \sinh kh_1 - \omega^2 \cosh kh_1)} \right] a^2 \right\} \quad (\text{A.13})$$

where  $A_r = \frac{2\sqrt{gh_1}}{\omega} \left| \frac{\rho_1 g G + i \rho_1 \rho_2 g \nu_2 \omega}{4 \rho_2^2 \omega^2 (\nu_2^2 + G^2 / \rho_2^2 \omega^2)} \right|$  is defined as the amplitude ratio.

*Note 5:* The dissipation mechanism employed here is that due to Yamamoto and Takahashi (1985), attributed to wave-induced motion in the soil bed. Based on a theoretical analysis for two elastic spheres, Mindlin and Deresiewicz (1953) found that the nonlinear elasticity and the energy dissipation of granular materials, e.g. soils, are due to Coulomb friction and are independent of the forcing frequency. In the frequency domain, the constitutive relation is approximately given by the linear model,  $\tau = \bar{G} \gamma$ , where  $\tau$  = shear stress,  $\gamma$  = shear strain and  $\bar{G} = G(1 + i\delta)$  is the complex shear modulus. The real part,  $G$ , is the dynamic shear modulus, and  $\delta$  is the specific loss given by  $\delta = \Delta W / 2\pi W$ , in which  $\Delta W$  = energy loss per cycle and  $W$  is the maximum elastic energy given by  $W = 0.5G\gamma'^2$ , where  $\gamma'$  = shear strain amplitude, both being expressed per unit area. The effect of soil Coulomb friction on the attenuation of water waves is approximately estimated by the analytical solution obtained by Yamamoto et al. (1978) for the quasi-static response of a homogeneous half-space of porous elastic medium to water

waves. It is assumed that the soil moduli,  $G$  and  $\delta$ , are constant throughout the bed. It is noted that the pure shear strain condition is induced in the bed by the water wave for the entire phase. The magnitudes of the shear stress,  $\tau_m$ , and the shear strain,  $\gamma_m$ , are only a function of depth,  $z$ , and are given by  $\tau_m = -p_0 k_0 z e^{k_0 z}$  and  $\gamma_m = -(p_0/G) k_0 z e^{k_0 z}$ , respectively. Here  $p_0$  is the amplitude of bottom pressure given by  $p_0 = \rho_1 g a (1/\cosh k_0 h_1)$ , which is the wave-induced dynamic pressure component based on linear wave theory.

The energy loss,  $\Delta W$ , due to soil Coulomb friction is given by:

$$\Delta W = 2\pi\delta \int_{-h_1}^{-\infty} \frac{1}{2} \tau_m \gamma_m dz \quad (\text{A.14})$$

which after integration becomes:

$$\Delta W = \frac{\pi}{2} \frac{(\rho_1 g)^2 a^2 \delta}{k_0 G \cosh^2 k_0 h_1} \quad (\text{A.15})$$

where  $k_0$  is the wave number for a rigid bottom. Accordingly, the rate of energy dissipation becomes:

$$\epsilon_D = \frac{\Delta W}{T} = \frac{(\rho_1 g)^2}{4} \frac{\omega \delta a^2}{G k_0 \cosh^2 k_0 h_1} \quad (\text{A.16})$$

*Note 6:* Here the approximate analysis assuming quasi-static motion of homogeneous soil bed (see Note 5) is improved upon by utilizing the dynamic theory for the case of a homogeneous half space of Coulomb-damped poroelastic medium to account for the coupling of water waves and the bed motion (Yamamoto, 1982; 1983). While two separate expressions for wave attenuation coefficient, due to soil Coulomb friction and percolation, respectively, are obtained, only the former is used here based on the premise that typical permeability in mud is very small. Substituting into the steady state wave energy equation for a constant water depth,  $C_g dE/dx = -\epsilon_D$ , and assuming an exponential decay law then leads to:

$$\epsilon_D = \left[ \frac{\rho_1^2 g^2}{4} \right] \left\{ \frac{\omega \delta a^2}{G k_0 \cosh^2 k_0 h_1} \left[ \frac{1}{(1 - \omega^2/\omega_0^2)^2 + \delta^2} \right] \right\} \quad (\text{A.17})$$

where  $\omega_0^2 = 2Gk_0^2/\rho_2$ .

*Note 7:* This semi-empirical approach is based on field measurement in East Bay, Louisiana in water depth of 20 m where the bottom sediments are composed of clays and silts. The instruments used included a wave staff, a pressure

sensor and a bottom-emplaced accelerometer. The general characteristics of the data showed that the motions can be adequately described in terms of the following harmonic functions:

$$p = p_0 + \rho_1 g A \cos(k_r x - \omega t) \quad (\text{A.18})$$

$$h_2 = h_{20} + M A \cos(k_r x - \omega t + \theta) \quad (\text{A.19})$$

where  $p$  = wave-induced bottom pressure,  $p_0$  = steady-state bottom pressure,  $A$  = surface wave amplitude,  $h_{20}$  = depth of mud over which motion occurs,  $M$  = proportionality constant between the amplitudes of the mud wave and the pressure wave; and  $\theta$  = phase angle between the crest of the pressure wave and the crest of the mud wave. The mean rate of energy dissipation is then computed based on the average energy transmitted through the sea/sediment interface per unit area over one wave cycle:

$$\epsilon_D = \frac{1}{T} \int_0^T p \frac{dh_2}{dt} dt \quad (\text{A.20})$$

where  $dh_2$  = an infinitesimal increase in the height of the interface. Using linear wave theory to interpret bottom pressures in terms of surface wave height, and upon integration, the mean rate of energy dissipation due to mud wave motion becomes:

$$\epsilon_D = \left[ \frac{\rho_1 g}{2} \right] \left[ \frac{\omega M \sin \phi a^2}{\cosh^2 k_r h_1} \right] \quad (\text{A.21})$$

where  $\phi = 180^\circ - \theta$ . Values of  $M$  and  $\phi$  can be obtained either from a theoretical approach or field measurement.

*Note 8:* The energy dissipation per unit volume in a linear viscoelastic medium over one cycle is given by:

$$\Delta E = \int_{\omega t = \pi - \delta'}^{\omega t = 2\pi - \delta'} \tau \dot{\gamma} dt = \pi \gamma_0^2 G'' \quad (\text{A.22})$$

where  $\delta'$  = loss angle,  $\tau$  = shear stress,  $\dot{\gamma}$  = shear rate,  $\gamma_0$  = shear strain at steady state,  $G''$  = loss modulus. Hence, the rate of energy dissipation (per unit volume) becomes:

$$\epsilon_v = \left[ \frac{\omega}{2\pi} \right] \Delta E = \frac{1}{2} \omega^2 \gamma_0^2 \mu' \quad (\text{A.23})$$

where  $\mu'$  = dynamic viscosity.

By defining an average value of  $\dot{\gamma}$  by (Schreuder et al., 1986):

$$\langle \dot{\gamma} \rangle = \frac{\int_0^T \dot{\gamma} d(\omega t + \delta')}{\int_0^T d(\omega t + \delta')} = \frac{2\omega\gamma_0}{\pi} \quad (\text{A.24})$$

then,

$$\varepsilon_v = \left[ \frac{\pi^2}{8} \right] (\mu' \langle \dot{\gamma} \rangle^2) \quad (\text{A.25})$$

The same expression can also be obtained by considering the response of a viscoelastic material to a small-amplitude oscillatory shear. Given  $\tau = \tau_0 e^{-i\omega t}$ ,  $\gamma = \gamma_0 e^{i(\omega t + \delta')}$ ,  $G^* = \tau/\gamma = G_0 e^{-\delta'} = G' - iG''$  where  $G^*$  = complex shear modulus,  $G'$  = storage modulus and  $G''$  = loss modulus, the time-averaged energy dissipation per unit volume over a wave period,  $\varepsilon_v$ , reads:

$$\varepsilon_v = \frac{1}{T} \int_0^T \text{Re}(\tau) \text{Re}(\dot{\gamma}) dt = \frac{G'' \gamma_0^2 \omega}{2} \quad (\text{A.26})$$

where Re denotes real part. By writing the complex viscosity as  $\mu^* = \mu' + i\mu''$ , it can be shown that  $G'' = \omega\mu''$  and, hence, the equivalence of the right-hand sides of Eq. A.23 and Eq. A.26.

Assuming a uniform energy dissipation per unit volume across the depth of mud layer in analogy with that of uniform energy dissipation in the water column due to breaking-induced turbulence, the mean rate of energy dissipation *per unit area* can be written as:

$$\varepsilon_D = \int_{z_h}^{-\infty} \varepsilon_v dz \quad (\text{A.27})$$

Given  $h_2 = h_2(x)$  as the equilibrium mud thickness,

$$\varepsilon_D = \left[ \frac{\pi^2}{8} \right] (\mu' \langle \dot{\gamma} \rangle^2 h_2) \quad (\text{A.28})$$

The above expression can then be evaluated by selecting an appropriate viscoelastic model, e.g. Voigt body, to compute the relevant input parameters.

APPENDIX B. A SUMMARY OF SOME WAVE-MUD MODELING STUDIES

Investigator(s)	Water Column	Mud	Modeling Depth	Theory	Brief Description
Gade (1957, 1958)	Inviscid	Viscous <sup>a</sup>	Shallow water	Linear	Analytical approach for wave attenuation; laboratory tests on wave amplitude decay and interfacial profiles, using a two-fluid system (kerosine overlying water-sugar solution).
Mallard and Dalrymple (1977)	inviscid	Elastic <sup>a</sup>	Mud thickness unbounded	Linear	Analytical approach for soil stresses, displacement and wave kinematics. Soil inertia neglected. No energy dissipation since viscous property of mud not considered.
Dalrymple and Liu (1978)	Viscous	Viscous <sup>a</sup>		Linear	Analytical approach for wave attenuation. Model valid for any water depth and both deep and shallow mud layers; boundary layer approximation; explicit solutions.
Dawson (1978)	inviscid	Elastic <sup>a</sup>	Mud thickness unbounded	Linear	Same as Mallard and Dalrymple (1978), but soil inertia taken into account.
Hsiao and Shemdin (1980)	Inviscid	Viscoelastic <sup>a</sup> (Voigt)		Linear	Analytical approach for wave attenuation.
MacPherson (1980)	Inviscid	Viscoelastic <sup>a</sup> (Voigt)		Linear	Analytical approach for wave attenuation.
Yamamoto (1982, 1983); Yamamoto and Takahashi (1985)	Inviscid	poroelastic <sup>b</sup>	Multi-layered mud	Linear	Based on nonlinear poroelastic theory that includes nonlinear and imperfect elasticity of soil skeleton. Bed response nonlinear and dynamically amplified; primary dissipation mechanism internal Coulomb friction between grains. Arbitrary distribution of continuously varying soil properties with depth. Quasi-static response more appropriate for hard bed such as sands, while dynamic response for soft beds such as clays.
Mehta and Maa (1986); Maa and Mehta (1987, 1989)	Viscous	Viscoelastic <sup>a</sup> (Voigt)	Multi-layered mud	Linear	Analytical approach with laboratory tests on wave attenuation and mud motion.

Investigator(s)	Water Column	Mud	Modeling Depth	Theory	Brief Description
Shibayama et al. (1986)	Viscous	Viscous <sup>a</sup>		Linear	Analytical approach using explicit velocity field of Dalrymple and Liu (1978) and laboratory tests on mud mass transport and attenuation rate.
Suhayda (1986)	Inviscid	Viscoelastic <sup>a</sup> (Nonlinear)	Mud thickness unbounded	Linear	Analytical approach based on the explicit results of MacPherson (1980); assumptions of small interfacial oscillations and infinite mud thickness. Nonlinear expressions relating shear strain to shear stress and damping ratio.
Mei and Liu (1987)	Inviscid	Viscoplastic <sup>a</sup> (Bingham, thin layer)	Shallow water; thin mud layer	Linear and Solitary	Analytical approach for wave attenuation. Laminar constitutive model and interfacial shear stress $\ll$ mud yield stress. Predicts continuous to intermittent mud motion.
Tsuruya et al. (1987)	Viscous	Viscoplastic <sup>a</sup> (Bingham)	Multi-layered mud	Linear	Analytical approach by extending Dalrymple and Liu's (1978) viscous-fluid model to Bingham fluid. Laboratory tests on mud mass transport and wave attenuation. Equivalent viscosity that takes into account the non-Newtonian mud rheology is introduced in an approximate fashion into the Newtonian equations of motion and solved iteratively.
Foda (1989)	Inviscid	Stratified Elastic <sup>a</sup>	Deep water; mud thickness unbounded	Non-linear	Analytical approach for wave attenuation. Wave energy lost to highly dissipative sideband oscillations, which in turn lose energy due to viscous dissipation whose action is enhanced by the interaction of standing elastic shear waves with viscous boundary layer.
Liu and Mei (1989)	Viscous	Viscoplastic <sup>a</sup> (Bingham)	Shallow water; thin mud layer	Solitary	Analytical approach that includes interfacial shear through boundary layer approximation. Wave dissipation due to bottom mud shear layer and turbulent interfacial stress. Predicts continuous to intermittent mud motion.

Investigator(s)	Water Column	Mud	Depth	Modeling Theory	Brief Description
Jiang and Zhao (1989)	Viscous	Viscous <sup>a</sup>	Shallow water	Solitary	Analytical approach and laboratory tests on wave attenuation based on boundary layer approximation.
Chou (1989)	Viscous	Viscous/ Viscoelastic/ Elastic <sup>a</sup>	Three-layered mud	Linear	Analytical approach for wave attenuation and fluidization. A generalized viscoelastic model where the bed consists of two layers with viscous/viscoelastic properties overlying a half-plane of viscoelastic/elastic muds, and a viscoelastic boundary layer approximation.
Shibayama et al. (1989)	Viscous	Viscoelastic <sup>a</sup>	Multi-layered mud	Linear	Analytical approach and laboratory tests on mud mass transport.
Sakakiyama and Bijker (1989)	Viscous	Viscous <sup>a</sup>		Linear	Analytical approach based on Dalrymple and Liu's (1978) viscous fluid model with laboratory tests on mud mass transport.
Jiang et al. (1990)	Viscous	Viscous <sup>a</sup>	Shallow water	Cnoidal (1 <sup>st</sup> order)	Analytical approach for wave attenuation based on boundary layer approximation. A more general model that includes those of Jiang and Zhao (1989) for solitary waves and Dalrymple and Liu's (1978) for their explicit solutions based on boundary layer approximation under shallow water waves.
Shibayama et al. (1990)	Viscous	Viscoelastic and/or viscoplastic <sup>a</sup>		Linear	Extension of the model of Shibayama et al. (1989) to include viscoplastic bed when the shear stress is greater than the Bingham yield stress.
Feng (1992)	inviscid	Power Fluid <sup>a</sup>	Shallow water	Linear	Analytical approach and laboratory tests on wave attenuation and mud fluidization. Power fluid (Sisko) model obtained empirically.
Isobe et al. (1992)	Inviscid	Non-Newtonian <sup>a</sup>		Linear	Numerical approach for wave attenuation and mud mass transport in which an empirical rheologic mud model based on multi-linear approximation to experimental stress-strain rate curves is derived.

Investigator(s)	Water Column	Mud	Modeling Depth	Theory	Brief Description
Jiang (1993)	Viscous	Viscoelastic <sup>a</sup>		Non-linear	Analytical approach and laboratory tests on wave attenuation and mud mass transport.
Cueva (1993)	Viscous	Viscoelastic (Voigt)		Linear	Analytical approach for wave attenuation based on boundary layer approximation

<sup>a</sup> Mud is assumed as a single-phase continuum.

<sup>b</sup> Two-phased system consisting of soil skeleton and pore fluid in relative motion.

# REPORT DOCUMENTATION PAGE

Form Approved  
OMB No. 0704-0188

Public reporting burden for this collection of information is estimated to average 1 hour per response, including the time for reviewing instructions, searching existing data sources, gathering and maintaining the data needed, and completing and reviewing the collection of information. Send comments regarding this burden estimate or any other aspect of this collection of information, including suggestions for reducing this burden, to Washington Headquarters Services, Directorate for Information Operations and Reports, 1215 Jefferson Davis Highway, Suite 1204, Arlington, VA 22202-4302, and to the Office of Management and Budget, Paperwork Reduction Project (0704-0188), Washington, DC 20503.

<b>1. AGENCY USE ONLY (Leave blank)</b>		<b>2. REPORT DATE</b> July 1994	<b>3. REPORT TYPE AND DATES COVERED</b> Final report	
<b>4. TITLE AND SUBTITLE</b> Fluid Mud and Water Waves: A Brief Review of Interactive Processes and Simple Modeling Approaches			<b>5. FUNDING NUMBERS</b> WU 32590	
<b>6. AUTHOR(S)</b> Ashish J. Mehta, Say-Chong Lee, Yigong Li				
<b>7. PERFORMING ORGANIZATION NAME(S) AND ADDRESS(ES)</b> Coastal and Oceanographic Engineering Department University of Florida Gainesville, Florida 32611			<b>8. PERFORMING ORGANIZATION REPORT NUMBER</b>	
<b>9. SPONSORING/MONITORING AGENCY NAME(S) AND ADDRESS(ES)</b> U.S. Army Corps of Engineers, Washington, DC 20314-1000 U.S. Army Engineer Waterways Experiment Station, 3909 Halls Ferry Road, Vicksburg, MS 39180-6199			<b>10. SPONSORING/MONITORING AGENCY REPORT NUMBER</b> Contract Report DRP-94-4	
<b>11. SUPPLEMENTARY NOTES</b> Available from National Technical Information Service, 5285 Port Royal Road, Springfield, VA 22161.				
<b>12a. DISTRIBUTION/AVAILABILITY STATEMENT</b> Approved for public release; distribution is unlimited.			<b>12b. DISTRIBUTION CODE</b>	
<b>13. ABSTRACT (Maximum 200 words)</b> <p>A review of field and laboratory data indicated that bottom mud can appreciably damp surface water waves in coastal areas. The interactive feature is the ability of waves to fluidize bottom mud and sustain it in a fluidized state as long as the wave action continues. This report reviews iterative procedures and simple model approaches for studying the basics of the interaction between progressive water waves and a compliant mud bed in a shallow coastal environment. Possible applications include designing offshore structures-energy absorbing berms-as buffers against shoreline wave attack using dredged material. The mud is assumed to be a continuum, and the suspension is assumed to have sediment and water phases. Constitutive relationships are developed to describe mud rheology. Mud can be highly rigid and weakly viscous or can be purely viscous fluid. Fluidization of the mud by waves proceeds as the space filling structure of the mud is broken and the stress between particles greatly diminished. An empirical relationship with which to estimate the depth of fluidization is presented. Models for water waves over mud are first presented, then compared to laboratory data. Field data are used to make example applications of the models.</p>				
<b>14. SUBJECT TERMS</b> Berms Dredged material Fluidization			Mud rheology Shoreline protection Wave damping	Wave modeling
			<b>15. NUMBER OF PAGES</b> 92	
			<b>16. PRICE CODE</b>	
<b>17. SECURITY CLASSIFICATION OF REPORT</b> UNCLASSIFIED	<b>18. SECURITY CLASSIFICATION OF THIS PAGE</b> UNCLASSIFIED	<b>19. SECURITY CLASSIFICATION OF ABSTRACT</b>	<b>20. LIMITATION OF ABSTRACT</b>	

Destroy this report when no longer needed. Do not return it to the originator.